SDC-92-328

SDC
SOLENOIDAL DETECTOR NOTES

SDC ENDPLUG CALORIMETER-WBS 2.2.10
GENERAL CONFIGURATION

January 11, 1993

W.L. Pope, R.W. Kadel, C. Hearty, M.D. Hoff & Y. Minamihara
Lawrence Berkeley Laboratory

SDC Endplug Calorimeter-WBS 2.2.10 SDC-92-328
General Configuration

W.L. Pope, R. W. Kadel, C. Hearty, M. D. Hoff & Y. Minamihara

Lawrence Berkeley Laboratory

January 11, 1993

ABSTRACT

This document provides a description of the SDC Calorimeter's Removable Hadronic Endplug. This monolithic endplug provides an approximately 100 tonne removable section ($2.0 \leq \eta \leq 3.0$) from remaining hadronic regions of the endcap calorimeter so that radiation damaged scintillating tiles (and fibers) can be periodically replaced without major rework or disassembly of the entire endcap calorimeter.

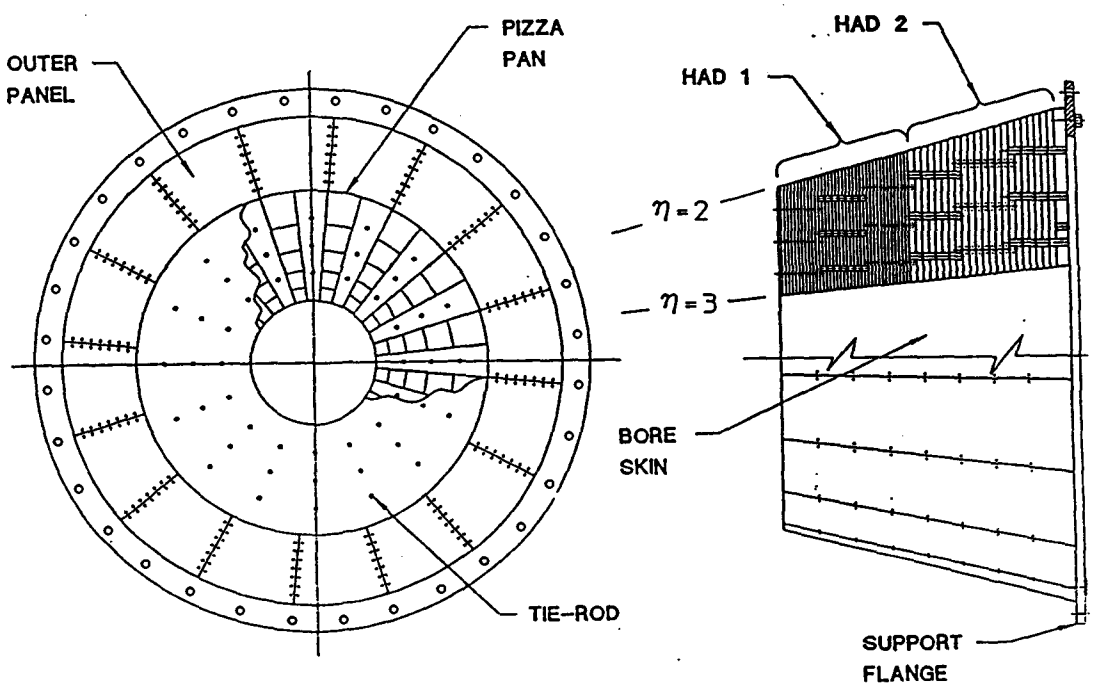

CONTENTS

1 Introduction
- 1.1 Radiation Dose and Damage Estimates
- 1.2 Alternative Endcap Considerations

2 Physics Parameter Requirements
- 2.1 Hadronic Endplug Parameters
- 2.2 The $|\eta| = 2$ Crack
- 2.3 General Absorber Configuration Considerations
- 2.4 Magnetic Field Considerations.
- 2.5 Electron Identification and Hadron/EM cuts.

3 Endplug Configuration Overview

4 Endplug Construction Details
- 4.1 Absorber Structure Parts Description
- 4.2 Absorber Assembly
- 4.3 Tile/WLS Fiber Configuration
- 4.4 Pizza Pans (or Megatiles) and Source Tube Details
- 4.5 Fiber Routing and PMT Mounting
- 4.6 Flange Light Seal and Fiber Disconnect Junction Box
- 4.7 Light Budget
- 4.8 Tile Calibration
  - CDF upgrade source
  - flexible composite wire
  - hydraulic source positioning option

5 Assembly Operations at LBL
- 5.1 Absorber Structure and Source Tube Completion
- 5.2 Optical System Completion
- 5.3 Optical System Testing

6 Endplug Support and Neighboring Interfaces
- 6.1 Endplug Support
- 6.2 Endplug-to-Endcap Interface
- 6.3 Endplug-to-EC/EM Interface
- 6.4 Endplug-to-Forward Muon System Interface

7 Loads & Structural Analyses
- 7.1 Operational Loads and Modeling Considerations
- 7.2 FEA Model Description
- 7.3 FEA Modeling Results
- 7.4 Endplug Stiffness
- 7.5 Future Structural Design and FEA Efforts

8 Installation and Removal
- 8.1 SSCL Surface Assembly Building Operations
- 8.2 Hall Operations
- 8.3 Future Fixture Design Work

9 Cost and Schedule
- 9.1 SDC Cost Estimate
- 9.2 Vendor Quotations
- 9.3 Schedule

10 Summary

11 References

12 Figures

1. INTRODUCTION

Scintillator based calorimetry was chosen by SDC because of its signal speed and absence of a containment vessel for the active medium, implying a relatively "hermetic" calorimeter. Furthermore, the safety issues involved in a scintillator calorimeter are straightforward and do not require special safety systems targeted solely at the calorimeter. The critical issue for scintillator calorimetry is the finite lifetime and consequent reduction in light yield of the scintillators and fibers in the radiation field of the detector. In its acceptance of scintillating plastic calorimeter, one of the mitigating factors acknowledged by the SDC collaboration was that the volume of the calorimeter expected to experience radiation damage is small. It seems therefore prudent to design the system so that these small sections of the calorimeter where damage is anticipated can be exchanged with minimal impact on the rest of the experiment or the schedule.

1.1 Radiation Dose and Damage Estimates

Figure 1.1 shows a cross section of the SDC calorimeter, indicating the barrel and endcap sections. Figure 1.2 shows the expected radiation dose in the endcap region after 10 years of running at a luminosity of 10^{34} sec^{-1} cm^{-2}. The radiation dose in the endcap is greatest at electromagnetic shower maximum, between 5 and 6 radiation lengths deep into the electromagnetic calorimeter. For any given angle with respect to the interaction point, the maximum radiation dose in the hadronic calorimeter is about 4 times less, and is greatest at the front of the hadron calorimeter. Over the surface of the calorimeter, the maximum radiation dose varies as $1/(r^2 \sin^3(\theta))$ or about a factor of 100, from 5 Mrad at pseudo rapidity ($\eta = - \ln\{\tan(\theta/2.)\}$) of 3 to 50 krad at $|\eta| = 1.4$, after 10 years of running at a luminosity of 10^{33} sec^{-1} cm^{-2}. Hence, the sections of the calorimeter closest to the beam line receive the highest dose, and the total volume of the calorimeter receiving a high dose is relatively small.

The sensitivity of plastic scintillator and fibers to radiation damage has been measured, and is shown in Figure 1.3. As can been seen, after about 1 Mrad of radiation, the scintillator tile/fiber combinations have lost about 50% of their total light yield. This result was obtained with scintillating tiles made from SCSN 81, BCF-91a wave length shifting fiber and BCF-98 clear readout fibers. A 50% reduction in light yield corresponds to a 7.5% addition (in quadrature) to the constant term in the calorimeter resolution (Ref. 1.1). The maximum radiation dose from Figure 1.2 and the light output from Figure 1.3, indicate that the scintillator in the hadronic calorimeter for $|\eta| \gtrsim 2$ near hadronic shower maximum in the HAC1 section of the calorimeter will need replacement during the life time of the detector, particularly if the accelerator exceeds its design luminosity.

In addition to this radiation dose calculated directly from the rate of minimum bias events, there are three other contributions to the radiation damage that are more difficult to estimate. Two of these involve *all* the tiles near the $\eta = 3$ boundary, regardless of their depth in the calorimeter as measured from the interaction region.

- Neutron damage/Forward calorimeter and quadrupole. The front face of the forward calorimeter, the low beta quads and the $\eta = 3$ boundary of the endplug, form the boundary of a neutron bottle which will trap neutrons boiled off the front face of the forward calorimeter and quadrupoles. One would estimate that these neutrons would deposit their energy in the first 1 - 2 interaction lengths of material at the boundary of this bottle. Hence, we expect a higher rate of damage to all the

scintillators along the $\eta = 3$ boundary of the endplug, regardless of their depth into the calorimeter as measured from the interaction point.

• Beam line related effects: The radiation damage estimates ignore damage due to beam-gas interactions, beam-pipe interactions and secondary interactions from particles from minimum bias events interacting with the beam pipe or other structures. These will all contribute to a higher, but currently unknown radiation dose, particularly for all the tiles along the $\eta = 3$ boundary, regardless of their depth in the calorimeter.

• Magnetic focusing. The radiation dose plotted in Figure 1.2 does not include magnetic field effects. Given the coil radius of 1.7 meters and the field strength of 2.0 T, the capture p_t of tracking volume is 0.5 GeV. All charged particles with p_t below 0.5 GeV will deposit their energy in the endcaps. Assuming that the average p_t at the SSC is 0.6 MeV, this means that about 13% of the particle flux that might have otherwise struck the barrel will be focused on the endplug instead. The total energy deposited from minimum bias events between $\eta_0 \geq \eta \geq 0$ is given by $H \langle p_t \rangle \sinh(\eta_0)$, where H is the height of the rapidity plateau and $\langle p_t \rangle$ is the mean p_t. Using these numbers, and modeling the single particle p_t dependence as $dN/dp_t = A\, p_t \exp(p_t/p_0)$, where A is a constant and $p_0 = \langle p_t \rangle = 600$ MeV, we estimate magnetic focusing contributes only a 1% increase in the total hadronic radiation dose in the endplug as compared to the raw rate calculated without the magnetic field.

1.2 Alternative Endcap Considerations

In the SDC Technical Design Report, the hadronic endcap includes a removable endplug to permit the replacement of radiation damaged scintillator tiles in the angular range $2.0 \leq |\eta| \leq 3.0$. The endplug, which weighs approximately 100 tonnes, is supported from the rear of the calorimeter's endcap and can be removed without dismantling the rest of the endcap calorimeter. Other techniques have been proposed which require dismantling most of the endcap to replace radiation damaged scintillator or fibers. We see several reasons why the removable endplug concept should be maintained:

• Damage to the calorimeter: The volume of damaged scintillator is expected to be relatively small. About 10% of the total number of tiles (or 7% of the scintillator volume) will require replacement. It seems dangerous to tear down all of the endcap calorimeter so that only 10% of it can be refurbished. The potential for damage to the part of the calorimeter system not needing replacement is high.

• Collateral damage: Removal of all the scintillators from the endcap calorimeter implies removal of all of the infrastructure from the calorimeter surface: electronics, PMTs, cooling systems, experimental power, equipment power, high voltage, cables, trigger hardware, source systems, fire protection and other safety systems, as well as those pieces of other subsystems that rely on the endcap for mechanical support or experimental utilities distributed from the endcap. Given the large number and variety of systems connected to the endcap, it is likely that a complete disassembly of the endcap calorimeter could cause significant damage to other systems.

• Schedule: The schedule for replacement of the damaged scintillator can be minimized by almost complete preparation of the new scintillator and pizza pan

assemblies prior to disassembly of the endplug. In a system of monolithic pizza pans extending from $1.4 \leq |\eta| \leq 3.0$, the new scintillators could not be installed into the pizza pans until the old scintillators had been removed. In this case, the schedule would also have to include down time for removal and eventual reinstallation of all the other systems and detector utilities and cables.

- Cost: With the removable endplug, refurbishment costs are fairly well restricted to replacement of the damaged scintillator, without involving the undamaged portion of the calorimeter or ancillary systems. A design requiring removal of all the scintillator needs to include not only the cost of the scintillator replacement, but also the cost of the disassembly and reinstallation of other affected systems.

For these reasons we conclude that the original plan for an endplug hadron calorimeter should be pursued, and in the following we describe a well-developed mechanical design. The physics parameters of the endplug are described in the next section, followed by a discussion of the mechanical implementation. Fabrication of the absorber structure, the scintillator tile/fiber assemblies, fiber and source tube routing as well as PMT mounting are also described in this section. Section 5 discusses initial assembly operations. The support of the endplug and interfaces to adjoining systems are discussed in Section 6. Mechanical and electromagnetic loads and the structural analyses indicating how these loads are carried by the structure are discussed in Section 7. Section 8 discusses the installation and removal of the endplug at the SSCL. Finally, we present a cost estimate in Section 9 and a summary in Section 10.

2. PHYSICS PARAMETER REQUIREMENTS

2.1 Hadronic Endplug Parameters

Because the reasons for the endplug calorimeter are environmental, rather than based on unique physics requirements, the parameters of the endplug are identical to those of the endcap calorimeter in general. They are listed in Table 2.1, as taken from the SDC Detector Parameters Book.

Table 2.1: Hadronic endplug parameters

Parameter	HAC1	HAC2
Longitudinal readouts	1	1
Lateral Segmentation ($\delta\eta \times \delta\phi$)	0.2 x 0.2	0.2 x 0.2
Absorber Layers	19	11
Absorber Thickness (mm)	42.0	90.0
Scintillator Thickness (mm)	4.0	4.0
Cell Thickness (mm)	48.0	96.0
Depth	5.04 λ	5.99 λ
Channels (both endcaps)	320	320

We note that the transition between tower sizes in the endcap occurs at $|\eta| = 2$, so that the segmentation of the electromagnetic endcap calorimeter is four times (except $2.6 \leq |\eta| \leq 3.0$) the segmentation of the hadron calorimeter behind it. Above this boundary the segmentation in the hadron calorimeter is $\delta\eta \times \delta\phi = 0.1 \times 0.1$. Below this boundary, which also corresponds to the outermost boundary of the endplug, the transverse segmentation is $\delta\eta \times \delta\phi = 0.2 \times 0.2$.

To minimize dead regions while still maintaining a solid mechanical structure, half thickness absorber plates in the endplug are alternated with scintillator tile assemblies, analogous to the structure of the barrel. Figure 2.1a shows a cross section through one layer of the hadronic endcap (for the baseline wedge module endcap option) and endplug, with alternating wedges of scintillator and absorber plates. In the subsequent scintillator layer the scintillator and wedge plates exchange positions such that layer-to-layer tile ϕ edges in the endplug are projective. Figure 2.1b shows an analogous cross section for another endcap configuration which utilizes radially withdrawn pizza pans. The further details of this endplug assembly are explained in Section 4.

2.2 The $|\eta| = 2$ Crack

The crack between the endplug and the endcap should be as small as possible, but large enough to accommodate:

- Readout fibers and their covers and connectors,
- Mechanical tolerances,
- Mechanical distortions of the endcap calorimeters due to gravity,
- Mechanical motion due to magnetic forces on the endplug.

We imagine that to accommodate these needs, the gap between the endcap and endplug needs to be about 10 mm wide. As is the case for the barrel, it is possible to put a "dogleg" in the gap between endcap and endplug hadron calorimeters so that the crack between them is non projective.

2.3 General Absorber Configuration Considerations

Besides the appropriate segmentation, and granularity and mechanical strength needed to satisfy the requirements of hadron calorimeter, the endplug design must be consistent with the overall flux return path through the steel of the calorimeter as a whole. Additionally, the arrangement of absorber in the endplug must not compromise the e/had cuts necessary to identify electrons in the ECEM. We address these two issues below.

2.4 Magnetic Field Considerations.

Similar to the design in the barrel, the endplug design features steel absorber wedge plates alternating azimuthally with scintillators in pizza pans. To complete a layer (or "cell") of absorber and scintillator, these wedge plates and pizza pans exchange position in the following depth layer in the calorimeter. The purpose for these alternating layers is to maximize the acceptance of the calorimeter while maintaining strong mechanical links between the absorber plates to carry the mechanical and electromagnetic loads. We show in Section 7 how the endplug is designed to withstand the 100 tonne gravitational loads and the estimated 300 tonne magnetic load. In the layout of the endplug, we have paid special attention to the boundaries of the steel plates to keep them aligned with the neighboring steel plates in the endcap hadron calorimeter so as to make the flux return path as uniform as possible. We have shown two examples of the steel layout in Figures 2.1a and 2.1b, where

the wedge plates in the endplug have been positioned so as to correspond to two different mechanical structures in the endcap hadron calorimeter. We note that the azimuthal asymmetry in the magnetic field introduced by this azimuthal distribution of steel should be small compared to the azimuthal variation in the flux return caused by the 32 steel pads spanning the 8 cm gap between the endcap and barrel calorimeters.

The axial stiffness of the endplug absorber structure is also a very important factor in the design. This should be at least as stiff as the combined stiffness of the coil (relative to the cryostat) and its external cryostat (relative to the barrel calorimeter). The required minimum stiffness is 10 tonne/mm (Ref. 2.1). The calculated endplug stiffness is described in Section 7.4.

2.5 Electron Identification and Hadron/EM cuts.

Additionally, we have been concerned with the potential azimuthal variation of absorber in the first layers of the endplug hadron calorimeter and its impact on the identification of electrons. Were the alternating structure of wedge plates and scintillators to be naively extended to the front of the endplug, there would be different amounts of steel absorber between the *last* scintillator of the ECEM and the *first* scintillator of the hadron calorimeter. We have therefore slightly modified the structure of the endplug so that the first scintillator in the hadron calorimeter is covered by the same absorber thickness.

This is accomplished by the addition of sixteen 24 mm thick steel wedge shaped plates on the front surface of the endplug (see Figure 1.1). Including the first full absorber plate, there is always 42 mm of steel in front of every scintillating tile in the first "cell" of the hadron calorimeter.

To maintain continuity between the endplug and the endcap, this 24 mm plate can also be incorporated in the endcap calorimeter. With this addition, electron showers that leak into the hadron compartment should be uniformly sampled, regardless of the location of the particle.

We are confident that the endplug absorber can be designed to correspond to any reasonable steel configurations in the endcap hadron calorimeter (e.g. see Figure 2.2).

3. ENDPLUG CONFIGURATION OVERVIEW

Each endcap calorimeter (Figure 3.1) spans the region $1.4 \leq |\eta| \leq 3$, and consists of an electromagnetic section (EC/EM), an outer hadronic region (EC/Had), and a smaller, approximately 100 tonne, conical shaped ($2 \leq |\eta| \leq 3$), monolithic, removable hadronic endplug. Absorber plates in the entire endcap are oriented perpendicular to the beam axis. The depth segments of the endplug match the corresponding depth segments in the surrounding EC/Had. The endplug's front face is adjacent to the back face of the EC/EM. The endplug's back face is approximately coplaner with the back face of the endcap.

Portions of the EC/EM and endplug calorimeters are subjected to the highest radiation exposure (damage and radioactivation) within the Central calorimeter. These two calorimeter sub-systems have been configured for relatively easy removal from the endcap so that tiles and fibers can be replaced. This operation takes place after the endcaps have been

axially withdrawn to suitable locations within reach of the hall's crane; requiring withdrawal of the detector's Forward Muon system.

Radiation damaged tile replacement operations are expected to take place during long scheduled detector shutdowns after operational periods of *about 4 years* (depending upon beam luminosity, η location, depth, and light output degradation).

The monolithic endplug, Figure 3.2, is an assembly of annular shaped absorber plates, trapezoidal shaped "wedge" plates, and trapezoidal shaped "pizza pans", with 5 scintillating tiles within each pizza pan. Pizza pans and tiles are inserted into the absorber structure from its outer, $|\eta| = 2$, boundary. Source tubes, which are adjacent to tile faces in each absorber slot, enter the endplug from its inner, $|\eta| = 3$, boundary.

There are two each absorber plates and two half-layers of wedge plates and two half-layers of pizza pans in a typical endplug hadronic "cell". Table 3.1 provides thickness details of endplug cells.

TABLE 3.1

HAC1

Absorber plate thickness	(mm)	18
No. of absorber plates/cell		2
Pan slot (and abs. wedge) thickness	(mm)	6
Abs. thickness/cell (2x18 + 6)	(mm)	42
Scintillator thickness	(mm)	4.0
Pizza pan thickness	(mm)	1.016
Cell thickness (2x(18 + 6))	(mm)	48
No. of HAC1 cell layers		19
Cell density	(g/cm^3)	7.140
No. of HAC1 Interaction Lengths	(lambda)	4.95

HAC2

Absorber plate thickness	(mm)	42
No. of absorber plates/cell		2
Pan slot (and abs. wedge) thickness	(mm)	6
Abs. thickness/cell (2x42 + 6)	(mm)	90
Scintillator thickness	(mm)	4.0
Pizza pan thickness	(mm)	1.016
Cell thickness (2x(42 + 6))	(mm)	96
No. of HAC2 cell layers		11
Cell density	(g/cm^3)	7.505
No. of HAC2 Interaction Lengths	(lambda)	6.00

Total endplug depth (at $\eta = 3$) 12.03
(assuming EC/EM depth of 1.08 lambda)

Table 3.2 provides tower size and quantity information for each section in an endplug. Each endplug consists of 32 sectors in ϕ. Quantities listed apply to each endplug.

TABLE 3.2

HAC1	Eta region	$\delta\eta$	$\delta\phi$	No. of towers/sector
	2.0-2.2	0.20	$\pi/16$	1
	2.2-2.4	0.20	$\pi/16$	1
	2.4-2.6	0.20	$\pi/16$	1
	2.6-2.8	0.20	$\pi/16$	1
	2.8-3.0	0.20	$\pi/16$	1
			No. of tiles per cell sector	5

HAC2	Eta region	$\delta\eta$	$\delta\phi$	No. of towers/sector
	2.0-2.2	0.20	$\pi/16$	1
	2.2-2.4	0.20	$\pi/16$	1
	2.4-2.6	0.20	$\pi/16$	1
	2.6-2.8	0.20	$\pi/16$	1
	2.8-3.0	0.20	$\pi/16$	1
			No. of tiles per cell sector	5

Total number of endplug tiles:

HAC1: (No. of HAC1 cell layers) x (No. of tiles per cell sector) x (No. of ϕ sectors) = 19 x 5 x 32 = 3040 tiles

HAC2: (No. of HAC2 cell layers) x (No. of tiles per cell sector) x (No. of ϕ sectors) = 11 x 5 x 32 = 1760 tiles

Total number of endplug tiles = 3040 + 1760 = 4800

4. ENDPLUG CONSTRUCTION DETAILS

4.1 Absorber Structure Parts Description

The absorber structure of the 100 tonne, conical-shaped endplug consists of alternating layers of annular steel absorber plates and trapezoidal-shaped steel wedge plates, all fastened together by short, steel tie-rods. The tie-rods are welded to the outboard face of each pair of absorber plates. In addition, the outer edge of each wedge plate is slot-welded to adjacent absorber plates. The combination of tie rods and peripheral slot-welds enable the plate/rod structure to resist gravity and magnetic forces at acceptable stress levels. The endplug is cantilever supported from the back face of the endcap calorimeter using an annular-shaped bolted flange.

The endcap, which may either be constructed from large, annular plates (a monolith) or from keystone-shaped wedge modules, has a similar distribution of absorber plate layers. Previously described Figures 2.1a and 2.1b illustrate typical cross-sections perpendicular to the beam indicating tiles and absorber material in the hadronic endplug and hadronic endcap for the forgoing endcap construction options. Note that tiles and absorber "line up" across the endcap/endplug interface for either endcap configuration option, providing nearby tower and magnetic flux continuity.

The endplug's absorber structure (see 20M6006) is divided into 2 longitudinal sections, HAC1 and HAC2 whose principle differences are the thickness of the absorber plates and the size and radial locations of the tie-rods. For practical reasons, the diameter of the tie-rods is constant in each hadronic section. The HAC1 and HAC2 sections are each further divided into 3 sub-regions of about 8 to 14 plates each. Within each of these sub-regions, the tie rod diameter and hole patterns through the absorber plates and wedge plates are identical.

Drawing 20M6046 shows fabrication details of a "generic" HAC1 absorber plate, and 20M6086 is a similar generic HAC2 absorber plate.

Drawing 20M6034 shows a "generic" HAC1 wedge plate; corresponding plates in HAC2 are virtually the same. Finally, Figure 2 of 20M6016 shows the typical azimuthal orientation of the 16 each, 11.25 degree ($2\pi/32$) wedge plates (all 6 mm thick) between absorber plates. This wedge plate pattern is alternately rotated +/- 22.5 degrees after each additional absorber plate layer, providing radial slots in the structure for subsequent insertion of pizza pans and scintillator tiles.

At the back of the endcap is an annular Endcap Adapter Ring (equipped with 32 protruding studs) to which the endplug's Support Flange (20M6143) attaches.

Purchased stock for the forgoing absorber plate fabrications could consist of flame cut blanks for the 42 mm (1.65 inch) thick HAC2 section parts and either flame cut or waterjet cut blanks for the 18 mm (0.708 inch) thick HAC1 section parts. The 6 mm thick wedge plates could be blanchard ground from waterjet cut blanks, with virtually no additional profile machining required for finish parts (only hole drilling).

Finally, 20M6154 and 20M6164 show details of the small, shallow grooves for source tubes in the HAC1 and HAC2 absorber plates, respectively. The 16 each, small straight slots in these plates could be cut using one of several conventional machining methods, but unless the cutting speed is high, the cost would be prohibitive. After considering several possibilities including milling, grinding (with an abrasive cut-off wheel), and cutting with a carbide bladed skill saw, we initially selected plasma arc "gouging" (Ref. 4.1) for producing these small grooves.

In this well developed commercial process, we could use a suitably guided and driven, plasma-arc gouging torch. Although the groove shape is more V-like, the finish is acceptable, and speeds of about 6 feet per minute can be achieved. Based upon recent groove samples cut at LBL (in 25 mm thick plate), distortion (warping) does not appear to be a problem. Clean-up operations are limited to surface flash removal (with a metal scraper) and wire brushing--both very fast operations. The short radiused end of these slots could be done either with a milling cutter (at the time the plate's holes are drilled) or with a router and a guiding template.

However, Barnes (Ref. 4.2) has recently shown that the z-position of the source relative to tiles has a significant influence on calibration sensitivity. When the source is located in a small groove in the absorber plate such that part of the tile is "obscured", the response at the tile is sensitive to the source's z-position at about the 30 %/mm level. On the other hand, when the source is located "in air" (adjacent to the face of the tile), this sensitivity drops to about 3 %/mm.

Because of this new information, we have changed our original plan of routing the source guide tube *within* the absorber structure, and in Section 4.4 we describe a modified design which achieves the reduced position sensitivity while retaining low cost fabrication means. The cost of the "grooves" is reduced by machining a wider (and shallower) profile using a much larger diameter milling cutter (see Section 4.4).

4.2 Absorber Assembly

The stacking/welding sequence of the endplug's absorber structure assembly is shown in the azimuthal cross-section Plug Assembly drawing, 20M6006, and the Plug Assembly Sequence drawing, 20M6016.

After individual absorber plates have had their tie-rods welded at the back side into close-fitting holes using suitable tie rod alignment shims as shown in Figure 1 of 20M6016, assembly starts with the HAC2 strongback plate inverted and positioned on four temporary post supports. A conical tooling fixture provides radial alignment as absorber plates are stacked.

As each absorber plate (which may be out-of-flat by as much as 0.1 inch) and each group of 16 blanchard-ground wedge plates are added to the "stack", the plate is locally compressed (Ref. 4.3) and welded to the upstanding end of the previous plate's tie-rods. This sequential plate-to-tie rod welding operation, produces a progressively more rigid, endplug structure with minimal residual thermal stress and consequent out-of-plane distortions. After the tie rods have been welded, the outer periphery of each wedge plate is slot-welded to its two adjacent absorber plates as shown in Figure 2 of 20M6016.

4.3 Tile/Wave Length Shifter (WLS) Fiber Configuration

Trapezoidal shaped scintillating tiles within the endplug are configured as shown in Figure 4.1, with a single, 1 mm diameter fiber readout to each tile. The "sigma" style, WLS fiber groove path is machined into the tiles with a high speed ball-mill type cutter. The groove path enters tangentially from one face of the tile, similar to tiles used in LBL's 4 x 4 tower Test Station Module of the monolithic EC/EM (Ref. 4.4). The inboard end of the WLS fiber is vacuum coated with Aluminum (sputtered) to improve light collection.

The endplug tile/fiber design has a fused joint from 1 mm diameter WLS fiber (within the tile) to 1 mm clear plastic readout fiber, reinforced with a thin metal or plastic tube (1.5 mm outer diameter) close to the tile. The clear fiber is routed radially outward over the face of tiles (or megatiles--see section 4.4), along the $\eta = 2$ boundary and through the support flange, to a single commercial optical disconnect on the back of the endcap.

To increase light output and minimize coupling between adjacent tiles, the four transverse edges of each tile are painted with a white acrylic paint. In addition, each tile is circumferentially wrapped with Tyvek or aluminized Mylar sheet before installation into the pizza pans. We will place a 0.005 inch thick sheet of Kapton over the reflective wrapping on the 5 tiles as they are installed into the pizza pans, to act as an "anti-abrasion strip" (for the reflective wrapping) when pizza pans are subsequently slipped into absorber slots.

As an alternative to this baseline design, we will consider multiple fibers (possibly of smaller diameter) per tile to improve radiation hardness, if uniformity is acceptable (Ref. 4.5).

4.4 Pizza Pans (or Megatiles) and Source Tube Details

We have been considering two types of construction for the 5 tiles which are installed in each absorber slot of the endplug: a) individually wrapped tiles contained in 0.5 mm thick pizza pans (to facilitate handling and installation), and b) megatiles with a continuous reflective over-wrap and no pizza pans. Recent endplug tile designs explored have also only considered tile-source tube arrangements in which the tube is in air and "sees" the entire tile (Ref. 4.2). With structurally sound, light reflecting adhesive joints between individual tiles and acceptable low levels of light coupling, megatiles provide the handling capability with an advantage of not requiring additional absorber space for the pizza pan--see Table 4.1.

TABLE 4.1 Endplug Absorber Slot Dimension Contributors--after Freeman (Ref. 4.6)

Tile Construction Option	Megatile	Pizza Pan
Component	thickness (mm)	thickness (mm)
Tile	4.0 (+/-0.2)	4.0 (+/-0.2)
1 mm Clear Fiber Splice	1.5	1.5
Optical Wrapping (3 layers)	0.5	0.5
Pizza Pan	0.0	1.0
Insertion Clearance	0.2	0.2
Required Slot Dimension	6.2 (+/-0.2)	7.2 (+/-0.2)

Note that the baseline, 6 mm thick, absorber slot is inadequate for either of the above endplug tile options, but close for megatiles. Although we might be able to show in Section 4.7 (Light Budget) that endplug tiles could be thinner or that smaller diameter fiber could be used, we ignore these potential refinements for now (the trade-offs can be studied later), because similar absorber slot dimensions will also be necessary for the outer endcap hadronic modules if radially withdrawable megatiles are considered, as we believe FNAL will propose.

Either the megatiles or the 0.5 mm thick stainless steel pans are laterally positioned in the 6 mm thick (nominal) trapezoidal slots in the absorber structure by the wedge plates. Figure 4.2a, an edge view of a typical slot in the absorber structure, shows the combined assembly of a megatile and a "source tube strip". Figure 4.2b shows a similar edge view for the pizza pan option. The source tube strip, with its attached z-plane section of source guide tube (the 1.3 mm diameter baseline source guide tube is shown), is installed from the $\eta = 3$ side and becomes semi-permanently attached to the absorber structure, whereas pizza pans or megatiles can be withdrawn from the outer, $\eta = 2$ boundary (Ref. 4.7).

The source guide tube is brazed or spot welded to the lateral center each of the 5 spring tabs which are die stamped into the approximately 75 mm wide x 0.5 mm thick source tube strip, Figure 4.3. The flexible spring tabs ensure that the guide tube is locally pressed against the transverse center of each tile. The source tube strip occupies the rectangular-shaped open region in the front face of the pizza pan in that option. Centering of the source guide tube (and strip) with respect to tiles to the +/- 2 mm lateral position requirement is easily obtained when the shallow U-shaped stamped section of the source tube strip is placed in the approximately 9.5 mm wide x 0.9 mm deep groove, milled into the absorber plate. These grooves will be positioned in phi to an accuracy of about +/- 0.25 mm. The strip has identical die-stamped features at each end to reduce costs. One of the subsequently bent tabs at each end allow attachment to the adjacent absorber plate with small, ring shanked nails. The other bent tabs at each end of the strip provide a reasonably precise radial positioning means for the tiles (or megatiles). Except for variable lengths and die stamped spring tab locations, all of the source tube strips are identical.

The pizza pan's simple configuration details are illustrated in Figure 4.4. These pizza pans offer the advantage that tile fibers (and splices) are protected against damage when pans are inserted into the absorber slots. The approximately 77 mm wide opening in the front face provides insertion clearance around the source tube strip. The small hole in the spot-welded bent tab at the outer edge of the pizza pan allows a screw attachment to the adjacent absorber plate. The inner and outer profiles of the pizza pans are configured in the simplest possible form to eliminate the cost of expensive, variable-dimension blanking and folding die tooling.

4.5 Fiber Routing and PMT Mounting

Pizza pans and tile/fiber units are installed into the endplug using a "last-in/first-out" assembly sequence. That is, those tile *layers* closest to the interaction point are removed first and installed (or reinstalled) last. This sequence permits the organized placement and tape down of fibers (and fiber layers) during pan/tile (or megatile) installation. Each clear fiber is equipped with a single commercial optical disconnect which resides in a junction box near the outer perimeter of the endplug support flange.

With the junction box opened and the fibers disconnected, the endplug can be withdrawn without disturbing PMT assemblies which are mounted at the outer circumference of the endcap. PMTs are mounted here (as opposed to the rear of the endplug) because the close proximity of the Detector's first muon chamber, FW1, would limit PMT access. With the PMTs on the endcap, the clear fiber length is about 2 m longer than with PMTs on the endplug.

We have investigated various means of routing the 4800 endplug fibers from the pizza pans to the PMTs, while providing light seals, minimizing light loss, and providing space for PMT mounting and access (Ref. 4.8). These functions must exist without compromising our ability to quickly remove and replace the 100 tonne endplugs and radiation damaged tiles therein. After the clear fibers exit the pizza pans (or megatiles), they are gathered into thin layers at the outer η boundary (inside a light-tight, conical sheet metal cover skin) and follow the small η "gap" between the EC/Had and the endplug to the PMTs. The proposed locations of PMTs and disconnects are shown in the endcap cross-section, Figure 4.5.

Figure 4.6 shows details of the clear fiber routing over the face of tiles and at the outer η boundary. As the 5 fibers exit a pizza pan (or megatile), the group is curved 90 degrees with about a 50 mm bend radius (at the outermost tile) to exit tangent to the outer surface of the absorber structure, and taped into position. Outside the pizza pan the 5 fibers are then curved through another relatively long radius, 90 degree arc (directed toward the rear of the endplug) and taped down to the $\eta = 2$ surface of the absorber structure. As subsequent groups of tiles and pizza pans (or megatiles) are installed (starting at the back of the endplug) their 5 fibers are joined with previous bundles until there are 25 fiber "mini-bundles" which are routed to junction boxes outside the endplug through light sealed, "split-tube conduits" imbedded in the endplug support flange.

4.6 Flange Light Seal, Split Conduit, and Fiber-Disconnect Junction Box

Figure 4.7 shows a typical radial cross-section through the back of the endcap, the endplug, and its support flange illustrating the path fibers take from under the thin, light-tight metal cone to the disconnect junction boxes. The endplug support flange (20M6143) is equipped with 64 milled radial slots which will contain 64 each split, circular conduits through which the fibers pass. These conduits are sealed light-tight into the flange slots using foam rubber gasketing stock which has a circular inner hole and a square outer cross-section (see Figure 4.7, section A-A).

In addition to their light sealing functions, the 32 each, junction boxes with their split-tube fiber conduits, Figure 4.8, provide two other useful functions: a) a light path physical separation means between tiles and PMTs for endplug removal, and b) a fiber withdrawal means between pizza pans (or megatiles) and optical disconnects for tile replacement. When the junction boxes are opened and the fibers disconnected, the endplug can be withdrawn from the endcap without disturbing the PMTs. The "inboard flange" of the junction box is also constructed from two mating halves which split when the box's joint is opened, allowing the clear fibers (between tiles and the disconnect) to be withdrawn. The exposed seams between the two halves of the split fiber conduits and the two halves of the junction box flange are externally wrapped with a suitable light-tight seal after the conduit gaskets have been compressed into the support flange slots, finalizing the light seal.

At the outboard end of each junction box (Figure 4.8) is a single metal conduit which extends to the PMT mounting/access boxes on the outer radius of the endcap. This tube is light-sealed to the junction box retractable lid using a conventional rubber grommet. The outermost end of this tube has a flange, which is sealed light-tight with a suitable gasket to the mounting box. There is one mounting box for each of the 32 phi sectors. Each contains ten PMTs, five for HAC1 and five for HAC2, giving a total of 320 PMTs per endplug. A total of 150 fibers enter each mounting box.

4.7 Light Budget

To estimate the photoelectron budget we begin with values for the standard tile/fiber combination for the barrel and translate them into the endcap environment. The light yield in the barrel is 4 photoelectrons per minimum ionizing particle assuming SCSN 38 scintillator and 2 meters of clear, 1 mm diameter readout fiber and no fiber disconnects.

Table 4.2: Light yield estimates for Endplug

Parameter	Reduction in Light yield	Net light yield/mip
Light yield barrel hadron	-	4.0
Use SCSN 81 scintillator	0.76	3.0
Attenuation due to extra clear fiber path length (assume 7 meter attenuation length), 4.6 m longest path	0.68	2.1
Attenuation of 1 fiber disconnect at 0.84 each	0.84	1.8

For the hanging file calorimeter, with 5 cm (2 inch) steel plate sampling, the resolution was 5.7% at an energy of 227 GeV or $85\%/\sqrt{E}$ (Ref. 4.9), assuming no constant term. For this result there were an average of 1.3 photoelectrons per minimum ionizing particle (Ref. 4.10). The smallest η boundary of the endplug is 2, and hence we can expect an E_t resolution two times better, or no worse than about $44\%/\sqrt{E_t}$. This is well within the SDC standard of $75\%/\sqrt{E_t}$. We conclude there is significant freedom on the placement of the optical components (e.g. disconnects or the photomultiplier tubes).

4.8 Tile Calibration

The source calibration in the endplug will use a traveling radioactive point source, similar to the arrangement adopted for the CDF Endcap upgrade (Ref. 4.11) and planned for the SDC Barrel calorimeter. Figure 4.9 schematically shows the routing of source tubes from the endplug's inner, $\eta = 3$, boundary over each of the 80 tiles in a given longitudinal layer. This routing configuration allows the convenience of tile and fiber removal from the outer boundary without disturbing the source tubes, and helps to minimize the radial "gap" at $\eta = 2$ between the endcap hadronic structure and the removable hadronic endplug. The source wire is inserted into thin tubes of about 1.3 mm diameter and is directed over the front face of each

tile by a suitable driver mechanism (Ref. 4.11) mounted on the back of the endplug. The source is alternatively inserted into appropriate endplug layer tubes by the driver, to pass in close proximity (+/- 0.5 mm) to the face of each tile within +/- 2 mm from its transverse center.

This source routing path for the endplug has the disadvantage of three or four relatively short radius (about 50-75 mm) 90 degree turns in series (and thus very high potential friction) between the driver mechanism and the tiles. Because the CDF "source positioning wire" (a small, solid metal wire in a thin metal tube) is relatively stiff in bending, excessive friction could develop while negotiating small radius bends, limiting its applicability to short circuits (about 7 m) with no more than 2 or 3, longer radius (approximately 75-100 mm), 90 degree bends (Ref. 4.11).

However, the first author feels a limiting factor of the CDF "source positioning wire" design for endplug applications may be repeated stress beyond the elastic limit. If the 0.028 inch (0.71 mm) O.D. outer tube were bent around 1.75 inch (45 mm) radius arcs as the endplug requires at $\eta = 3$, the tube would be subjected to stresses well above 100 ksi. Although the CDF tube is free of local stress concentrations, few steel alloys can survive repeated flexures of this magnitude. Those alloys available in such small bore tubing form are even more limited. Consequently, we have been investigating two other alternatives: a) a more flexible, "composite source wire", and b) a hydraulically positioned source.

Flexible, "Composite Source Wire"

Figure 4.10 is a drawing of the flexible composite source wire. In this "wire" configuration, a central, flexible aircraft cable provides high axial "pull" stiffness, and a surrounding extension spring (also flexible in bending but stiff in compression) provides "push" stiffness when guided by the surrounding source tube. This composite wire has greater *elastic bending flexibility* than the CDF version, allowing repeated insertion past small bend radii at modest stress levels without fatigue failure. Although it is larger in diameter than the CDF design, frictional drag forces appear to be comparable.

The radioactive source is encapsulated (welded into a small cylindrical hole) in a short, smooth bull-nosed fitting at one end of the composite wire which is hard soldered to the cable. The "driven end" of the wire has a cylindrical fitting which is also hard soldered to the cable. This latter fitting is installed after the spring, with the cable under a modest tensile preload.

Source Wire Forces. Intuitively, one would expect the insertion/withdrawal forces between the composite wire and the (curved) source guide tube to be a function of the number of bends, or wrap angle, the friction coefficient, the bend radius, and the bending stiffnesses of the cable and spring.

Some insight into relationships between parameters affecting frictional behavior in the source wire/tube insertion/withdrawal process can be obtained by analogy with a simple friction brake mechanism. If the wire (brake band) was constructed from an ideally flexible "string", the axial string (band) tension, F1, which must be provided by the driver (band to resist drum motion), is a function of the total wrap angle around the tube (drum), α, the friction coefficient, f, and the drag force (band tension), F2, applied at the string's (brake

band's) "fixed" end. In the brake example (Ref. 4.12), the tension ratio is given by: $F1/F2 = \exp(\alpha f)$. If we arbitrarily assume $\alpha = 2\pi$, and $f = 0.6$, this force ratio becomes 43.4! The effectiveness of the band tension, F1, in the brake application, and conversely, the importance of minimizing the source wire drag, F2, in our case, should be quite clear.

In our situation, the effective axial drag force, F2, can be estimated as the product of the transverse force (composite wire bending stiffness and bend radius) and the friction coefficient at each contact point between the tube and the wire--particularly in tube bend regions. To keep F2 small, it is important to select appropriate tube and spring material combinations (to minimize f), and cable and spring materials and section properties (to minimize bending stiffness). Our calculations suggest it may also be desirable to have the spring custom wound with an initial preload as small as practical within "closed coil" spring fabrication constraints, because this initial (compressive) spring preload increases its bending stiffness.

There are a number of other factors which have conspired to make the composite wire's development "interesting", including: material selections, tube-to-spring relative diameter selections, tube joints and flattening at bends, lubrication (or lack of) in a high radiation environment, electroplating, and corrosion and wear considerations.

We have built two prototype composite wires similar to that shown in Figure 4.10, initially using off-the-shelf commercial components with minor modifications, to *measure* the forgoing forces without becoming too influenced by our "speculations" above. The initial performance (Ref. 4.13) is very encouraging--these move *elastically* through twice the number of small bends needed in the endplug with small driver forces. The smallest unit built so far has a spring outer diameter of 0.070 inches (1.78 mm), which might be acceptable for hadronic applications. We have not reviewed the availability of suitable smaller cables and springs for electromagnetic source wire applications. Much work remains to achieve a predictable and highly reliable design.

Hydraulic Source Positioning Option (a low friction source positioning concept)

Another potentially attractive, low friction method would utilize a hydraulically positioned source (Ref. 4.14). In this adaptation the source would be installed in a small (about 1 mm in diameter), spherical metal capsule which would reside in a slightly larger tube filled with a viscous liquid. The tube would be part of a closed fluid circuit, and the source would be driven over the faces of tiles in the calorimeter by a suitable, small hydraulic metering pump.

If the tube is about 1.2 mm I.D., and the fluid viscosity is the order of 20-30 centistokes, and the hydraulic circuit path length for a typical endplug cell layer (Figure 4.11) is about 45 m (150 feet), the fluid velocity can be about 10 cm/s (0.3 ft/s) with a total circuit pressure drop not exceeding about 400 psi.

For this hydraulic option to be technically viable in the endplug, the source (and its capsule) would need to be non-magnetic, have a moderately long life, a high specific activity, and be safely encapsulated (welded, for example) within the metal sphere.

We have performed terminal velocity tests of this concept utilizing 3.17 mm (1/8 inch) diameter solid metal and plastic spheres of various densities in a 4 mm diameter vertical glass tube filled with Silicone fluid with a kinematic viscosity of about 50 centistokes (these sphere and tube sizes and fluid viscosity were selected for convenience only) to verify the predictability of the sphere drag force using existing, semi-empirical creeping flow correlations (Ref. 4.15, 4.16) which are accurate to within about a factor of 3 for our geometric conditions (Dtube/Dsphere of approximately 1.2).

If the source capsule were neutrally buoyant, it would travel around the various inclined legs of the the above circuit at precisely the velocity of the driven fluid. However, it does not appear to be possible to construct a neutrally buoyant source/capsule near 1 mm in diameter with the desired properties. Nevertheless, calculations of the terminal velocity of source/capsule spheres with a sphere-to-fluid specific gravity ratio the order of 3-5 in a vertical tube (Poiseuille flow) suggest that the relative velocity (sphere-to-fluid) would be small. Thus, for all practical purposes, the sphere would move with the fluid at about 10 cm/s in all branches of the circuit shown in Figure 4.11.

LBL physicists working with a commercial source vendor (Ref. 4.17) have tentatively identified a candidate source/capsule with the requisite properties. This could be a 10-15 mCi gamma source (Zn^{65}) contained within a 1 mm diameter, welded Titanium sphere. After the source pellet is installed in a 0.5 mm hole in the sphere's center followed by a short, 0.5 mm diameter Ti plug, the sphere would be EB welded shut, Figure 4.12. The pellet would be subsequently enriched in a nuclear reactor. Because Zn^{65} has a relatively short half-life (244 days--decaying to Copper), several "cold" source spheres would be initially fabricated and stored for subsequent bombardment and use.

This hydraulic source positioning concept would require extensive development which is not included in the baseline endplug's estimated cost (Section 9, below). We will explore it further only if we cannot make the mechanically driven, flexible source wire work reliably.

Similarly, we will stop all work on the flexible composite source wire, if the CDF design (*the SDC baseline*) is found to be satisfactory for all calorimeter subsystems. A change from 300 series stainless steel tubing in the CDF design to either MP35N (Ref. 4.18) or Elgiloy (Ref. 4.19) would improve the tube's fatigue performance.

5. ASSEMBLY OPERATIONS AT LBL

After the endplug absorber structure has been welded into a 100 tonne assembly by an outside fabricator, it will be lifted with a mobile truck crane (e.g. Bigge) and a pick-up and rotation fixture (Figure 5.1) and transported with a vertical axis orientation on a suitable truck carrier to LBL, where subsequent assembly work will be performed.

At LBL, the structure will be off-loaded and placed inside the selected assembly building on a large, thick steel plate equipped with four each, stout vertical "posts" welded on a 2.5 m circle on the steel plate (tooling used by the structure's vendor during assembly). The Endplug Adaptor Ring and Support Flange will be placed over the 4 posts onto the steel plate prior to off-loading the absorber structure. Assembly work at LBL will be done with the vertical axis endplug orientation on a platform as shown in Figure 5.2.

Assembly work at LBL, which will take several months, consists of:

5.1 Absorber Structure & Source Tube Completion:

- lifting and temporary bolting of the Adaptor Ring and Support Flange to the rear of the absorber structure,
- installation of an annular-shaped wooden working platform around the endplug and above the temporary location of PMT mounting/access boxes and source drivers (Figure 5.2),
- small hole drilling and tapping for pizza pan attachment screws (as applicable),
- small hole drilling for source tube strip attachment nails,
- absorber structure final cleaning operations,
- attachment of source tube strips (with their z-plane source tubes) into the pizza pan (or megatile) slots,
- completion of source routing tubes to the rear of the endplug at the inner η boundary,
- installation of the light-tight sheet metal skin at the inner η boundary,
- installation of the endplug's source drivers at a suitable location under the working platform near the platform's outer boundary,
- extension of source tubes at the rear of the endplug's inner η boundary to the source drivers.

5.2 Optical System Completion:

- installation of pre-wrapped tiles, fibers and pizza pans (as applicable) at the outer η boundary,
- routing of the clear fiber segments and their disconnects to the junction boxes and fiber tape-down,
- checking of each layer in the final assembly for integrity and light yield,
- installation of the 64 each foam-rubber-sealed, split fiber conduits (which terminate at the junction boxes) into the Plug Support Flange radial grooves,
- installation of the 64 each fiber junction boxes and their approximately 2 m long straight radial extensions to the PMT mounting/access boxes (temporarily supported from the working platform),
- routing of the clear fibers from their "cookies" through the conduits from the PMT access boxes to the fiber junction boxes, and attachment at disconnects,
- installation of the light-tight sheet metal skin sectors at the outer η boundary; screw attachment of the skin's rear flange to the Plug Support Flange (which seals the foam-rubber-covered conduits); screw attachment of the skin's front flange to the front HAC1 plate,
- light tight sealing of the axial seams of the outer sheet metal skin sectors,
- installation of an annular wooden ring simulating the Endcap Adaptor Ring--which bolts to the Endplug Support Flange over the rubber sealed fiber conduits--*roughly simulating* the horizontal axis installation/make-up of the endplug into the endcap.

5.3 Optical System Testing:

During the installation scintillators into the endplug it is essential that the proper installation of each tile/fiber combination be tested and the light yield be recorded. We foresee a "just in time" assembly scenario, where tiles and fibers are joined and inserted into the pizza pans (as applicable) just before the pizza pan assembly itself (or megatile) is installed into the absorber structure. This organization minimizes the assembly space and reduces the exposure of individual tiles or fibers to damage during the assembly stages.

We envision a two shift assembly procedure, where during the first shift pizza pans (or megatiles) are inserted into the calorimeter and their correct operation is verified in the next shift. We would use a large "dark box" or flexible light tight shroud to cover the partially assembled endplug for these quality control tests. The source tube system would be used to monitor the light from the individual tile/fiber combinations.

6. ENDPLUG SUPPORT AND NEIGHBORING SUBSYSTEM INTERFACES

6.1 Endplug support

The relatively rigid absorber structure design allows the 100 tonne endplug to be supported in cantilever fashion from the back of the endcap utilizing a simple, bolted annular support flange. The endcap, whether it consists of stacked, trapezoidal shaped modules as in the barrel, or is a monolithic structure of large, welded annular plates (like the endplug), will be equipped with a bolted-on annular Endcap Adapter Ring (20M6173). This adaptor ring is equipped with 32 each, 50 mm diameter studs which penetrate large clearance holes in the annular Plug Support Flange (20M6143) to simplify the installation.

The endplug is similarly equipped with an annular Plug Adapter Ring (20M6133), which bolts to the rear strongback plate. Figure 6.1 shows a typical cross-section through the endcap and endplug illustrating the structural support configuration in greater detail. To reduce relative stack accumulative tolerances, the Plug Adapter Ring is not machined to its final thickness dimension until the finished stack height of the endplug is known, and the endplug's cavity depth in the endcap is also known. Installation and removal of the endplug is discussed in Section 8.

Although formal discussions of the various interface boundaries around the endplug have not yet occurred at the SDC Calorimeter Sub-system Manager level, the next section attempts to establish some of the important interface considerations. These future discussions could lead to appropriate Interface Control Documents (ICD) with formal SDC change control procedures.

6.2 Endplug-to-Endcap Interface ($\eta = 2$)

The $|\eta| = 2$ crack between the endplug and the endcap should be as small as possible, but large enough to accommodate:

- Readout fibers and connectors and their light-tight cover skin,

- Mechanical fabrication tolerances in the endcap and endplug,
- Mechanical distortions of the endcap calorimeters due to gravity,
- Mechanical motion due to gravity and magnetic forces on the endplug.

We estimate that to accommodate these needs, the gap between the endcap and endplug needs to be *about* 10 mm wide. As is the case for the barrel, it is possible to put a "dogleg" in the gap between endcap and endplug hadron calorimeters so that the crack between them is non projective.

6.3 Endplug-to-EC/EM Interface

Although FEA analyses on the endplug absorber structure is at a relatively mature state, we do not yet have final FEA calculations of the full endplug (and support flange assembly) inward z-deflection under the action of the steady state, axial magnetic field. However we feel the maximum z-deflection will be no more than about 3-4 mm (see Section 7.4).

Tentatively assuming this inward z-deflection plus about 3-4 mm of axial assembly clearance, we anticipate that the front HAC1 face of the removable endplug can be installed within *about* 6-8 mm from the rear plate of the EC/EM assembly.

6.4 Endplug-to-Forward Muon System Interface

During normal detector operations, the approximately 50 tonne Absorber Cone, which shields Forward Muon Chambers from albedo radiation at high eta, butts against the back of the endplug, but is physically attached to Forward Torroid One (FT1) of the Detector's Forward Muon System (Ref. 6.1). This absorber cone is configured to withdraw about 1 m into the bore of FT1, for the SDC's "Small Move" maintenance scenario.

Simply withdrawing this cone without providing suitable temporary shielding could expose personnel to dangerous radiation from the concentric beam pipe, so additional shielding means must be provided. One possible solution would be to have a small (say 5-10 tonne) concentric, inner cylindrical section of the absorber cone "permanently attached" to the back of the endplug, which would not move with the main outer absorber cone part. After these Detector interface issues have been resolved by the SDC Integration Group, the Calorimeter and Muon System groups will prepare appropriate interface control documents.

7. LOADS AND STRUCTURAL ANALYSES

7.1 Operational Loads and Modeling Considerations

In normal operation, the endplug structure and support flange to the endcap must operate within the elastic range and resist the 100 tonne gravitational load and forces from the 2 Tesla magnetic field (see Figure 1.1), which applies an axisymmetric distributed lateral load to the front HAC1 plate equivalent to *about* -90 psi (Ref. 7.1).

The endplug structure's tie rod design (size/number/radial distribution) must be compatible with these operational loads plus various other loading conditions, which include:

a) handling (pick-up with cone axis vertical and 90 degree turn),
b) shipping (cone axis vertical), and
c) installation and removal, with a suitable support fixture attached to the rearmost plate of HAC2 using a circular ring of bolts.

Fixtures to handle these loading conditions are described in Section 8.

Practical constraints limit the degree of "mesh" detail which can be built into the FEA model of the endplug. Because of the number of absorber plates and number of tie rods, for example, it is not possible to provide a very high resolution stress picture simultaneously for all welded joints between rods and absorber plates. Similarly, because the wedge plates are not welded to the absorber plates (except at their outer edge), numerous non-linear gap type elements are necessary in the model for accurate structural interface characterizations.

However, it is important to have an endplug model which accurately describes the stress state at welded joints--especially in those regions where the weld stresses are highest. It is also important to know the stress and/or lateral deflection distribution in absorber plates, because these cumulative axial deflections within the welded absorber structure plus deflections at the rear support flange joint due to the magnetic forces determine the minimum required axial installation clearance between the EC/EM and the endplug.

Anticipating the challenge of building an accurate, cost effective, isoparametric FEA model for the the endplug, LBL prepared a request for quotation and statement of work covering the expected analyses activities (Ref. 7.2). After reviewing the capabilities of various FEA codes, and the availability of suitably trained personnel within LBL, we contracted with MCR Associates, Sunnyvale, CA, the local ANSYS representative, to perform the initial FEA work.

7.2 FEA Model Description

MCR Associates have constructed a set of isoparametric FEA models for LBL which have been used to estimate the stress and deflection characteristics of the endplug for the previously described load cases. These models utilize the ANSYS Finite Element Code (Ref. 7.3).

The current endplug FEA structural model files (Ref. 7.4) prepared by MCR consist of:

- A highly detailed (approximately 9000 degrees of freedom), 3-D Tie Rod Model which uses eight-node brick elements and includes plasticity effects,

- A HAC2 System Model, which explicitly represents the endplug's bolted support flange and the last 4 endplug plate layers, utilizes non-linear gap elements between absorber and wedge plates, and simulates the slot welds to wedge plate outer edges. ANSYS "shell elements" are used for the plates, and "pipe elements" are used for the tie rods in the system model. Brick solid elements are used elsewhere.

• A HAC1 System Model, which explicitly represents the last 4 HAC1 plate layers, utilizes non-linear gap elements between absorber and wedge plates, and simulates the slot welds to wedge plate outer edges. ANSYS "shell elements" are used for the plates, and "pipe elements" are used for the tie rods in the system model. Brick solid elements are used elsewhere.

The local, generic tie rod model stiffness characteristics are used to adjust the properties of the pipe element tie rods attached between shell element plates in the system models, and to accurately predict the tie rod stresses produced by system model loads and displacements.

7.3 Modeling Results

Mark C. Rodamaker of MCR Associates, Inc. described recent FEA progress on the structural simulation of the endplug in Reference 7.4. This work was performed by MCR during June-July 1992 under contract to LBL (Ref. 7.5).

With three simple changes to our initial characterization of the endplug structure, the current design meets all physics and stress requirements with relative ease using conventional materials and a conservative set of assumptions. The changes were:

1) assume 35 mm diameter HAC1 tie-rods, and 50 mm HAC2 tie-rods,

2) increase the thickness of the strongback plate from 42 mm to 84 mm,

3) slot-weld simulation of the outer edge of all wedge plates to the outer edge of the adjacent absorber plates.

Change 3) above dramatically reduced previous peak tie rod loads and stresses and further stiffened the absorber structure axially and in transverse shear.

The conservative simplifying assumptions were:

1) The tensile preload in tie-rods, which might occur from differential thermal expansion during post weld cool-down, is zero;

2) the friction between adjacent plates throughout the absorber stack is zero.

MCR shows, through plastic simulation techniques, that although there is a *very small* inelastic zone (yielding) in the tie rod weld region at modest external loads due to an unavoidable stress concentration at the bottom of the "V-weld" (Figure 7.1), this zone remains localized and stable for external loads beyond about 1.4 times design conditions (see Fig. 28 and Fig. 41 of Ref. 7.4) with change 1) above, only.

With changes 1) and 2) above, the situation gets slightly worse at the rear of HAC2, because tie rod stresses increase (longer rods). The system is stable to only about 1.2 times design conditions (see Fig. 60 of Ref. 7.4). The forgoing alone, however, does not suggest that change 2) is undesirable.

With all 3 of the above changes, previous peak tie rod forces were reduced by about a factor of 10 to 16, as the slot welds contribute significantly to both axial and lateral strengthening. These perimeter welds carry a large fraction of the structure's axial load, but they are stressed to roughly half that of the tie-rods.

We can conservatively conclude that the very small inelastic zone in the tie rod welds in the current design will be localized and stable to external loads to well beyond two times design conditions, even though MCR has yet to "run" this case.

7.4 Endplug Stiffness

Because the existing endplug model only contains explicit characterizations of absorber plates in discrete regions (see Section 7.2), representations of its axial and lateral stiffness requires a combination of ANSYS calculations and extrapolations using hand calculations. These are conservative extrapolations.

The lateral stiffness of the endplug is very high. The (downward) deflection of the front of the 100 tonne endplug relative to its rear support is about one millimeter or less.

We have also calculated the axial stiffness of the endplug under the combined loadings of: 1) support flange stud preload, and 2) simulated magnetic forces. First we point out that the endplug's axial stiffness depends on the direction of the applied axial load. The endplug is much stiffer for outwardly applied axial loads, than for inwardly applied loads as considered here. Table 7.1 provides a list of the various compliance contributors in the HAC1 and HAC2 sections from FEA calculations, along with hand calculated estimates of region stiffness and the overall axial stiffness of the endplug relative to its support at the back of the endcap.

TABLE 7.1 Current Axial Stiffness of the Endplug. The listed stiffnesses assume a distributed axial pressure of -90 psi applied to the front HAC1 plate of the MCR models.

Component or region	Deflection, δz (mm)	Stiffness, kz[1] (tonne/mm)
Support and adaptor flanges[2]	0.0510	5908.22
Rear strongback (84 mm thick)[2]	0.2942	1023.64
Single HAC2 plate (42 mm thick) and tie rods[2,3]	0.0028	108787.11
HAC2 Section (tie rods and 21 plates)[4]	0.0581	5180.34
HAC2 Total (with flange and strongback)[4]	0.4034	746.71
Single HAC1 plate (18 mm thick) and tie rods[2,3]	0.0391	7694.87
HAC1 Section (tie rods and 38 plates)[4]	1.4874	202.50
HAC1 Total (ref)	1.4874	202.50
Estimated Endplug Axial Stiffness[4]	1.8907	159.30

[1] based on Fz = 301.188 tonnes (90 psi on area of HAC1 front plate in MCR model).
[2] ANSYS calculations using MCR model by C. Corradi (LBL), 12/19-21/92.
[3] calculation procedure revised after Mark Rodamaker review of 12/29/92. See *Note* below.
[4] hand calculation.

Note: The forgoing calculations for a single HAC1 or HAC2 plate *are approximations* which will be replaced by more exact calculations later (see Section 7.5). They are based upon use of the maximum absolute value of the difference between global SMN deflections of any two adjacent absorber plates as read from individual plate UY contour plots in the MCR model output routines. When the maximum absolute value of the difference between global *mean* deflection values [SMEAN = (SMX + SMN)/2] of any two adjacent plates is used, the estimated endplug axial stiffness is 149.07 tonne/mm (about 6.8 % lower, primarily due to an increase in the single HAC2 plate deflection). These single plate calculation procedures were used because only a few plates are explicitly modeled in each HAC section. We believe the final result is conservative because the extrapolations in each section used larger than average diameter plates. Due to mistakes (by the first author) in Table 7.1 results in a previous draft, it appeared that the endplug's stiffness was marginal. We apologize for the confusion. The Y-direction in the MCR models corresponds to the Z-direction in SDC coordinates.

If the endcap's compliance is small (as we expect), the 149 tonne/mm endplug stiffness obviously meets SDC solenoid requirements (Ref. 2.1), even though MCR has made no attempt to minimize plate deflection by optimizing the radial location of tie rods. Axial compliance of the endplug is dominated by absorber plate bending in the HAC1 section, which has the largest number of thin plates connected in "series", as expected.

Based upon this analysis, the endplug provides more than adequate axial stiffness for safe charging and operation of the solenoid. Although we can perceive at least three low cost means to further stiffen the endplug which have no physics impact, there appears to be no need to change the design.

LBL engineers (Ref. 7.6) have recently performed initial FEA optimizations of the radial tie rod locations at the front HAC1 plate (characterized in its simplest possible form) for simulated magnetic loading (-90 psi) only, using two rotation boundary condition extremes at the slot-welded outer edge. We used the RASNA FEA code (Ref. 7.7) for this preliminary work. Our version of the potentially powerful, developing (but currently, linear elastic) RASNA code has too limited a set of design optimization objective function alternatives to make decisive rod location selections. Nevertheless, we are able to conclude that the two boundary condition extremes have only a minor influence on plate stress optimized radial tie rod locations. The results of this LBL work will be shared with MCR for inclusion in their final report.

7.5 Future Structural Design and FEA Effort

Future endplug efforts will include improved stiffness calculations. The most direct way to do this (avoids extrapolations from single plate behavior) is with explicit characterizations of *all plates* in a new FEA system model of the endplug--a large model. These new calculations will include new magnetic force results as they become available from FNAL. We will also address design parameter refinements that would reduce endplug fabrication costs and/or insure reliability:

a) Find better tie rod radial locations which would reduce the peak load and/or load variations within given regions (front of HAC1, HAC1/HAC2 interface, and back of HAC2) allowing potentially smaller rod diameters to reduce fabrication costs.

b) Provide more detailed local slot-weld characterizations to verify that governing stress conditions do not simply shift from the tie rod welds to these absorber plate slot-welds.

c) The existing MCR model of the endplug support "lumps" the endplug support flange and adaptor ring as a stepped monolithic flange. This flange also does not include the large clearance holes (for the endcap adaptor ring bolts) or the deep radial slots for the clear fiber conduit seals (see Figure 6.1 and 20M6143). New FEA characterizations will be created.

d) FEA modeling of major installation/removal fixtures. The endplug installation and removal fixture has been conceptualized (see Section 8). Although the general behavior of this structure can be determined by "traditional means" (Ref. 7.8), finite element analyses methods will be applied to the initially adopted configuration to obtain precise detailed stress, stiffness and deflection characteristics for formal documentation. Much of this FEA work can be accomplished with existing linear elastic codes.

8. INSTALLATION AND REMOVAL

A conceptual description of endplug's final assembly, testing, and installation (and removal) operations to be conducted at SSCL site are outlined in detail in Reference 8.1. These operations require the use of 3 major fixtures:

1) a two piece, endplug pick-up and turnover fixture (TOF),
2) an endplug load transfer cradle (Cradle),
3) an endplug installation and removal fixture (PIF).

8.1 SSCL Surface Assembly Building Operations

The following paragraphs describe transportation, off-loading, and installation of the endplug(s) into the endcap(s), including the major load transfer operations.

We anticipate that the 100 tonne endplug will be truck transported from LBL to the SSCL above ground assembly building and off-loaded using a locally rented, two hook mobile truck crane (e.g. Bigge). The endplug is lifted and rotated 90 degrees using the TOF, and placed onto the Cradle, which is equipped with both Hilman rollers and hydraulic jacks. Later the endplug is attached to the PIF near the endcap for final assembly/test operations. After this attachment, the Cradle is jacked down (transferring the endplug's gravity load to the PIF), and the Cradle is removed. These load transfer steps can be easily visualized using the fixtures shown pictorially in Figure 8.1.

An approximate layout of the respective positions of endcap and endplug during final assembly is shown in Figure 8.2. Figure 8.3 shows a near final step in the installation of the endplug into the endcap in the surface assembly building. Although the EC/EM is shown in

place here, under currently perceived installation plans it would be installed later, allowing a direct view of the front of the endplug and its clearance from the endcap as it is installed.

After aligning and inserting the endplug into the endcap using suitable guide rails under the PIF's rollers, the support stud connections at the endplug's rear support flange are made-up and suitably torqued. The endcap and endplug and the PIF are then jacked up slightly using the endcap's hydraulic jacks (transferring the gravity load of the endplug and the PIF to the endcap), and the studs at the endplug/PIF joint are loosened. The endcap is then jacked down until the PIF's rollers are back on the floor rails (removing the PIF's gravity load from the endplug), and the PIF is removed. After subsequent endcap and endplug final assembly and testing activities, the endcap is ready to move to the below ground Hall.

8.2 Hall Operations

After the Forward Muon System (FMS) has been suitably withdrawn, removal of the endplug from the endcap (for radiation damaged tile and fiber replacement) is accomplished in the below ground Hall using the PIF and the procedures in the forgoing paragraph in reverse. Because the height of the endcap above the Hall floor is now greater than it was in the above ground assembly building (by roughly the height of the picnic tables), we modify the PIF with a box-shaped, vertical extension which we call a "Picnic Box" (see Figure 8.4) and suitable shims between the PIF's rollers and their mounting plates.

We will not attempt to describe these Hall operations in greater detail, because of ongoing design activities at FNAL and elsewhere associated with the calorimeter support structure (and provisions for moving it on the above ground roadway).

It should be noted that the Forward Muon System and the endcap calorimeter must also be withdrawn periodically to replace radiation damaged Tracker components and to refurbish tiles and fibers in the EC/EM calorimeter (see Figure 1.1).

8.3 Future Fixture Design Work

It is known that the cost of these installation and removal fixtures represent a significant fraction of the "cost delta" which could make the removable endplug option uncompetitive. We are looking at possible changes to the PIF which will allow elimination of the Cradle without compromising SSCL riggers' ability to perform the 100 tonne off-loading operations under safe, controlled conditions (see Figure 8.1).

Elimination of the Turn Over Fixture-to-Cradle transfer has the following additional benefit. We could ship the endplug to SSCL with tiles and fibers installed, without having to deal with potential problems of damage to fibers or the thin, light tight cover at the $\eta = 2$ boundary. We will make the Cradle elimination a high priority item.

9. COST AND SCHEDULE

This section provides the results of cost estimating activities and a schedule for endplug construction. Besides SDC estimates which include the cost of material, labor, EDIA and contingency, we also present recent vendor quotations for the cost of material and fabrication labor to construct the endplug absorber structure and its operational support flanges.

The SDC's cost estimating and scheduling procedures, which follow a formal Work Breakdown Structure basis, are described elsewhere (Ref. 9.1). The endplug hadronic calorimeter has been given the WBS designation: 2.2.10.

9.1 SDC Cost Estimate

Table 9.1 provides details of the SDC Calorimeter Group's estimate of the endplug's cost (Ref. 9.2) down to WBS level 4. Much greater detail (to level 7) can be found in the referenced document. In this table we also list the cost of Plug Components, WBS 2.2.10.1, and the Endplug/Endcap Joint, WBS 2.2.10.3, to level 5, so that comparisons with vendor quotations on the absorber structure and support flanges can be made.

TABLE 9.1 SDC Cost Estimate for the Endplug, WBS 2.2.10

WBS	Description	Materials & Manuf. Labor (K $)	EDIA (K $)	Contingency (K $)	Total (K $)
2.2.10	Endplug Calorimeter	4561	2963	2533	10056
2.2.10.1	Plug Components	2869	1067	1465	5400
2.2.10.1.1	Plug Abs. Structure	1579	380	757	2717
2.2.10.1.2	Scintillator Assemblies	961	428	505	1894
2.2.10.1.3	PMT Assemblies	152	102	54	309
2.2.10.1.4	Endplug Skin	39	33	36	108
2.2.10.1.5	Tile Calibration Sys.	110	62	69	240
2.2.10.1.6	Cable Brackets	13	31	22	66
2.2.10.1.7	Elec. Crate Brac'kts	13	31	22	66
2.2.10.2	Endplug Assembly	584	311	280	1175
2.2.10.3	Endplug/Endcap Joint	144	106	80	331
2.2.10.3.1	Endcap Flange	57	35	30	122
2.2.10.3.2	Endcap Flange Studs	15	18	10	43
2.2.10.3.3	Endplug Flange	57	35	30	122
2.2.10.3.4	Endplug Flange Hdwr	15	18	10	43
2.2.10.4	Equip., Tool., Fixtures	373	226	257	856
2.2.10.5	Endplug Assy Facility	167	113	90	369
2.2.10.6	Surface Assy at TOH	59	45	39	143
2.2.10.7	Program Management	141	936	172	1249
2.2.10.8	Endplug Prototype Mod	223	160	149	532

It can be noted from Table 9.1 that the absorber structure is one of the major endplug cost drivers. The SDC's estimated cost of material and manufacturing labor for the endplug absorber structure ($ 1579 K) was obtained by *scaling* (using cost per unit volume) from earlier quotations obtained by FNAL for 64 each, wedge-shaped hadronic barrel modules. These modules consist of stacked layers of milled and drilled, rectangular steel plates of similar thicknesses. The plates are plug-welded together, and two module sides are finish machined to final dimensions. The barrel quotation "scaling factor" used did not include the cost to machine source tube grooves in the barrel modules, so the scaled endplug values (Table 9.1) also do not.

9.2 Vendor Quotations

Because other construction features of the monolithic endplug are also dissimilar from barrel modules, we recently asked several large, U.S. industrial fabricators (including those who quoted to FNAL) to respond to a Request for Quotation (Ref. 9.3) by providing the cost of labor and materials to fabricate the two approximately 100 tonne endplug absorber structures (*including* source groove machining) and their support and adaptor flanges--items previously described in Section 4. Table 9.2 lists the rough, order-of-magnitude quotations (the RFQ was not expected to result in a purchase) from the five vendors who responded.

TABLE 9.2 Vendor Cost Estimates for the Endplug Absorber Structure (WBS 2.2.10.1.1), Endcap Flange (WBS 2.2.10.3.1) and Endplug Flange (WBS 2.2.10.3.3). These costs are for fabrication labor and material only--no EDIA or Contingency is included.

VENDOR	LOCATION	QUOTATION (K $)
A	Minnesota	1903.0
B	So. California	1937.4
C	So. California	
	Option 1--no abs. grinding	2806.6
	Option 2--with abs. grinding	2977.5
D	Wisconsin	5081.0
E	No. California	1905.0

Because of the two tight clusters of vendor quotes (A, B and E) and (A, B, C and E), one could conclude that, in competitive circumstances, the probable actual cost of the endplug absorber structure and its support flanges would be between about $ 1915 K and $ 2138 K (average of A, B, C-option 1, and E with D ignored), or about 13 - 26 % above the current SDC estimates for these items.

9.3 Schedule

Figure 9.1 shows some of the major milestones in the design, fabrication and installation phases of the endcap WBS 2.2, which includes the endplug. We feel the existing endplug design is on schedule.

10. SUMMARY

We have presented here the justification and design for the endplug hadron calorimeter. The radiation doses in this limited region are two orders of magnitude higher than in most of the remainder of the endcap. We find the inclusion of a removable endplug consistent with the original intent of the collaboration in selecting a tile/fiber calorimeter, as it was realized that the volume of scintillator subject to damage is small and in a well defined region. The boundaries of the endplug seem well tuned to :

- include the damaged parts of the detector and
- minimize disruption to the rest of the experiment..

Sources of radiation not included in the current dose estimates are 1) a small increased particle flux due to magnetic focusing of the solenoid, 2) beam-pipe interactions or secondary interactions from particles from minimum bias events interacting with the beam pipe or other structures, and 3) damage due to neutrons boiled off the forward calorimeter. These all increase the radiation damage to the endplug, particularly along the $\eta = 3$ boundary. It seems prudent to design the detector so that this relatively small part of the calorimeter can be replaced with minimum disruption to the experiment, thus avoiding :

- Possible mechanical damage to the other 93% of the scintillator, fibers or PMTs not needing replacement.
- Collateral damage to other detectors and utilities as the endcap is dismantled.
- Significant extra schedule delays due to removing 10 times the volume of the actual damaged scintillator, as well as disassembly and reinstallation of other detector systems in the disassembly path.
- Cost increments for the extra labor involved in removing the undamaged scintillator, calorimeter components and components of other systems.

Given the possible damage to the calorimeter or other parts of the detector we see good reason why the endplug was included in the overall design for the SDC.

The mechanical design of the endplug is well understood. There are first cut drawings of critical pieces supported by engineering calculations and finite element simulations of the absorber structure, including both gravitational and electromagnetic loads. The system for holding the tiles, fibers and source tubes inside the absorber structure is well defined, and an innovative technique for making the source carrier wire has been demonstrated. Overall, the selection of load paths, section sizes, weld locations and fabrication techniques appear

consistent with the needs of the experiment, and satisfy mechanical constraints and requirements, environmental issues and SDC cost expectations.

In a previous draft we raised an issue in Section 7.4 regarding axial stiffness of the endplug in the magnetic field. This issue has been resolved. The endplug appears to be at least a factor of 10 stiffer than that required by the solenoid.

We have described conceptual procedures for the installation of the plug into the rest of the endcap, including the functionality of the installation fixturing. There remains significant design work on these fixtures and on the nature of the endplug interface to its neighbors, including the endcap hadron calorimeter and the innermost muon chambers (FW1).

Less certain is the detailed optical design, including final choices of scintillator, tile and fiber and the exact fiber routing path in the tile or its eventual course to the PMT. These decisions await results from the current round of radiation damage tests. We have suggested locations for fiber disconnects and photomultiplier tubes. These tentative plans require further refinement in coordination with the rest of the endcap calorimeter.

To conclude, we propose this endplug hadron calorimeter design as a well reasoned, *low risk approach* to the inevitable problem of radiation damage to the scintillator tiles and fibers at large η values in the SDC calorimeter.

11. REFERENCES

1.1 Dan Green, "Radiation Damage in the SDC Hadronic Endcap Calorimeter", Fermilab, 11/25/92.
2. References for Physics Parameter Requirements
2.1 magnetic stiffness--TDR, Table 5-8, SDC-92-201, April 1, 1992.
3. References for Endplug Configuration Overview
4.1 Plasma Arc Cutting of Source Tube Grooves, SDC-92-372.
4.2 V. Barnes, source position sensitivity studies, presented at the 12/10/92 SDC Calibration Workshop at SSCL.
4.3 Absorber Plate Flattening Forces, SDC-92-325.
4.4 M. Hoff, "Scintillator Fabrication of the 4x4 Calorimeter Test Station Module", LBL-SD-020209, (1992).
4.5 multi-fiber--poor light uniformity--??'s presentation at SSCL, 12/11/92.
4.6 J. Freeman, tile assembly thickness, presented at SDC meeting 12/11/92 at SSCL.
4.7 pizza pan & source tube details, SDC-92-326.
4.8 fiber routing & PMT mounting, SDC-92-324.
4.9 light budget--TDR, p. 6-14, SDC-92-201, April 1, 1992.
4.10 P. Barbaro, private communication with R. Kadel.
4.11 CDF upgrade source (V. Barnes).
4.12 Friction brake band example.
4.13 flexible composite source wire (pope to do).
4.14 hydraulic source positioning.
4.15 Poiseulle #1
4.16 Poiseulle #2
4.17 source selection(Cris?).
4.18 MP35N is a registered trademark of SPS Technologies, Inc.
4.19 Elgiloy Co., A Katy Inds, Inc. Subs., Elgin, IL.
5. References for Assy Operations at LBL.
6.1 endplug-to-FMS interface (pvt comm--Bintinger, Thurston, Piles, 10/27/92 at SSCL).
7.1 magnetic forces based on 2-D FEA model,--Wand's E-Mail 1/29/92.
7.2 FEA Model Requirements, SDC-92-327.
7.3 ANSYS ref
7.4 MCR FEA, Report #2, SDC-92-330.
7.5 LBL PO#3512000.
7.6 Don Le calculations 11/92.
7.7 RASNA ref
7.8 hand calculations using Roark and Young on TK Solver Plus
8.1 SSCL surf assy operations, SDC-92-323.
9.1 SDT-00009.
9.2 SDT-000021, Project Cost/Schedule Summary Book, Oct. 25, 1992.
9.3 RFQ for Steel Endplug Fabrication, SDC-92-331.
10. References for Summary.

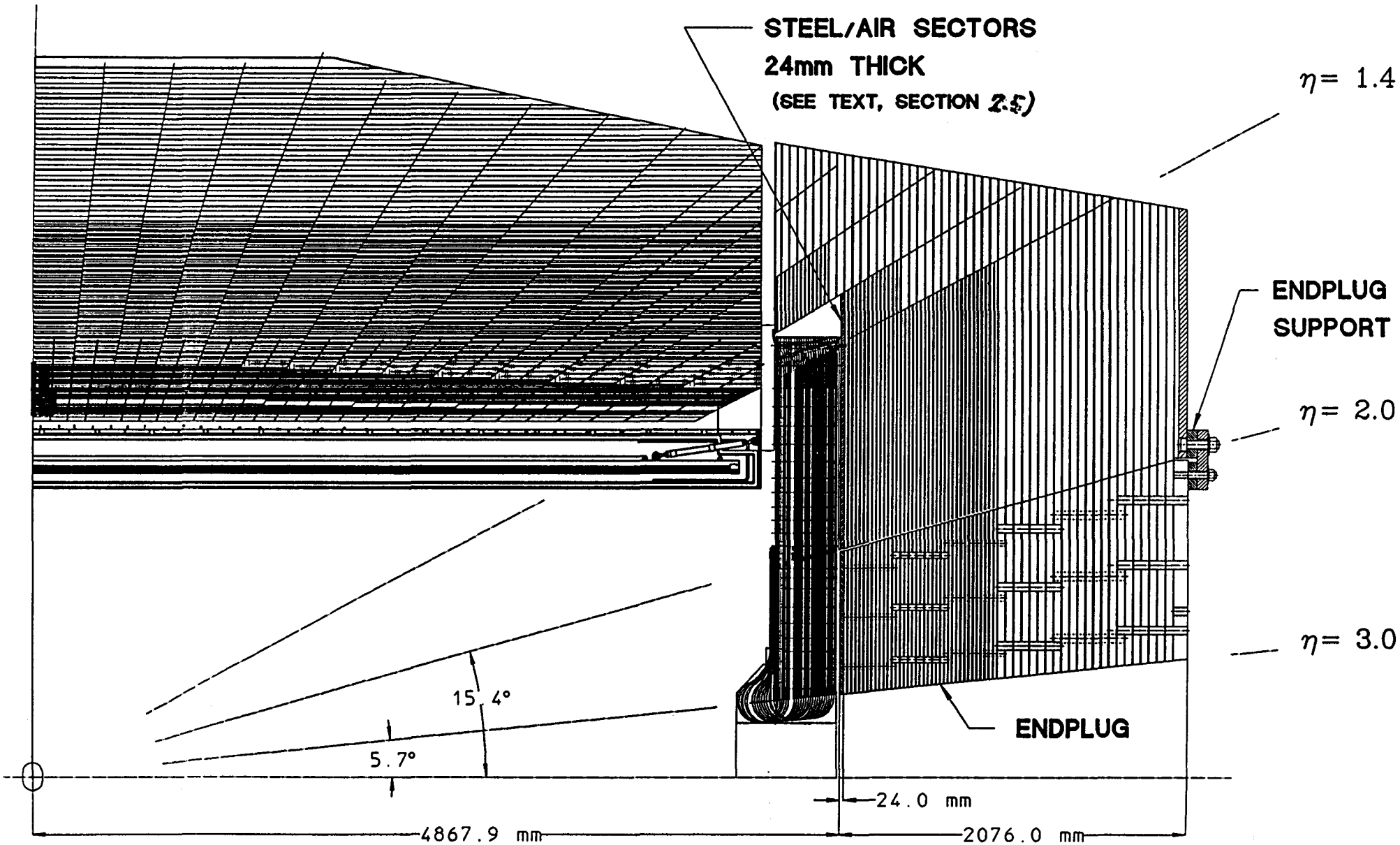

FIG. 1.1 CROSS-SECTION OF THE SDC CALORIMETER

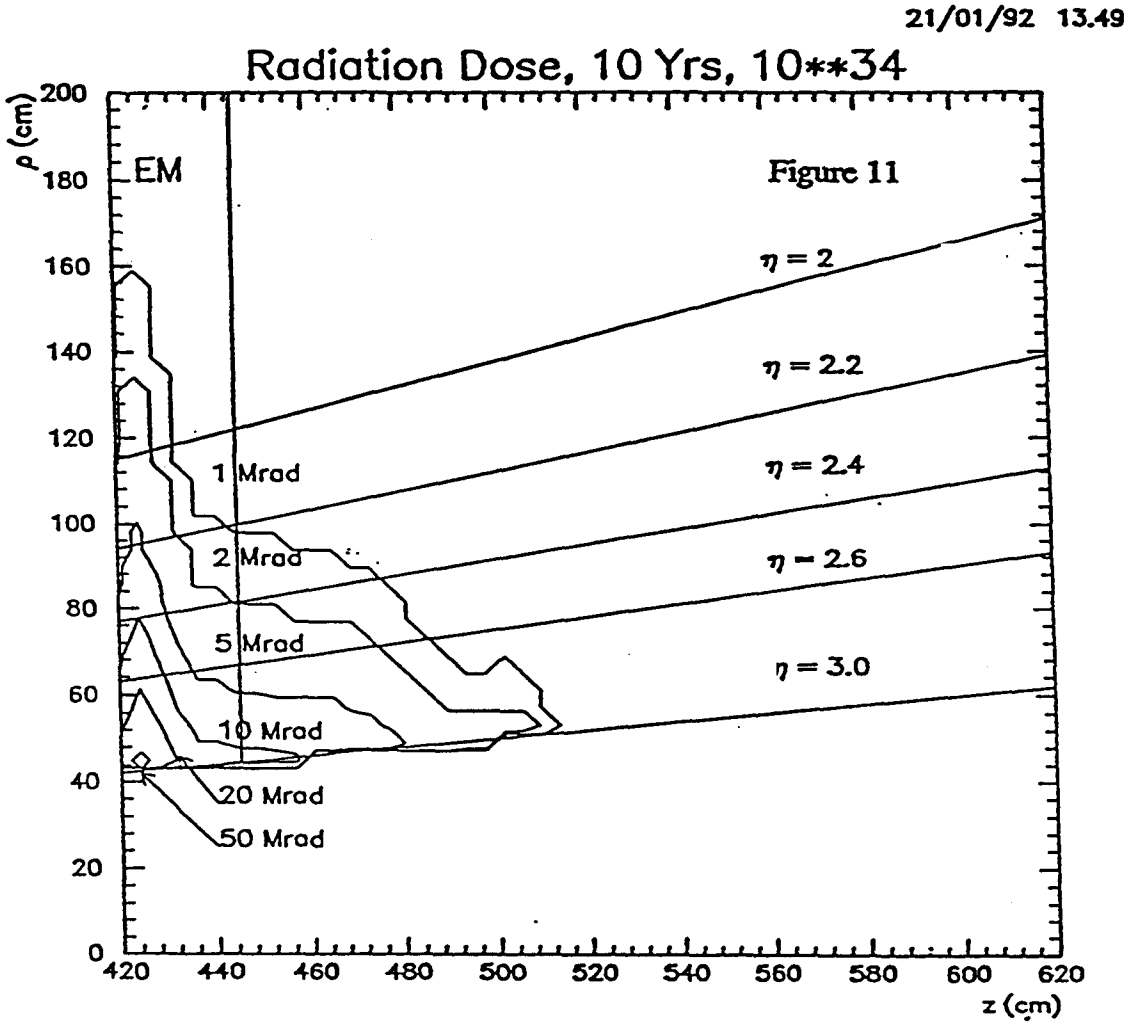
21/01/92 13.49
Radiation Dose, 10 Yrs, 10**34
ρ (cm)
EM
Figure 11
η = 2
η = 2.2
η = 2.4
η = 2.6
η = 3.0
1 Mrad
2 Mrad
5 Mrad
10 Mrad
20 Mrad
50 Mrad
z (cm)

FIG. 1.2

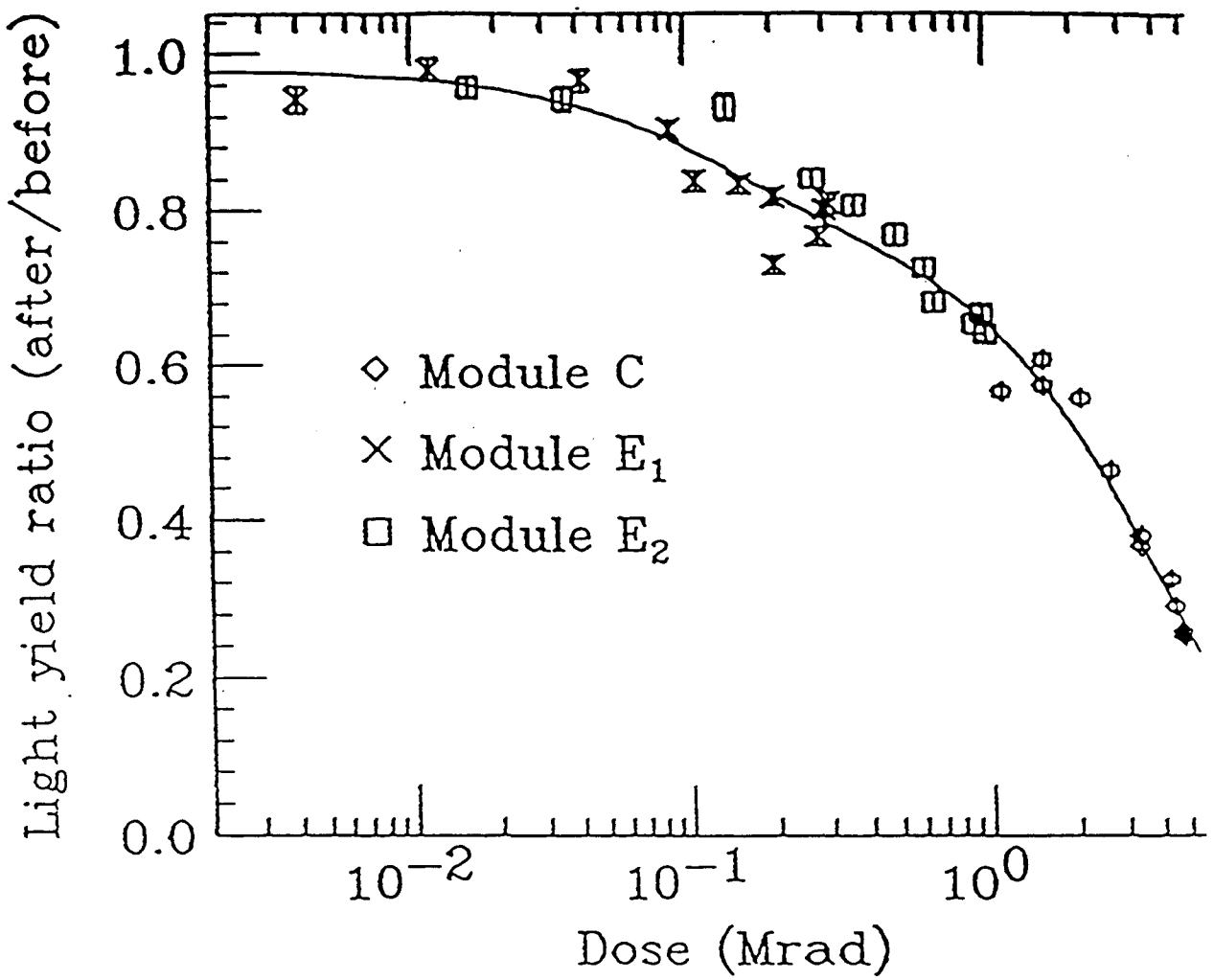

FIG. 1.3 . Light yield ratio for KEK tile/fiber assemblies as a function of dose. The KEK modules C, E_1, and E_2 are dismantled after irradiation with a 2.5 GeV electron beam and radiation damage of individual tile/fiber assemblies is measured by a ^{106}Ru source scan.

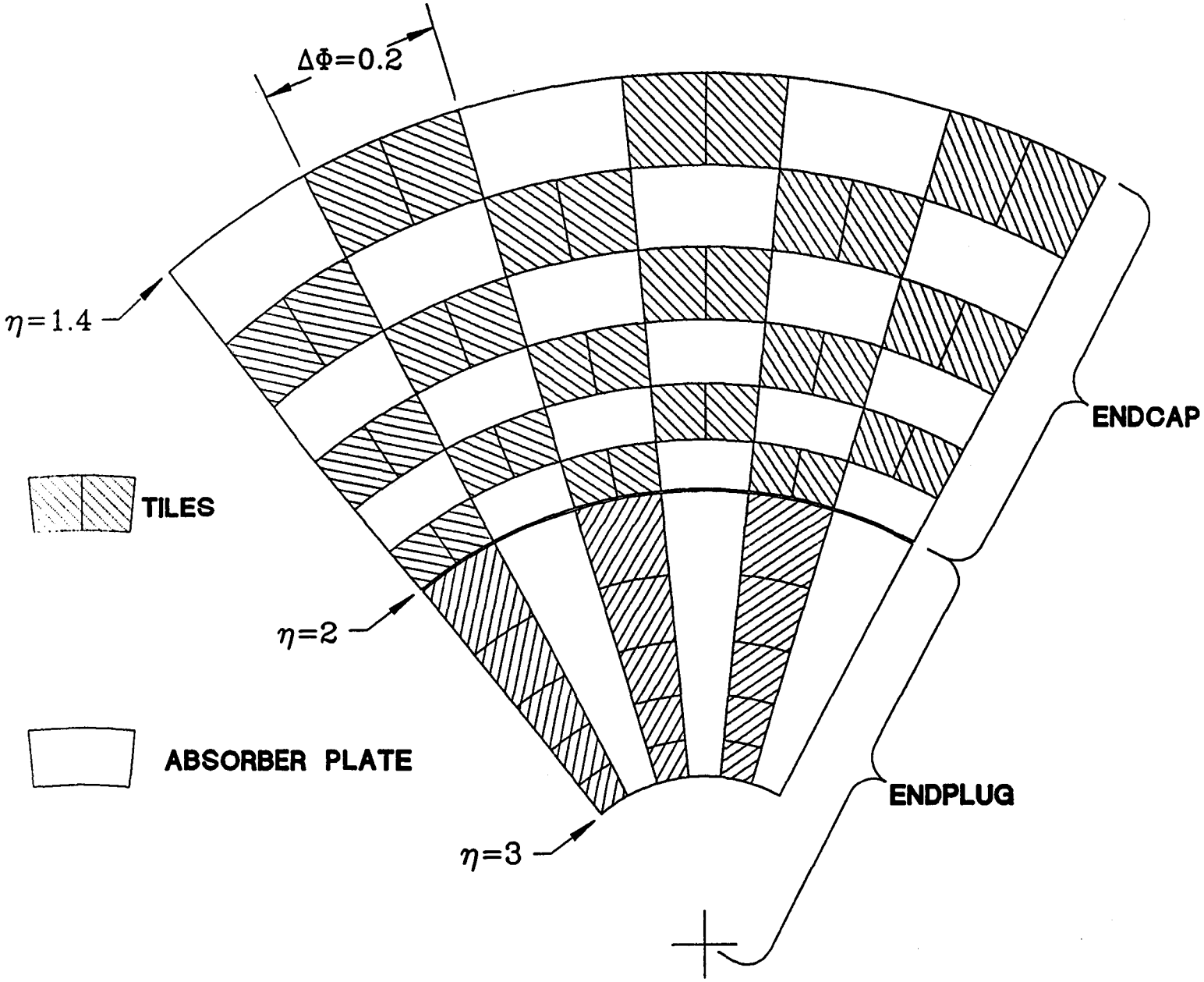

FIG. 2.1 a

CROSS SECTION THROUGH ONE LAYER OF THE ENDCAP AND ENDPLUG ILLUSTRATING ALTERNATING WEDGES OF SCINTILLATOR AND ABSORBER PLATES. THE BASELINE (ANL) WEDGE MODULE ENDCAP OPTION IS SHOWN.

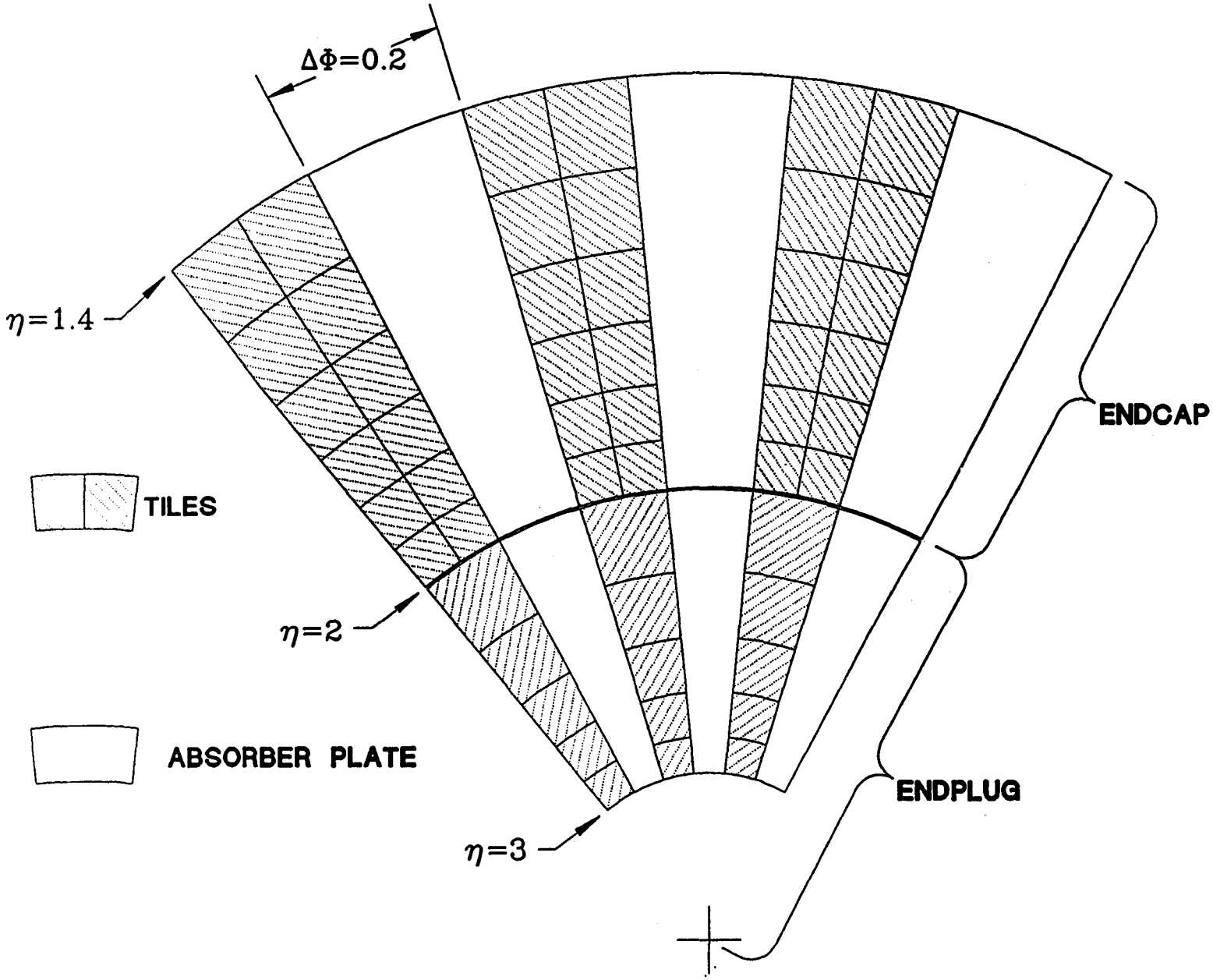

FIG. 2.1 b

CROSS SECTION THROUGH ONE LAYER OF THE ENDCAP AND ENDPLUG ILLUSTRATING ALTERNATING WEDGES OF SCINTILLATOR AND ABSORBER PLATES. A RADIALLY WITHDRAWABLE PIZZA PAN (OR MEGATILE) ENDCAP OPTION IS SHOWN.

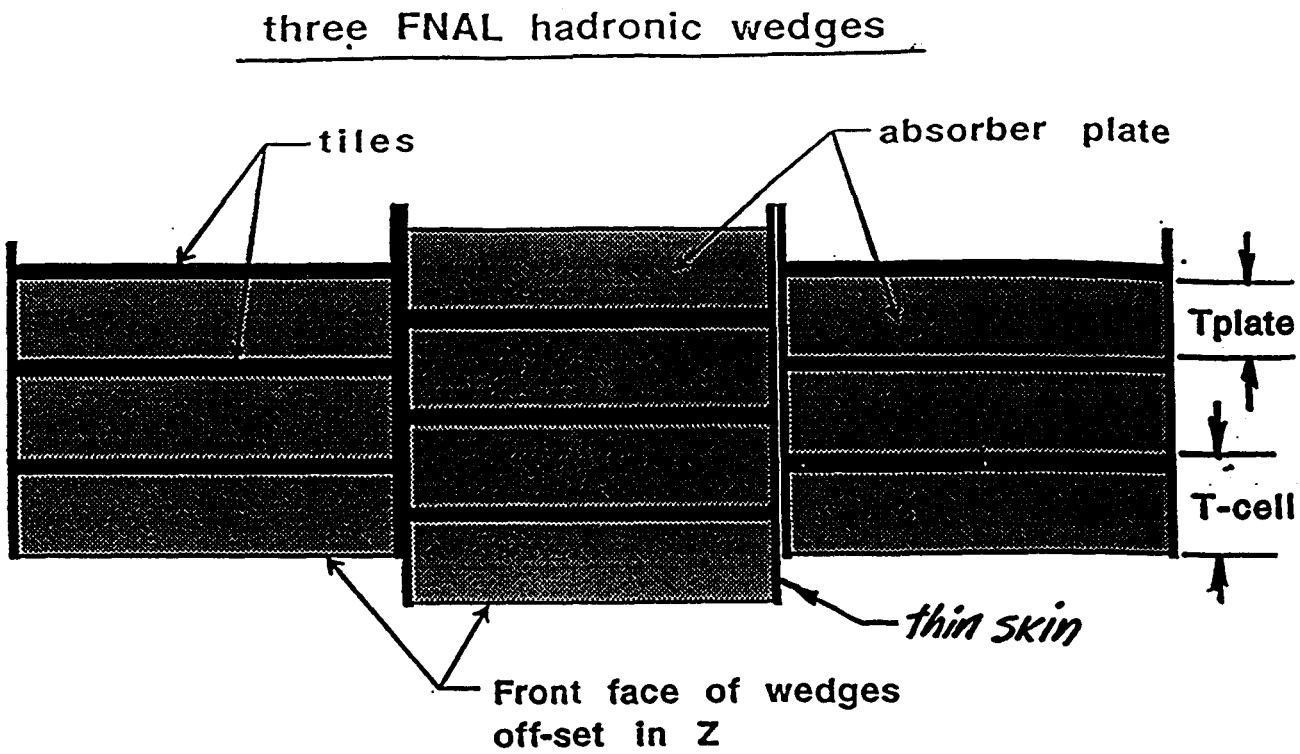

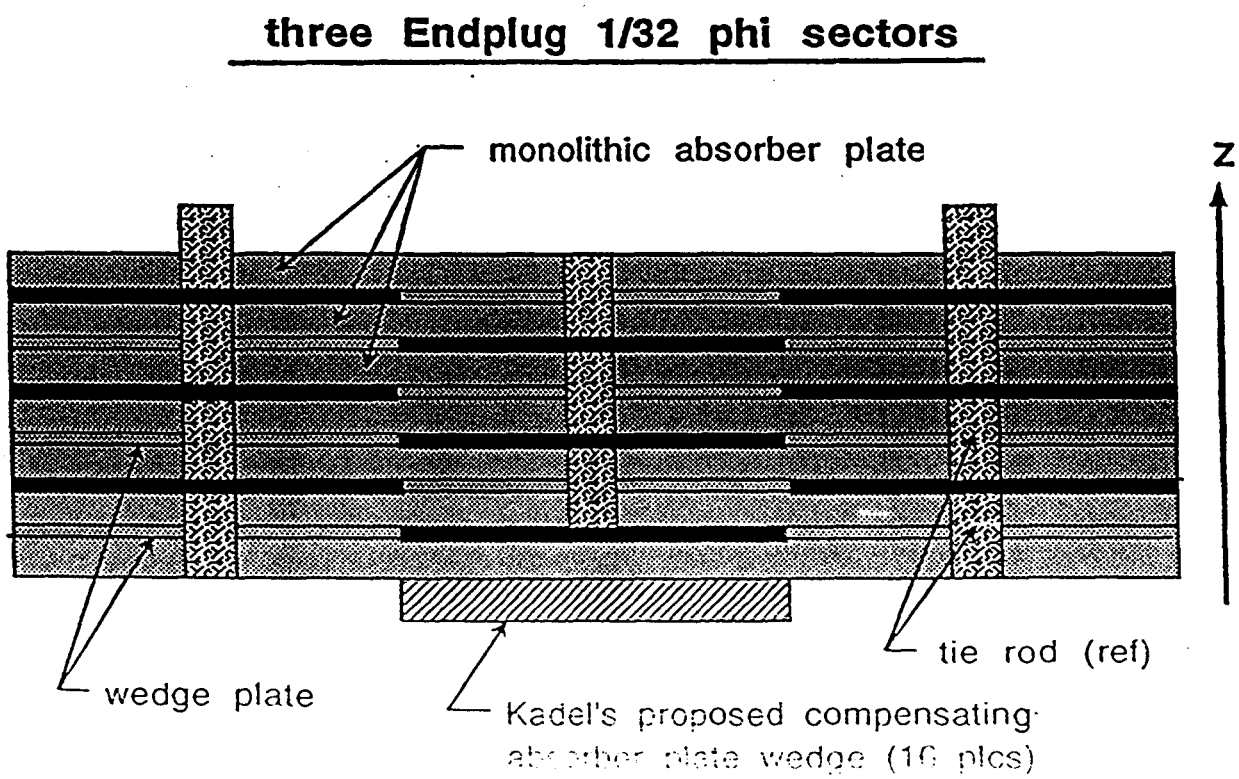

Figure 2.2 Compatibility of the Endplug with the new FNAL hadronic wedge design (the Endplug's plate thicknesses could change to suit FNAL)

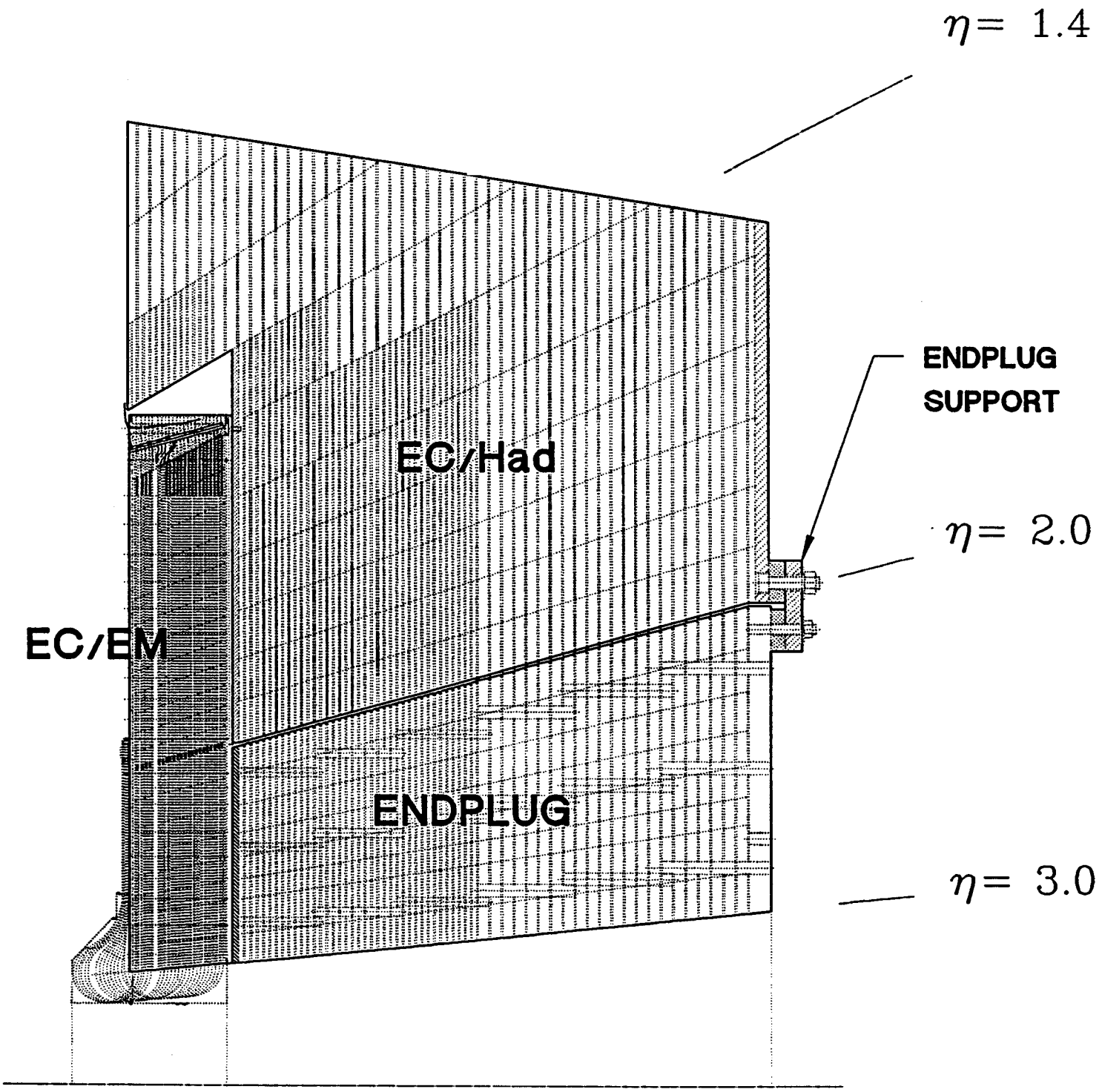

FIG. 3.1

CROSS–SECTION OF THE ENDCAP CALORIMETER

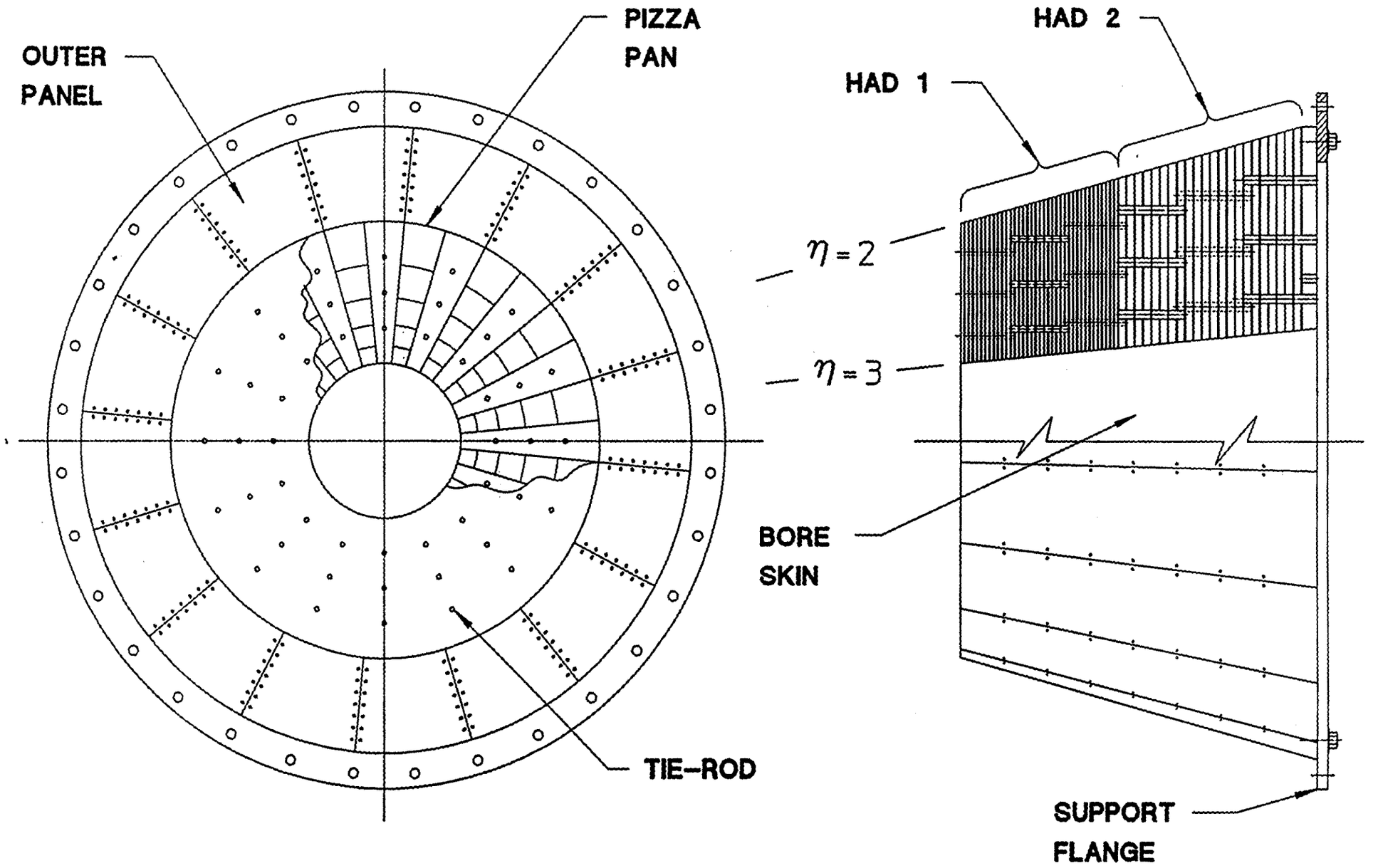

FIG. 3.2 CROSS-SECTION OF THE MONOLITHIC ENDPLUG

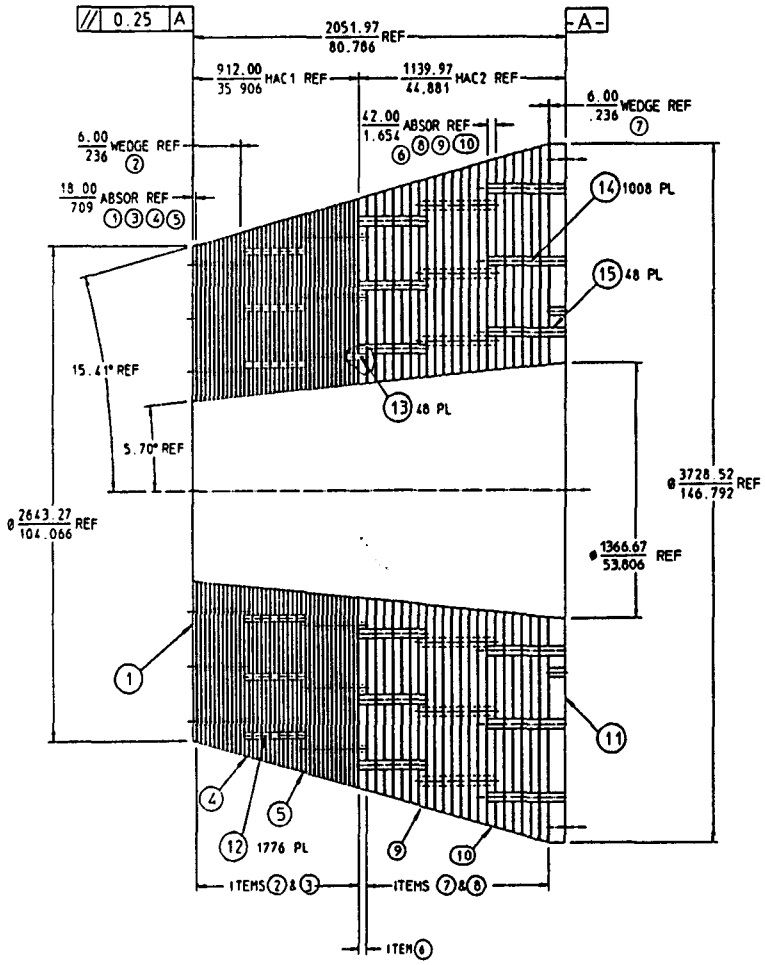

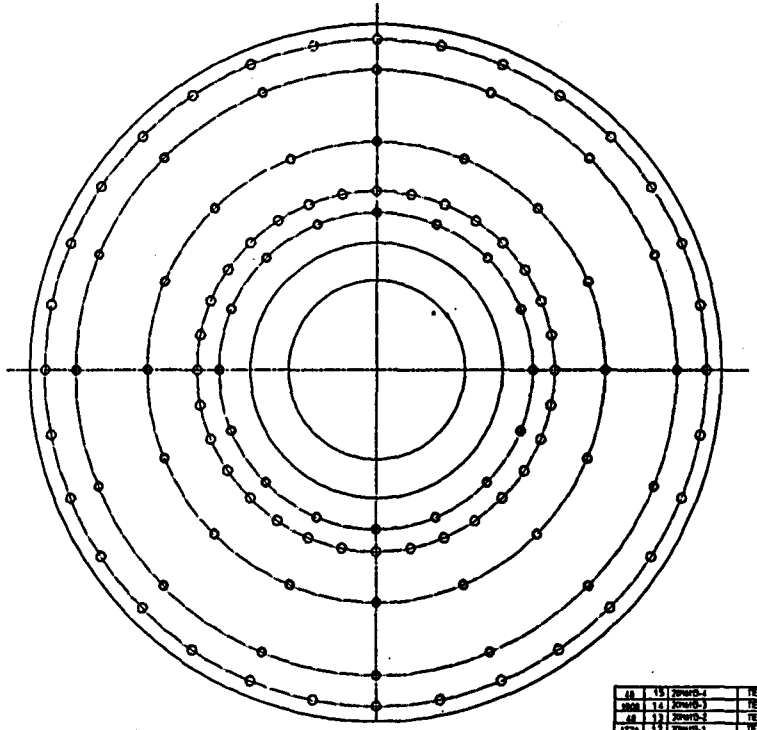

20M6006A

REQD	ITEM	PART NO.	DESCRIPTION
48	15	20M4B-1	TIE ROD - HAC3/STRONGBACK JUNCTION
1008	14	20M4B-1	TIE ROD - HAC2
48	13	20M4B-1	TIE ROD - HAC1/HAC2 JUNCTION
1776	12	20M4B-1	TIE ROD - HAC1
1	11	20M4B4	ABSORBER STRONGBACK PLATE
1	10	20M4B4-1	TRANSITION ABSORBER PLATE - HAC2
1	9	20M4B4-1	TRANSITION ABSORBER PLATE - HAC2
19	8	20M4B4-1thru9	GENERIC ABSORBER PLATE - HAC2
352	7	20M4B4-1thru52	GENERIC WEDGE PLATE - HAC3
1	6	20M4B4	TRANSITION ABSORBER PLATE - HAC1/HAC2
1	5	20M4B4-1	TRANSITION ABSORBER PLATE - HAC1
1	4	20M4B4-1	TRANSITION ABSORBER PLATE - HAC1
35	3	20M4B4-1thru35	GENERIC ABSORBER PLATE - HAC1
408	2	20M4B4-1thru35	GENERIC WEDGE PLATE - HAC1
1	1	20M4B4	ABSORBER PLATE, REF. - HAC1

REV	DIG	CHK	TOOL	DATE	CHANGES
A					GENERAL REVISION

UNLESS OTHERWISE SPECIFIED — SHOP ORDERS — REV. — DATE — DRAWN — DATE — MATERIAL — FINISH — DIMENSIONS ARE IN INCHES — DO NOT SCALE — DO NOT ADD OR DELETE — DO NOT DEVIATE FROM THIS DRAWING WITHOUT AUTHORITY — DIMENSIONS MARKED "REF" ARE FOR INFORMATION ONLY — DEFINITIONS: ANSI Y14.5M-1982 — DRAWN BY: H. HIRAHARA — DATE: 5-21-92

LAWRENCE BERKELEY LABORATORY
UNIVERSITY OF CALIFORNIA - BERKELEY

SSC

SDC 2.0 PLUG
PLUG ASSEMBLY

ASSEMBLY — 4213-01 — SCALE 1:10 — SIZE D — 20M6006 — REV A

42

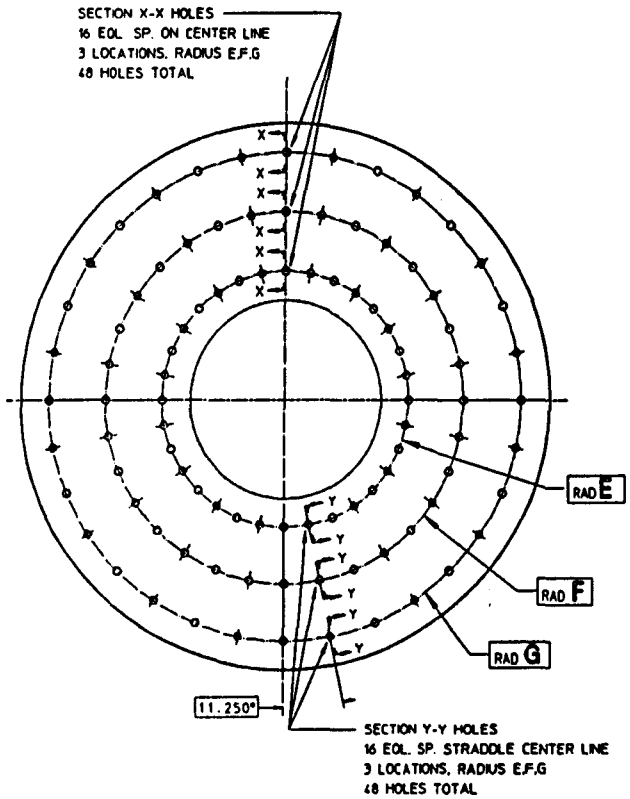

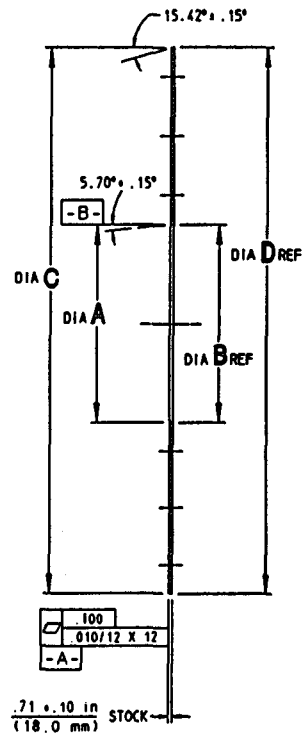

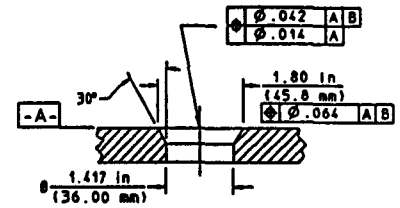

SECTION X-X
SCALE 1:1

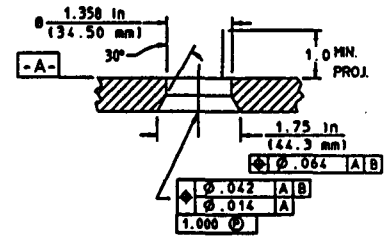

SECTION Y-Y
SCALE 1:1

VERSION NO. / ARBOR WAC	A (Ref.)	B (Ref.)	C (Ref.)	D (Ref.)	E Radius	F Radius	G Radius	WT. (LBS)
					(HOLE RADII FOR THE RODS)			
VER-1	37.985	38.009	104.890	104.979	38.149	38.589	47.988	1505.785
VER-2	38.053	38.195	105.109	105.890	38.149	38.588	47.988	1523.629
VER-3	38.248	38.384	105.630	106.021	38.149	38.588	47.988	1538.549
VER-4	38.431	38.572	106.181	106.542	38.149	38.588	47.988	1554.142
VER-5	38.619	38.761	106.673	107.064	38.149	38.588	47.988	1568.410
VER-6	38.808	38.950	107.194	107.585	38.149	38.588	47.988	1584.753
VER-7	38.997	39.138	107.715	108.106	38.149	38.588	47.988	1600.176
VER-8	39.185	39.327	108.236	108.627	38.149	38.588	47.988	1615.692
VER-9	39.376	39.515	108.757	109.148	38.149	38.588	47.988	1631.323
VER-10	39.563	39.704	109.278	109.669	38.149	38.588	47.988	1646.871
VER-11	39.751	39.893	109.799	110.190	38.149	38.588	47.988	1662.587
VER-12	40.129	40.270	110.841	111.232	38.624	38.788	48.988	1694.243
VER-13	40.317	40.458	111.363	111.754	38.674	38.788	50.988	1710.192
VER-14	40.506	40.647	111.884	112.275	38.674	38.788	50.988	1726.197
VER-15	40.695	40.836	112.405	112.796	38.674	38.788	50.988	1742.288
VER-16	40.883	41.025	112.926	113.317	38.674	38.788	50.988	1758.486
VER-17	41.072	41.213	113.447	113.838	38.674	38.788	50.988	1774.688
VER-18	41.261	41.402	113.968	114.359	38.674	38.788	50.988	1791.002
VER-19	41.449	41.591	114.489	114.880	38.674	38.788	50.988	1807.388
VER-20	41.638	41.779	115.010	115.401	38.674	38.788	50.988	1823.852
VER-21	41.827	41.968	115.531	115.922	38.674	38.788	50.988	1840.388
VER-22	42.015	42.157	116.052	116.444	38.674	38.788	50.988	1857.000
VER-23	42.204	42.345	116.574	116.965	38.674	38.788	50.988	1873.688
VER-24	42.581	42.722	117.616	118.007	38.149	41.063	53.007	1907.203
VER-25	42.770	42.911	118.137	118.528	38.199	41.063	53.007	1924.183
VER-26	42.959	43.100	118.658	119.049	38.199	41.063	53.007	1941.178
VER-27	43.147	43.288	119.179	119.570	38.199	41.063	53.007	1958.237
VER-28	43.336	43.477	119.700	120.091	38.199	41.063	53.007	1975.371
VER-29	43.525	43.666	120.221	120.612	38.199	41.063	53.007	1992.588
VER-30	43.713	43.855	120.743	121.134	38.199	41.063	53.007	2009.863
VER-31	43.902	44.043	121.264	121.655	38.199	41.063	53.007	2027.221
VER-32	44.091	44.232	121.785	122.176	38.199	41.063	53.007	2044.654
VER-33	44.279	44.421	122.306	122.697	38.199	41.063	53.007	2062.161
VER-34	44.468	44.609	122.827	123.218	38.199	41.063	53.007	2079.743
VER-35	44.657	44.798	123.348	123.739	38.199	41.063	53.007	2097.399

NOTES 1 ALL DIMENSIONS ARE IN INCHES UNLESS OTHERWISE SPECIFIED.

2 TOLERENCES APPLY TO INCH DIMENSIONS ONLY.

20M6046 B

REV	DR	CH	DW	DATE	
B					CHANGED TO SIZE 6 DIA
A					REVISED HOLE SIZE AND QUANTITY

CHANGES

UNLESS OTHERWISE SPECIFIED
.X ± .1 POL. ±
.XX ± 0.01 ANGLE ±1/2°
.XXX ± 0.010 FINISH 250
REMOVE ALL BURRS
DIMENSIONS ARE IN INCHES UNLESS OTHERWISE SPECIFIED
DIMENSIONS ARE FOR FINISHED PART AFTER ALL PROCESSES
DIMENSIONS ARE FOR FINISHED PART AFTER ALL PROCESSES

REQ'D	PART NO.	DESCRIPTION
		PLATE, LOW CARBON STEEL, SAE 1010

SHOP NOTES
DEGREASE
RINSHIWA

LAWRENCE BERKELEY LABORATORY
UNIVERSITY OF CALIFORNIA-BERKELEY

SSC
G - HACK
ER PLATE
SCALE 1:10
20M6046 B

43

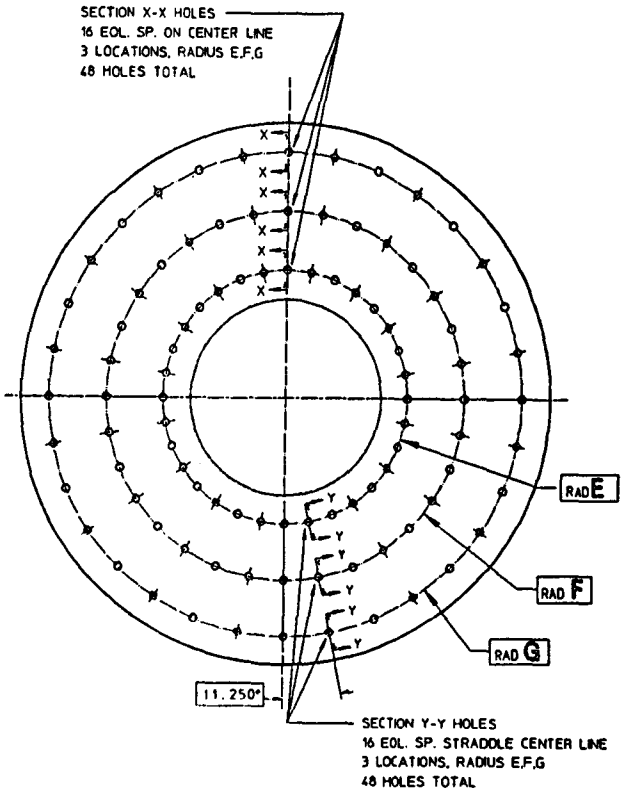

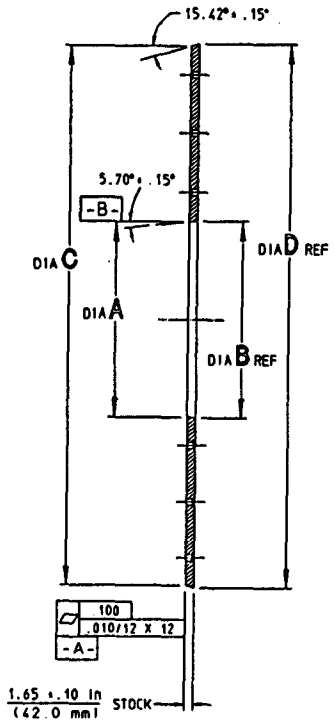

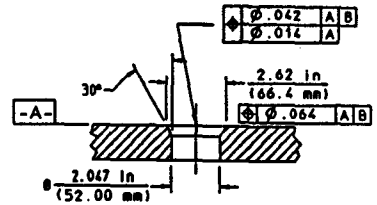

SECTION X-X
SCALE 1:1

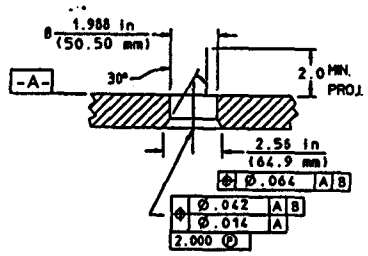

SECTION Y-Y
SCALE 1:1

NOTES: 1. ALL DIMENSIONS ARE IN INCHES UNLESS OTHERWISE SPECIFIED.

2. TOLERENCES APPLY TO INCH DIMENSIONS ONLY

VERSION NO.	A	B	C	D	E	F	G	WT.(LBS)
ABSOR HAC2	±0.010	(Ref.)	±0.010	(Ref.)	Radius	Radius	Radius	
					(HOLE RADII FOR TIE RODS)			
VER-1	45.222	45.553	124.911	125.523	29.868	43.576	57.183	5035.437
VER-2	45.600	45.930	125.953	129.866	29.966	43.576	57.183	5119.507
VER-3	45.977	46.307	126.996	127.908	29.966	43.576	57.183	5204.274
VER-4	46.354	46.685	128.038	128.956	29.968	43.576	57.183	5289.736
VER-5	46.732	47.062	129.080	129.992	29.968	43.576	57.183	5375.895
VER-6	47.109	47.439	130.122	131.634	29.986	43.576	57.183	5462.749
VER-7	47.864	48.194	132.207	133.119	31.677	46.860	68.442	5838.546
VER-8	48.241	48.571	133.249	134.181	31.677	46.060	60.442	5727.488
VER-9	48.618	48.948	134.291	135.283	31.677	46.060	60.442	5817.127
VER-10	48.996	49.328	135.303	136.246	31.677	46.060	60.442	5907.481
VER-11	49.373	49.703	136.378	137.266	31.677	46.060	60.442	5998.492
VER-12	49.750	50.080	137.418	138.330	31.677	46.080	60.442	6090.218
VER-13	50.128	50.458	138.460	139.372	31.677	46.060	60.442	6182.641
VER-14	50.862	51.212	140.545	141.457	33.365	48.544	63.702	6389.574
VER-15	51.260	51.590	141.587	142.499	33.365	48.844	63.702	6484.085
VER-16	51.637	51.967	142.629	143.541	33.365	48.544	63.702	6559.291
VER-17	52.814	52.344	143.671	144.583	33.365	48.544	63.702	6855.194
VER-18	52.392	52.722	144.713	145.626	33.365	48.544	63.702	6751.792
VER-19	52.770	53.100	145.755	146.669	33.365	48.544	63.702	6836.800

20M6086B

REV	DIS	CHK	DATE	CHANGES
B				CHANGED TO SIZE A DWG
A				REVISED HOLE SIZE AND QUANTITY

UNLESS OTHERWISE SPECIFIED

DESCRIPTION	PLATE, LOW CARBON STEEL, SAE 1010
SHOP OPERS	LAWRENCE BERKELEY LABORATORY, UNIVERSITY OF CALIFORNIA-BERKELEY
	SSC
	2.0 SOC PLUS - HAC2
DEGREASE	GENERIC ABSORBER PLATE
HIRAMIHARA	DETAIL (4213-01) — SCALE 1:10 — 20M6086 — B

REQ	ITEM	PART NUMBER	DESCRIPTION
			PLATE, LOW CARBON STEEL, SAE 1010

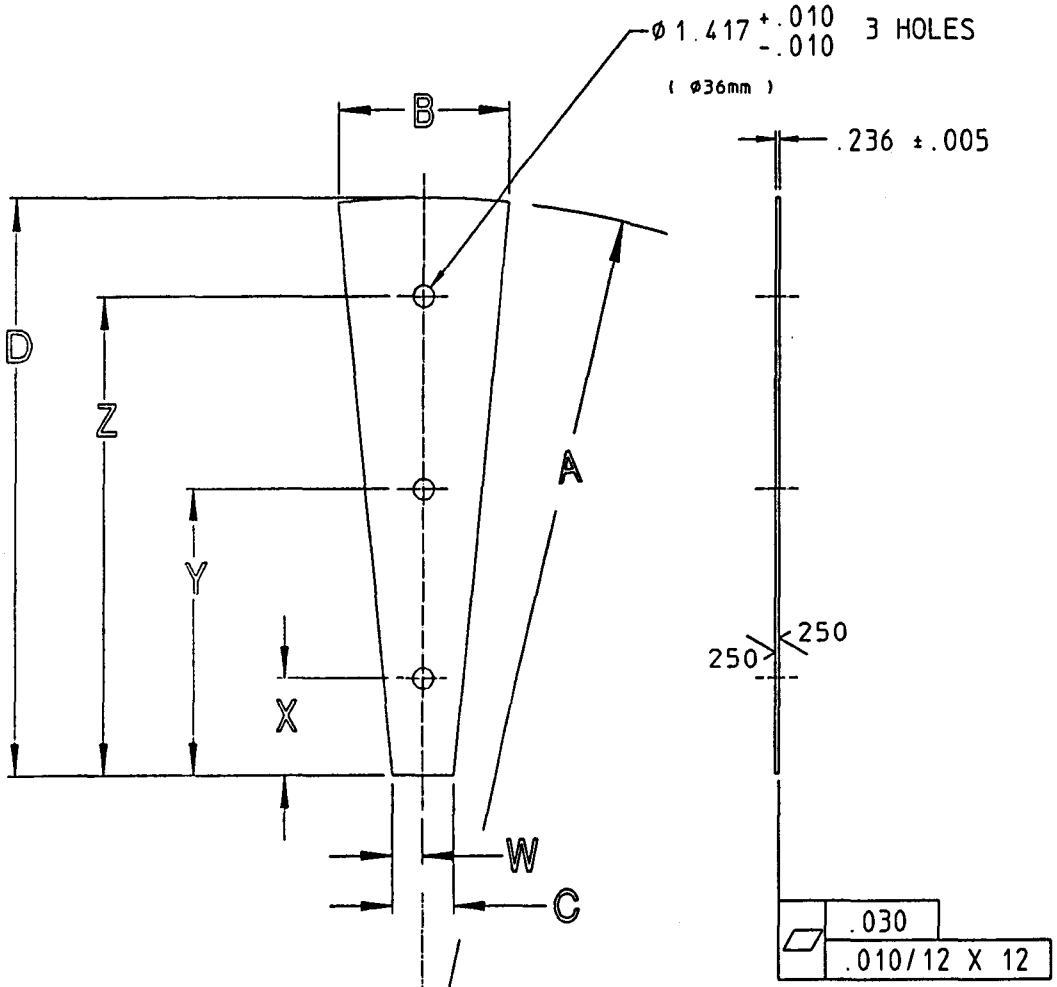

VERSION NO.	A RADIUS	B ±0.010	C ±0.010	D ±0.010	W ±0.005 -.010	X ±0.005 -.010	Y ±0.005 -.010	Z ±0.005 -.010	WT. lbs. each
VER-1	61.092	10.193	3.712	33.000	1.056	0.217	17.037	20.055	15.40
VER-2	62.253	10.244	3.730	33.226	1.065	0.122	17.542	20.960	16.56
VER-3	62.613	10.290	3.748	33.392	1.076	0.029	17.449	21.896	16.72
VER-4	62.774	10.340	3.767	33.619	1.083	0.934	17.354	20.772	16.87
VER-5	63.035	10.387	3.785	33.726	1.093	0.839	17.269	20.977	16.03
VER-6	63.299	10.440	3.804	33.881	1.102	0.745	17.185	20.863	16.19
VER-7	63.550	10.489	3.822	34.007	1.011	0.651	17.071	20.489	16.35
VER-8	63.810	10.550	3.841	34.223	1.920	0.556	16.976	20.564	16.61
VER-9	64.077	10.601	3.899	34.390	1.930	0.462	16.882	20.300	16.87
VER-10	64.337	10.652	3.878	34.596	1.939	0.369	16.788	20.206	16.03
VER-11	64.600	10.703	3.896	34.722	1.948	0.273	16.683	20.111	16.89
VER-12	64.856	10.754	3.915	34.888	1.957	0.179	16.599	20.017	17.15
VER-13	65.119	10.805	3.933	35.054	1.967	0.919	16.721	30.632	17.31
VER-14	65.375	15.057	3.952	35.221	1.679	0.818	16.620	30.737	17.46
VER-15	65.640	16.908	3.970	35.387	1.968	0.621	16.032	30.843	17.60
VER-16	65.900	10.959	3.989	35.553	1.984	0.327	16.438	30.849	17.81
VER-17	66.161	11.010	4.007	35.719	3.004	0.233	16.344	30.455	17.00
VER-18	66.421	11.061	4.026	35.886	3.013	0.138	16.249	30.360	18.14
VER-19	66.683	11.112	4.044	36.052	2.022	0.044	16.155	30.266	18.31
VER-20	66.942	11.163	4.063	36.218	2.031	0.950	16.061	30.172	18.46
VER-21	67.203	11.214	4.081	36.384	2.041	0.906	17.966	30.077	19.65
VER-22	67.463	11.265	4.100	36.550	2.050	0.761	17.872	29.983	18.02
VER-23	67.724	11.316	4.118	36.717	2.059	0.667	17.778	29.968	18.69
VER-24	67.984	11.367	4.137	36.883	2.069	0.572	17.683	29.794	19.16
VER-25	68.245	11.418	4.155	37.049	2.078	0.478	17.589	29.700	19.34
VER-26	68.505	11.469	4.174	37.215	2.087	0.909	16.713	32.817	19.51
VER-27	68.766	11.520	4.192	37.381	2.096	0.814	16.618	32.422	19.68
VER-28	69.027	11.572	4.211	37.548	2.106	0.720	16.524	32.329	19.88
VER-29	69.287	11.623	4.229	37.714	2.115	0.626	16.430	32.234	20.03
VER-30	69.548	11.674	4.248	37.880	3.124	0.531	16.335	32.139	20.21
VER-31	69.808	11.725	4.266	38.046	2.133	0.437	16.241	32.045	20.39
VER-32	70.069	11.776	4.285	38.212	2.143	0.343	16.147	31.951	20.57
VER-33	70.329	11.827	4.303	38.379	2.152	0.248	16.052	31.856	20.75
VER-34	70.590	11.878	4.322	38.545	2.161	0.154	15.958	31.762	20.93
VER-35	70.850	11.929	4.340	38.711	2.170	0.060	15.864	31.668	21.11
VER-36	71.111	11.980	4.359	38.877	2.179	0.966	16.769	31.573	21.29
VER-37	71.371	12.031	4.377	39.043	2.189	0.871	16.675	31.479	21.47
VER-38	71.633	12.082	4.396	39.210	2.198	0.777	16.581	31.385	21.65

20M6034A

REV	DWG	CHK	ZONE	DATE	CHANGES
A	MOH			*****	Ø1.417 WAS Ø1.355

UNLESS OTHERWISE SPECIFIED
TOL DIMENSIONS: .X ± —— FRAC. ± —— .XX ± —— ANGLES ± —— .XXX ± .020 FINISH 250/
THREADS ARE CLASS 2 CHAMFER END OF ALL SCREW THREADS 30°, ON 1.1 PITCH AND ROUND WITH RADIUS HALF ON MACHINE CUT THREADS.
BREAK EDGES .010 MAX. ON FINISHED WORK
REMOVE BURRS VOLS SPLINTER & LOOSE SCALE
REFERENCES: ANSI Y14.5 & B46.1.

SHOP ORDERS
ACCT. NO. SERIAL NO.
DATE ISSUED DATE RECEIVED DATE COMPLETED
DELIVER TO
MATERIAL DEGREASE
HEAT TREATMENT
PROCESS PLATE
DRAWN BY MINAMIHARA DATE 6-30-92
CHECKED BY DATE

LAWRENCE BERKELEY LABORATORY
UNIVERSITY OF CALIFORNIA-BERKELEY
SSC
2.0 PLUG - HAC 1
GENERIC WEDGE PLATE

PATENT CLEAR | DWG. TYPE DETAIL | SHOWN ON | SCALE NONE | DWG. NO. 20M6034 | SIZE A | REV.
INTERPRETED | REVISE ACT. NO. 4213-01 | CATEGORY CODE

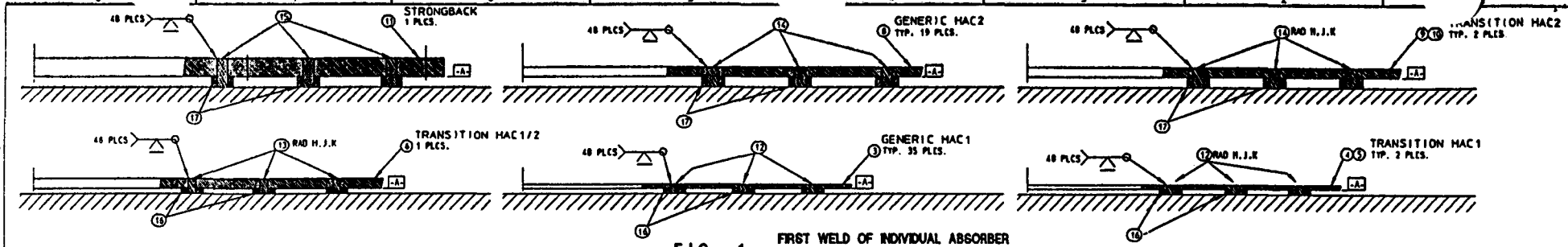

FIG. 1 FIRST WELD OF INDIVIDUAL ABSORBER PLATES TO TIE RODS.

NOTE 1. SLOT WELD ALL WEDGE PLATES ((ITEMS 2 & 7) TO THEIR ADJACENT ABSORBER PLATES AS SHOWN LEAVING A 1/2 IN. SPACE AT EACH END OF THE WEDGE PLATE. 16 PLACES EACH WEDGE PLATE LAYER, 60 LAYERS, 960 WELDS TOTAL.

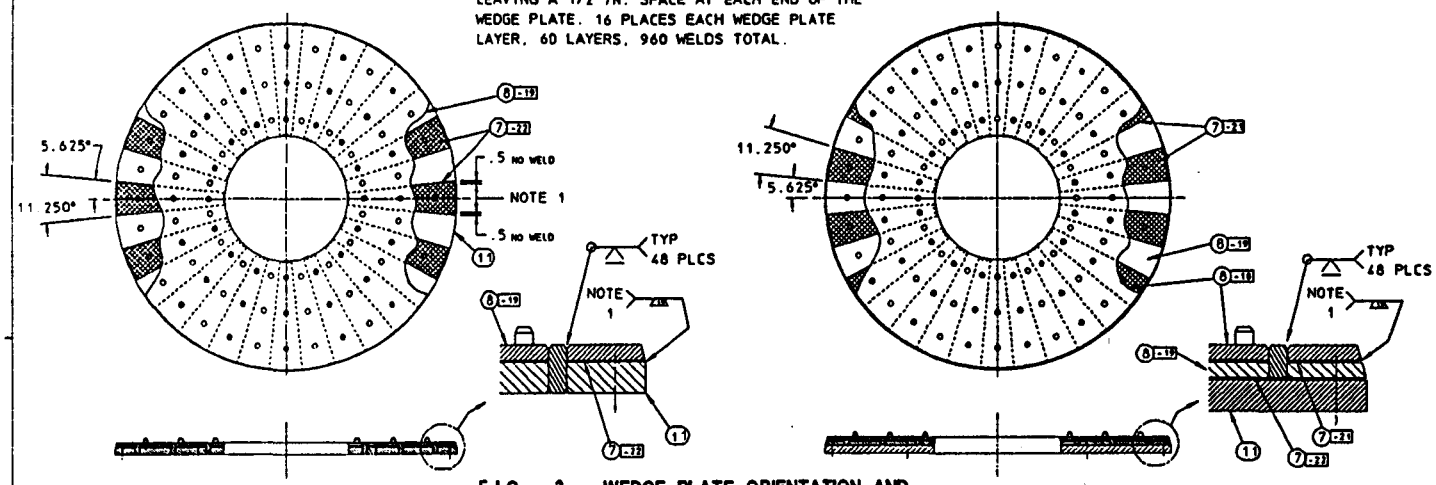

FIG. 2 WEDGE PLATE ORIENTATION AND STACK ASSEMBLY WELDING

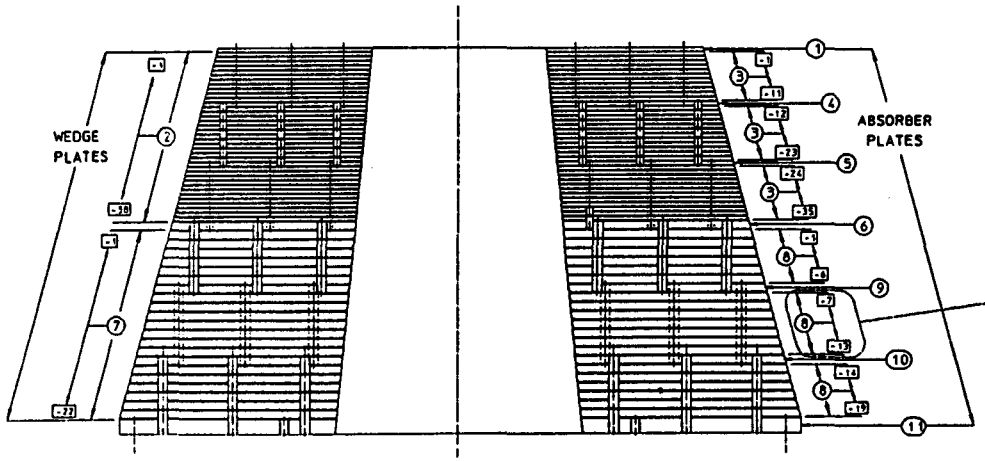

TYPICAL NOMENCLATURE:
CIRCLED NUMBERS (6) ARE ITEM NUMBERS. THEY REFER TO A DRAWING NUMBER.
BOXED DASHED NUMBERS [-7] ARE VERSION NUMBERS. THEY REFER TO A VARIATION (VERSION) OF A DRAWING.

FIG. 3 STACK SEQUENCE

A. Welding of First Tie Rod End to Absorber Plates—See Fig. 1

1. Place a large sheet (≈ 146 in. square or diameter) of soft, foam rubber (≈ 1 in. thick) on the work surface. Place 16 ea. long metal strips (≈ 1/8 in. thick x ≈ 7 in. wide x ≈ 56 in. long) in a fan-like pattern (see Fig. 2) on the foam pad. (the compressible foam rubber pad's compliance insures that the metal strips will press plug assembly shims, items 16 or 17, against the underside of slightly bowed absorber plates, placing the top ends of tie rods flush with the absorber plate's top surface for proper welding position. The metal strips also serve as lateral heat conductors, to prevent burning the foam).
2. Weld first end of tie rods, items 12-15, to absorber plate(s), items 3,4-6,8-11 as shown in Fig. 1, and grind welds flush (48 pics per plate).
3. Machine ≈1/8 x 3/32 radial grooves into plate (through welds) as shown on item 18 or 19 using a skill saw or router and template (16 pics per plate).
4. Machine ≈1/8 x 3/32 curved grooves into plate as shown on item 18 or 19 using a router and template (16 pics per plate).
5. Remove grinding dust, chips & cutting fluids with suitable solvent and oil-free house air.

B. Assembly Stacking/Welding—See Figures 2 & 3

Assembly stacking (Fig. 2 & 3) must anticipate subsequent pick-up of the ≈ 110 ton plug weldment. This can be accomplished with a pick-up fixture 20M(TBD), to be supplied by LBL. If item 11 is supported about 18 in from the shop floor on 4 each, stout "posts" placed on a circle of about 100 in. diameter.

1. Starting with the inverted strongback plate, item 11, place 16 ea. of wedge plates, item 7, over the up-protruding tie rods (alternating the azimuthal position of wedge plates in subsequent layers) as shown in Fig. 2.
2. Position items 7 as shown in Fig. 2, and tack-weld at the outer radius to the absorber plate beneath (2 pics per wedge plate, 32 pics per layer).
3. Invert subsequent absorber plates and add to the stack over previous plate's up-protruding tie rods as shown in Fig. 2.
4. Depending upon whether the added absorber plate's general curvature (out-of-flatness) is concave downward (upward), clamp the plate's inner (outer) edge down to the stack beneath with suitable clamps or loading fixture, and weld the inner-most (outer-most) ring of tie rods to the plate (16 pics).
5. Re-position the loading fixture to apply absorber plate flattening loads near the middle ring of tie rods, push the plate down to be flush with tie rod ends, and weld the middle ring of tie rods to the plate (16 pics).
6. Weld the 3rd ring of tie rods (inner-most or outer-most, per step 4) to the absorber plate (16 pics).
7. Perform the slot welding between wedge plates, item(s) 7, and adjacent absorber plates as shown detailed in Fig. 2 (16 places per layer, with no welding within 1/2 in. of the sides of item 7).
8. Grind tie rod-to-absorber plate welds from steps 4, 5 & 6 flush with the stack's top plate surface (48 pics).
9. Repeat Assembly steps 1 thru 8 for all layers of the plug assembly shown in Fig. 3 (61 pics total).
10. Remove slot weld spacer (step 7) from plate O.D.'s (16 pics, per wedge plate layer, 960 pics max, as req'd)
11. Remove grinding dust, chips & cutting fluids from stack slots and exterior with suitable solvent and oil-free house air.

20M6016

REQ	ITEM	PART NO.	DESCRIPTION
REF	19	20M6[illegible]	GENERIC SOURCE TUBE GROOVE - HAC1
REF	18	20M6[illegible]	GENERIC SOURCE TUBE GROOVE - HAC1
48	17	20M6[illegible]-2	PLUG ASSEMBLY SHIM
48	16	20M6[illegible]-1	PLUG ASSEMBLY SHIM
48	15	20M6[illegible]-4	TIE ROD - HAC2/STRONGBACK JUNCTION
1008	14	20M6[illegible]-3	TIE ROD - HAC2
48	13	20M6[illegible]-2	TIE ROD - HAC1/HAC2 JUNCTION
1728	12	20M6[illegible]-1	TIE ROD - HAC1
1	11	20M6[illegible]	ABSORBER STRONGBACK PLATE
1	10	20M6[illegible]-2	TRANSITION ABSORBER PLATE - HAC2
1	9	20M6[illegible]-1	TRANSITION ABSORBER PLATE - HAC2
19	8	20M6[illegible]-1 thru -19	GENERIC ABSORBER PLATE - HAC2
352	7	20M6[illegible]-1 thru -22	GENERIC WEDGE PLATE - HAC2
1	6	20M6[illegible]	TRANSITION ABSORBER PLATE - HAC1/HAC2
1	5	20M6[illegible]-2	TRANSITION ABSORBER PLATE - HAC1
1	4	20M6[illegible]-1	TRANSITION ABSORBER PLATE - HAC1
35	3	20M6[illegible]-1 thru -35	GENERIC ABSORBER PLATE - HAC1
600	2	20M6[illegible]-1 thru -38	GENERIC WEDGE PLATE - HAC1
1	1	20M6[illegible]	ABSORBER PLATE HAC1 - HAC1

UNLESS OTHERWISE SPECIFIED	SHOP PRACTICE	LAWRENCE BERKELEY LABORATORY UNIVERSITY OF CALIFORNIA/BERKELEY	
DIM. ±	MAC. ±		SSC
ANGLE ±0°0'5"			SSC 2.0 PLUG
MATERIAL			PLUG ASSEMBLY SEQUENCE
DRAWN		ACTIVITY CODE	SIZE TYPE	DWG. TYPE	SHEET OF	SCALE
		ASSEMBLY				N.T.S.
R. HALL HOFF	12/12					
		4213-01				20M6016

REV | ING | CH | CK | DATE | CHANGES

4

REQ	ITEM	PART NUMBER	DESCRIPTION
			PLATE, MILD STEEL, SAE 1020

APPROXIMATE WEIGHT OF THIS ITEM IS 3.940 LBS. 1.786 KG.

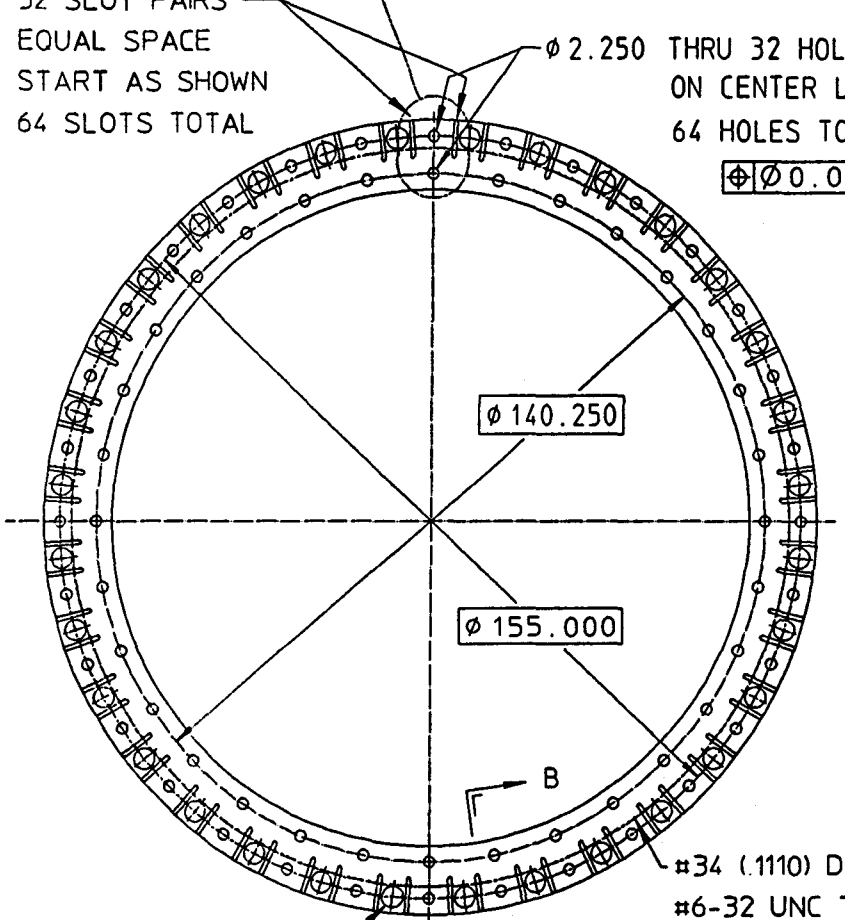

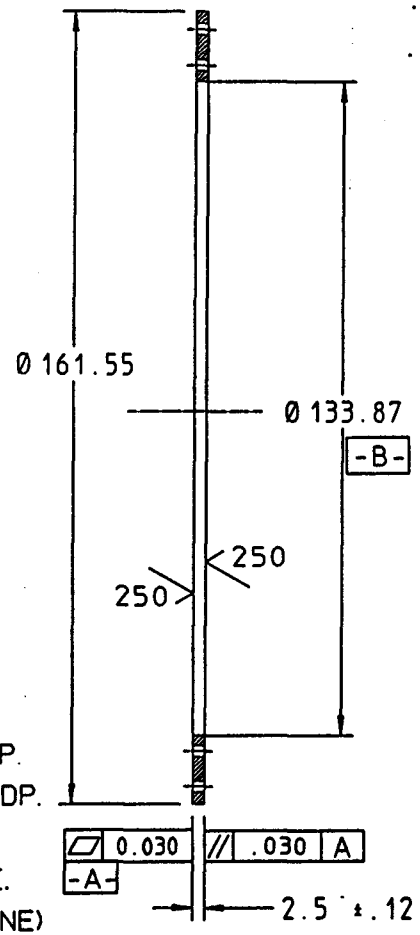

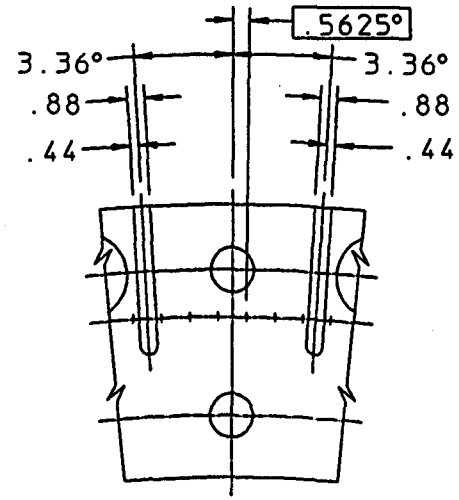

DETAIL 'A'
SCALE 1:4

20M6143A

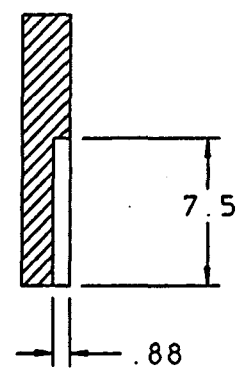

SECTION B-B
SCALE 1:4

REV	DWG	CHK	ZONE	DATE	CHANGES
A	MDH			9-26-92	ADDED SLOTS AND 4.5 DIA HOLES

UNLESS OTHERWISE SPECIFIED
TOLERANCES: .X ± 0.1 FRAC. ± ; .XX ± 0.03 ANGLES ± .03° ; .XXX ± 0.015 FINISH 250
THREADS ARE CLASS 2
CHAMFER ENDS OF ALL SCREW THREADS 30°.
CUT 1.5 PITCH THRD RELIEF WITH ROUND NOSE TOOL ON MACHINE CUT THREADS.
BREAK EDGES .016 MAX. ON MACHINED WORK
REMOVE BURRS [illegible] SPLATTER & LOOSE SCALE
REFER[illegible] Y14.5 & B46.1

SHOP ORDERS
ACCT. NO. | SERIAL NO.
DATE ISSD | DATE REQD | NO. REQD.
DELIVER TO
SURFACE TREATMENT: DEGREASE
IDENT. METH.: TAG
DWG. BY: MINAMIHARA | DATE 5-26-92
CHK. BY | DATE

LAWRENCE BERKELEY LABORATORY
UNIVERSITY OF CALIFORNIA-BERKELEY

SSC
2.0 SDC PLUG
PLUG SUPPORT FLANGE

PATENT CLEAR	DWG. TYPE	SHOWN ON	SCALE	DO NOT SCALE PRINTS
	DETAIL		1/20	
MICROFILMED	DESIGN ACCT. NO. 4213-01	CATEGORY CODE	DWG. NO. 20M6143	SIZE A / REV.

47

REQ	ITEM	PART NUMBER	DESCRIPTION

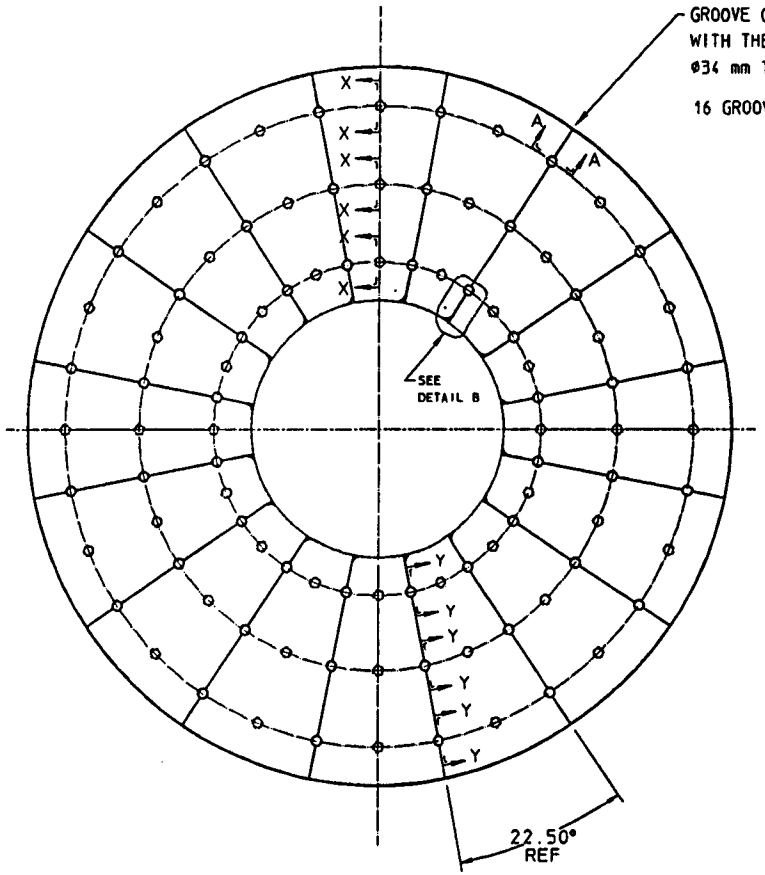

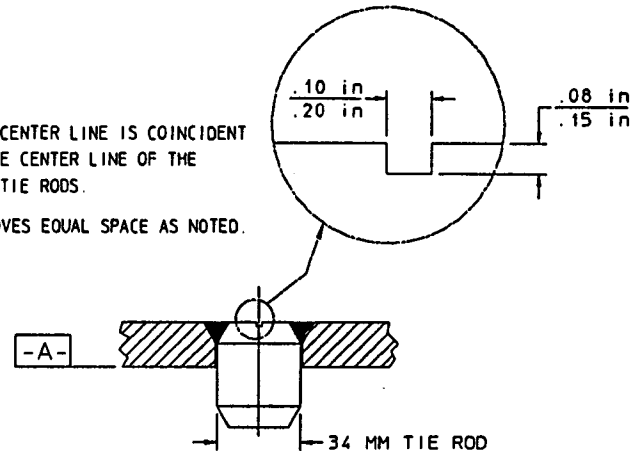

SECTION A-A
NOT TO SCALE

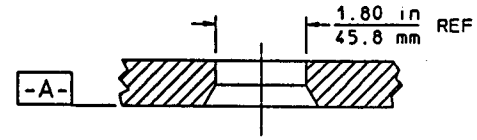

SECTION X-X
SCALE 1:1

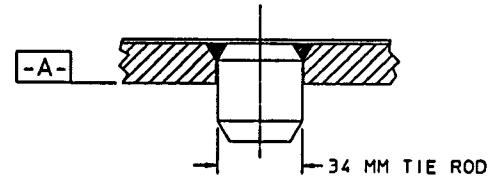

SECTION Y-Y
SCALE 1:1

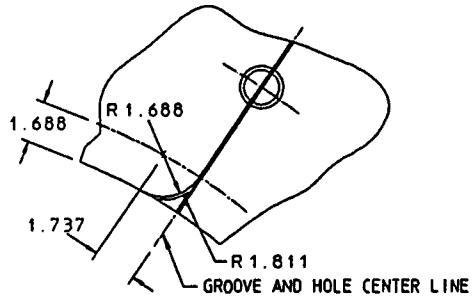

DETAIL B
NOT TO SCALE

NOTES:
1. ALL DIMENSIONS ARE IN INCHES UNLESS OTHERWISE SPECIFIED.
2. TOLERENCES APPLY TO INCH DIMENSIONS ONLY.
3. GROOVE MAY RUN THE ENTIRE RADIAL LENGTH OF PLATE (AS SHOWN) OR RUN RADIALLY FROM THE OUTSIDE DIAMETER TO TANGENT WITH THE RADIUS GROOVE.

20M6154

REV	DWG	CHK	ZONE	DATE	CHANGES

UNLESS OTHERWISE SPECIFIED
TOL. DIMENSIONS: X ± — FRAC. ± — .XX ± 0.06 ANGLES ± 1/4° .XXX ± 0.010 FRACTIONS 254/7°
THREADS ARE CLASS 2
CHAMFER ENDS OF ALL SCREW THREADS 30°, ON 1.5 PITCH AND COLD OF WITH ENDS FREE DIA. ON MACHINE CUT THREADS.
BREAK EDGES .010 MAX. ON MACHINED WORK
REMOVE BURRS WELD SPLATTER & LARGE SCALE
REFERENCES: ANSI Y14.5 & B46.1.

SHOP ORDERS
ACCT. NO. SERIAL NO.
DATE CODE DATE CODE NO./NO.
DELIVER TO
SURFACE TREATMENT DEGREASE
FINISH
PLATE
DRAWN MATT HOFF DATE 6-18-92
CHK. DATE
APP. DATE

LAWRENCE BERKELEY LABORATORY
UNIVERSITY OF CALIFORNIA-BERKELEY
SSC
2.0 SDC PLUG
GENERIC SOURCE TUBE GROOVE - MAC 1
PATENT CLEAR | DWG. TYPE DETAIL | SHOWN ON 20M6016 | SCALE TENTH | DO NOT SCALE DRAWING
INTERPRETER | DESIGN ACCT. NO. 4213-01 | CATEGORY CODE | DWG. NO. 20M6154 | SIZE | REV.

48

REQ	ITEM	PART NUMBER	DESCRIPTION

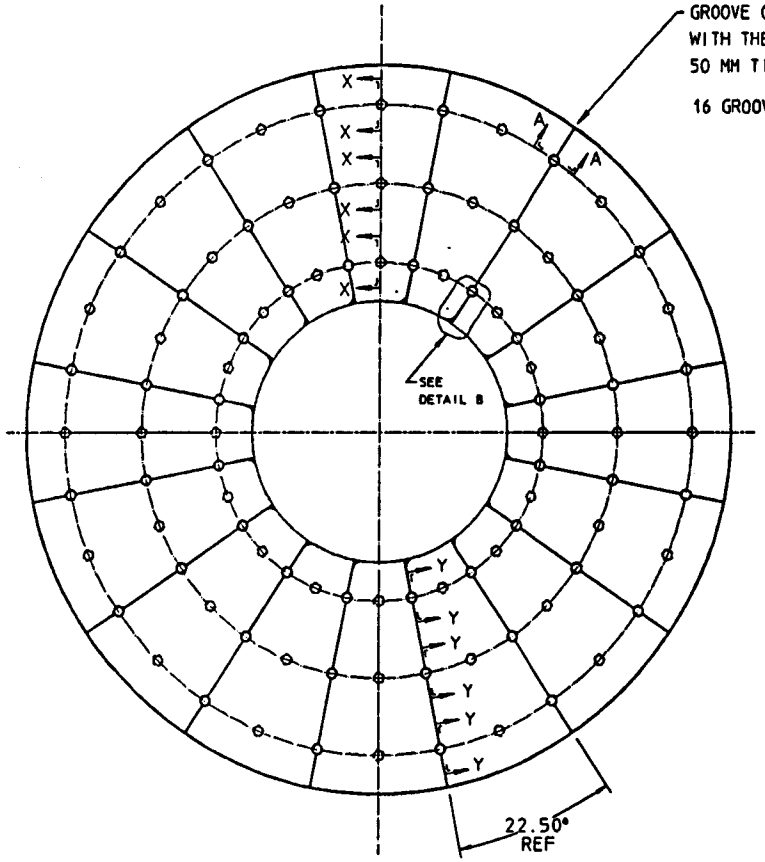

GROOVE CENTER LINE IS COINCIDENT WITH THE CENTER LINE OF THE 50 MM TIE RODS.

16 GROOVES EQUAL SPACE AS NOTED.

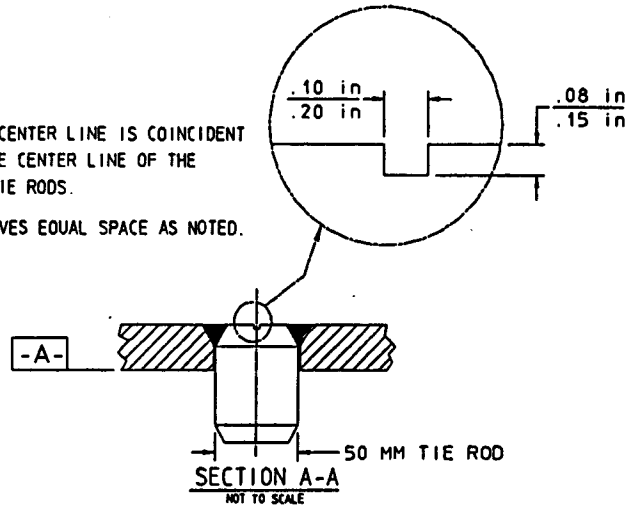

TYPICAL ENTIRE GROOVE LENGTH

SECTION A-A
NOT TO SCALE

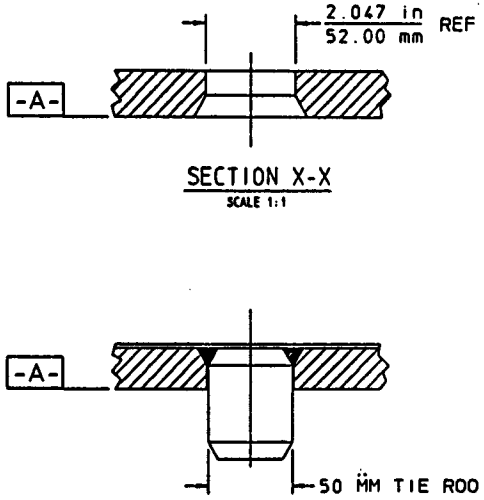

SECTION X-X
SCALE 1:1

SECTION Y-Y
SCALE 1:1

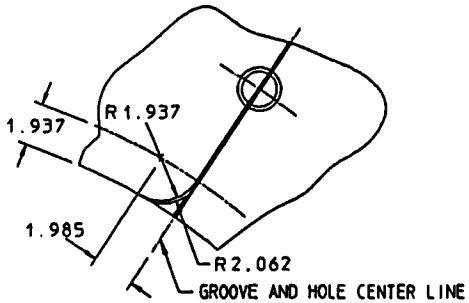

DETAIL B
NOT TO SCALE

NOTES:
1. ALL DIMENSIONS ARE IN INCHES UNLESS OTHERWISE SPECIFIED.
2. TOLERENCES APPLY TO INCH DIMENSIONS ONLY.
3. GROOVE MAY RUN THE ENTIRE RADIAL LENGTH OF PLATE (AS SHOWN) OR RUN RADIALLY FROM THE OUTSIDE DIAMETER TO TANGENT WITH THE RADIUS GROOVE.

20M6154

REV	DWG	CHK	ZONE	DATE	CHANGES

UNLESS OTHERWISE SPECIFIED
TOL DIMENSIONS: .X ± —— FRAC. ± —— .XX ± 0.06 ANGLES ± 1/4° .XXX ± 0.010 FINISH 250
THREADS ARE CLASS 2
CHAMFER ENDS OF ALL BORED THREADS 30°, ON 1.1 PITCH TWO FULL OF WITH ROOTS ARE FULL ON MACHINE CUT THREADS.
BREAK EDGES .010 MAX. ON UNCHANGED AREA.
REMOVE BURRS HOLD FLATNESS & LARGE SCALE
REFERENCES: ANSI Y14.5 & B46.1.

SHOP ORDERS
ACCT. NO. SERIAL NO.
DATE ISSUED DATE REQ'D REV. ORDER
SUPPLIER
SURFACE TREATMENT DEGREASE
DRAWN BY MATT HOFF DATE 6-11-92
CHK. BY
APP. BY
ENG. BY
MFG. BY

LAWRENCE BERKELEY LABORATORY
UNIVERSITY OF CALIFORNIA-BERKELEY

SSC
2.0 SDC PLUG
GENERIC SOURCE TUBE GROOVE - HAC 2

PATENT CLEAR | DWG. TYPE DETAIL | SHOWN ON 20M6016 | SCALE TENTH | 20 MM SCALE
MODIFIED | REVISION ACT. NO. 4213-01 | CATEGORY CODE | DWG. NO. 20M6164 | SIZE | REV.

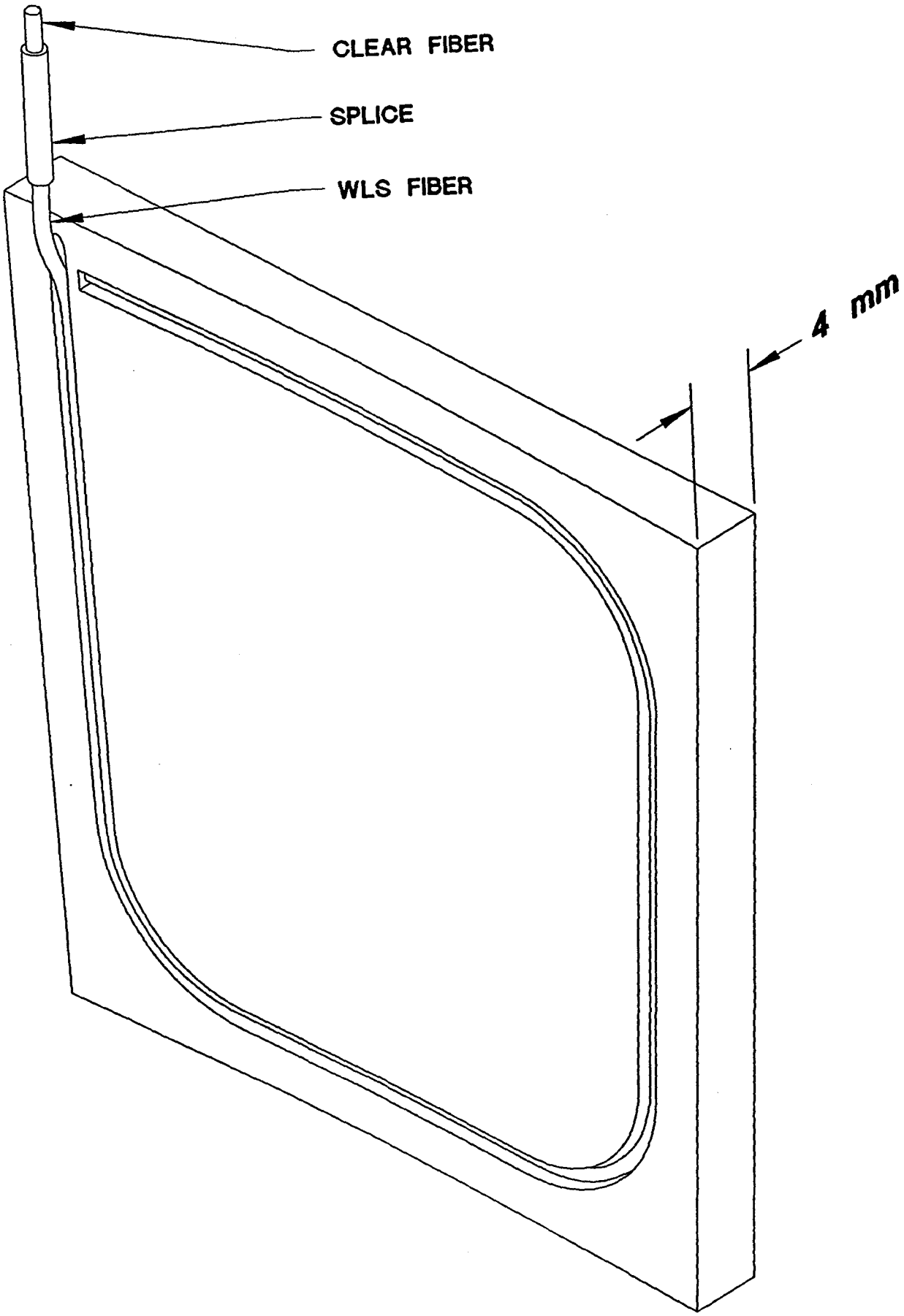

FIG. 4.1

TYPICAL ENDPLUG SCINTILLATING TILE CONFIGURATION

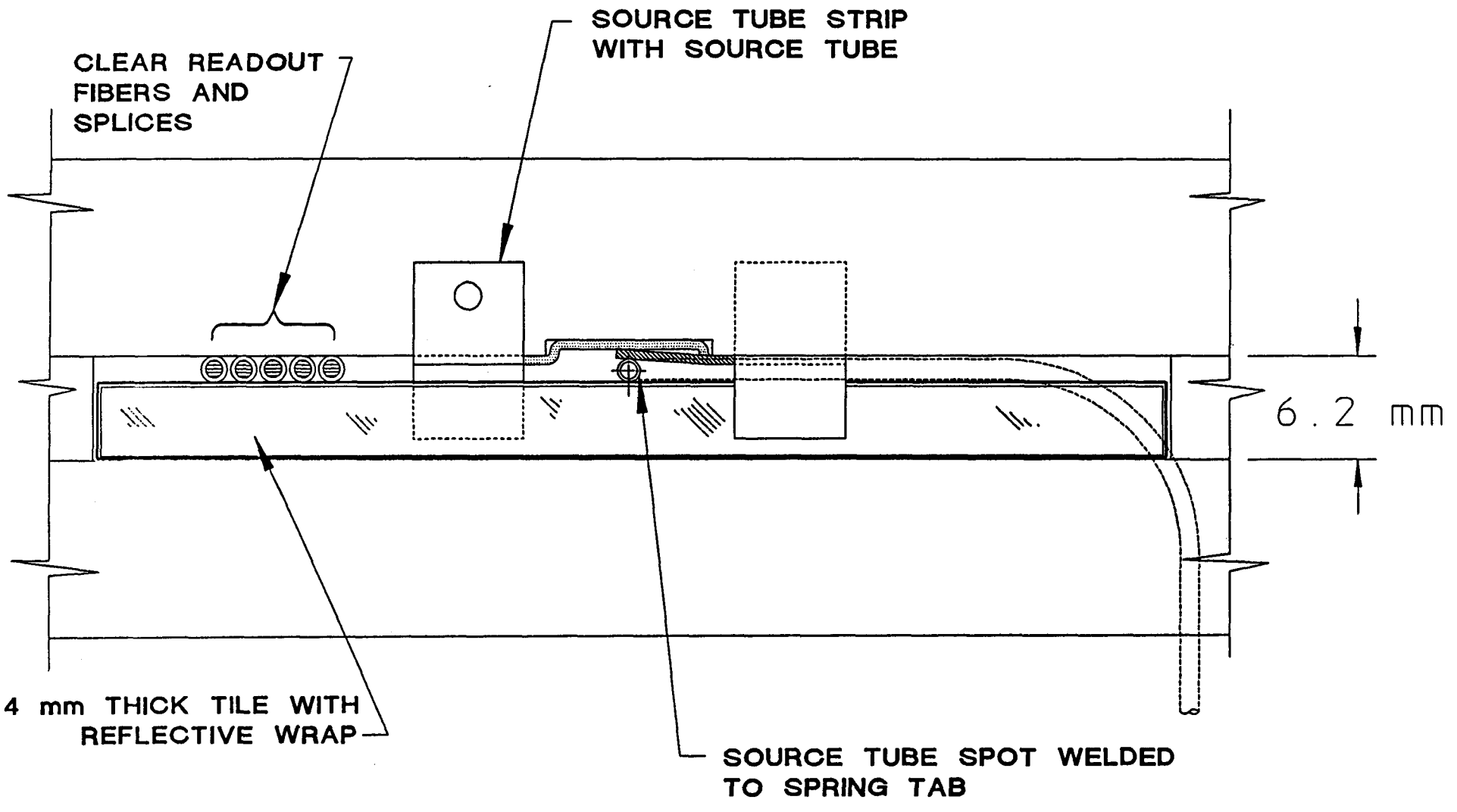

FIG. 4.2a

OUTER EDGE VIEW OF ABSORBER SLOT (MEGATILE CONFIGURATION)
NOT TO SCALE. DIMENSIONS ARE AGGERATED FOR CLARITY.

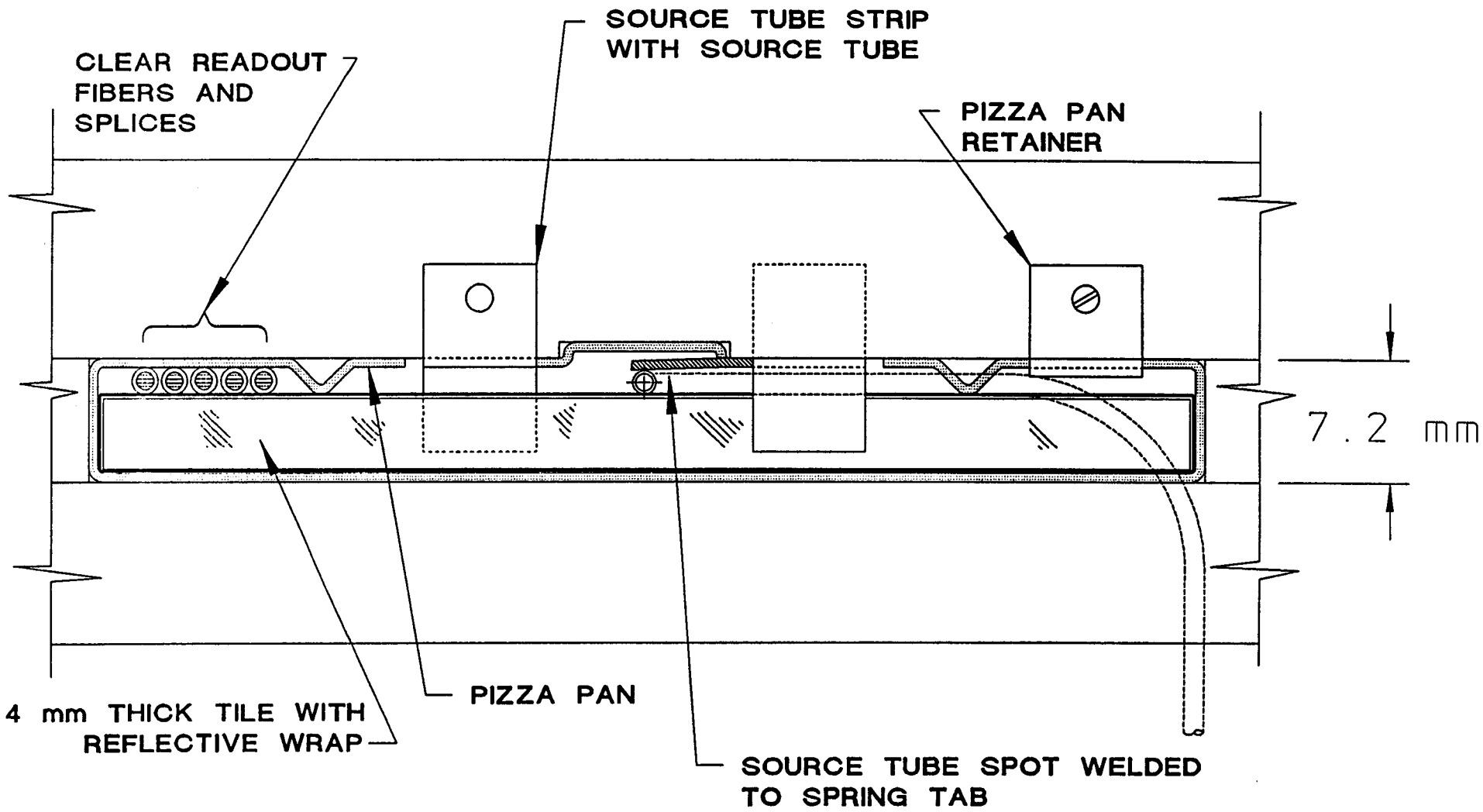

FIG. 4.2b

OUTER EDGE VIEW OF ABSORBER SLOT (PIZZA PAN CONFIGURATION)
NOT TO SCALE. DIMENSIONS ARE EXAGGERATED FOR CLARITY.

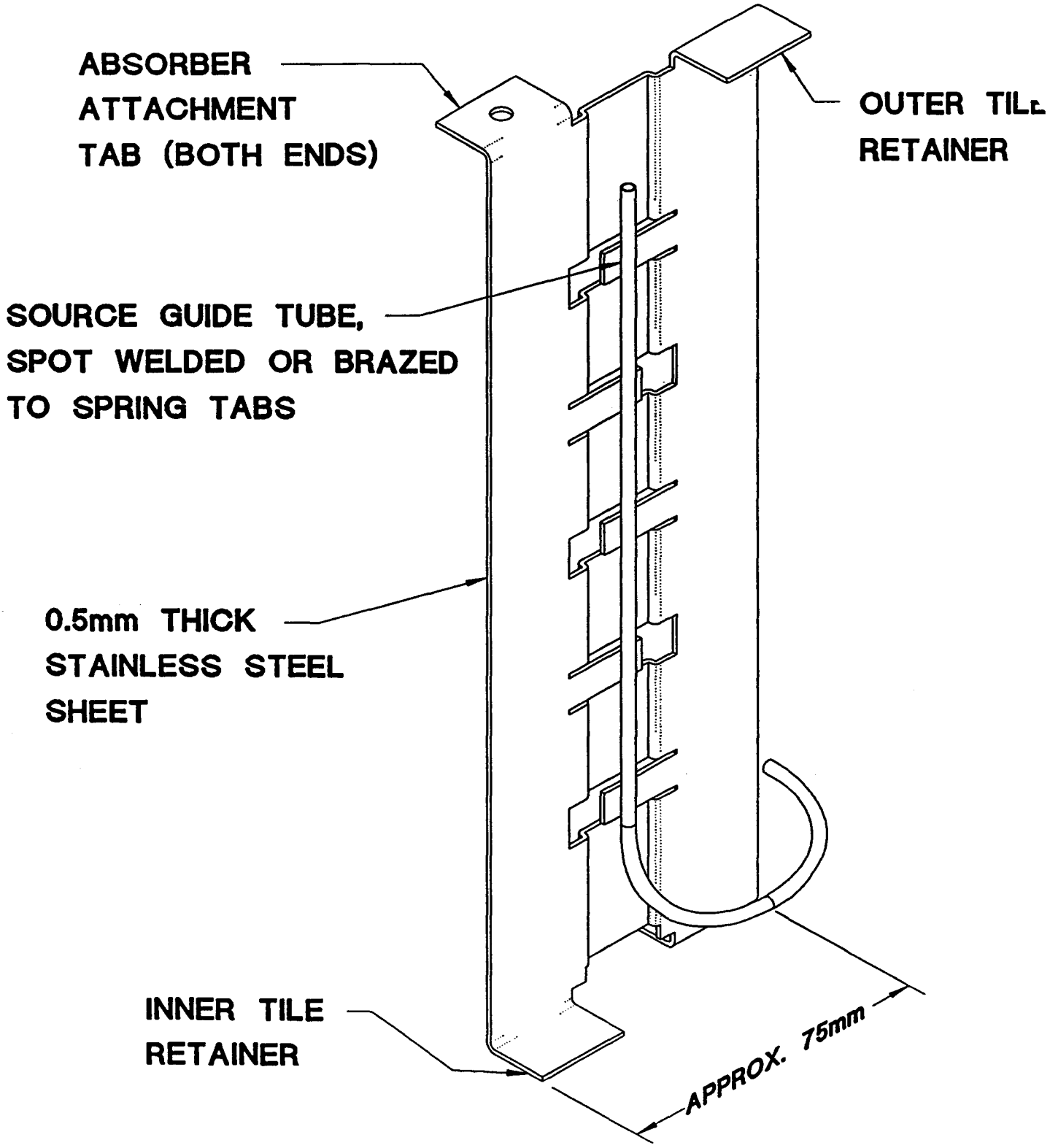

FIG. 4.3

SOURCE TUBE STRIP/SOURCE TUBE SUB-ASSEMBLY
NOT TO SCALE

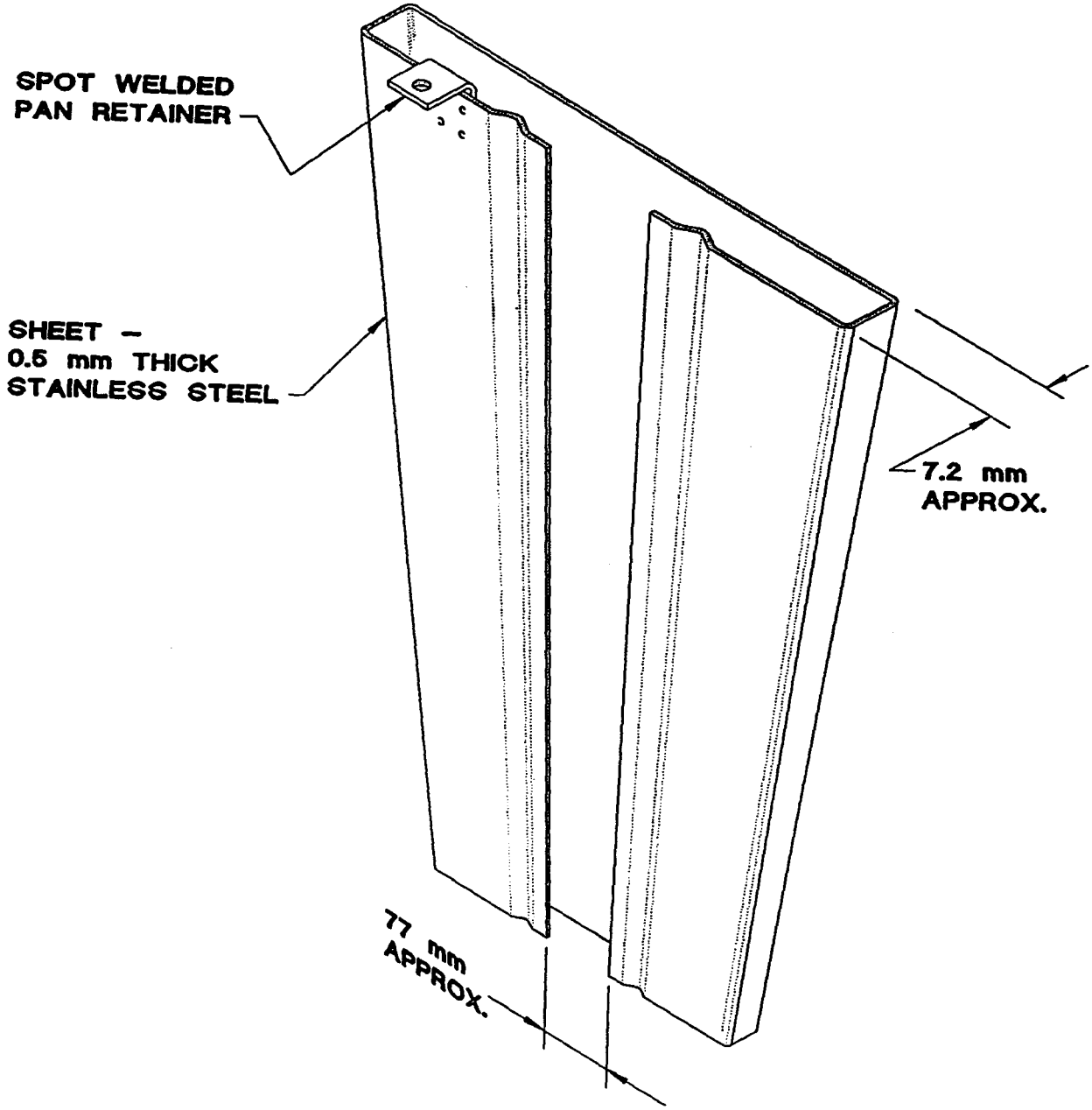

FIG. 4.4

ENDPLUG PIZZA PAN SHEET METAL WORK.
NOT TO SCALE. DIMENSIONS EXAGGERATED FOR CLARITY.

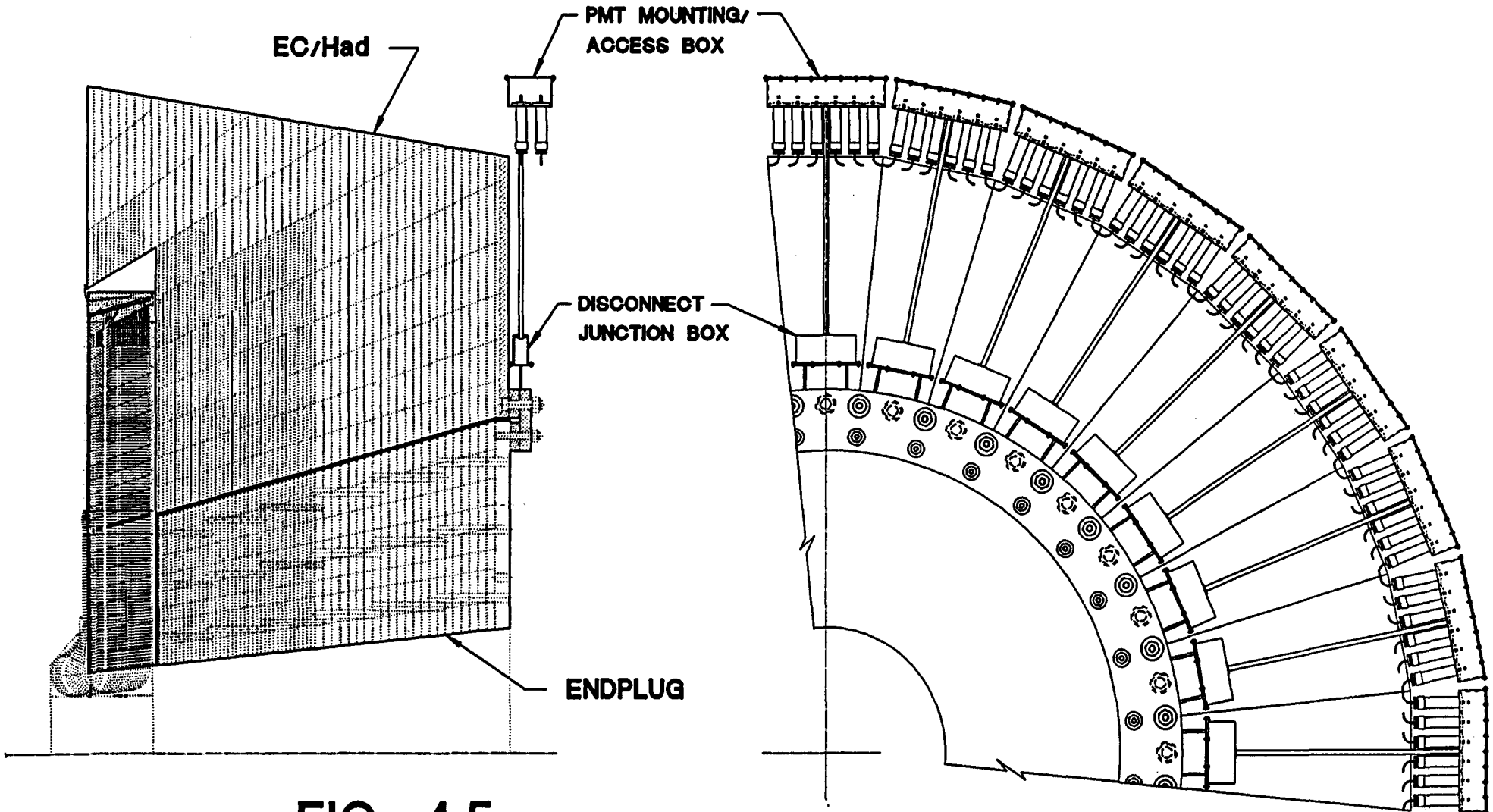

FIG. 4.5 CROSS-SECTION AND END VIEW OF THE ENDCAP

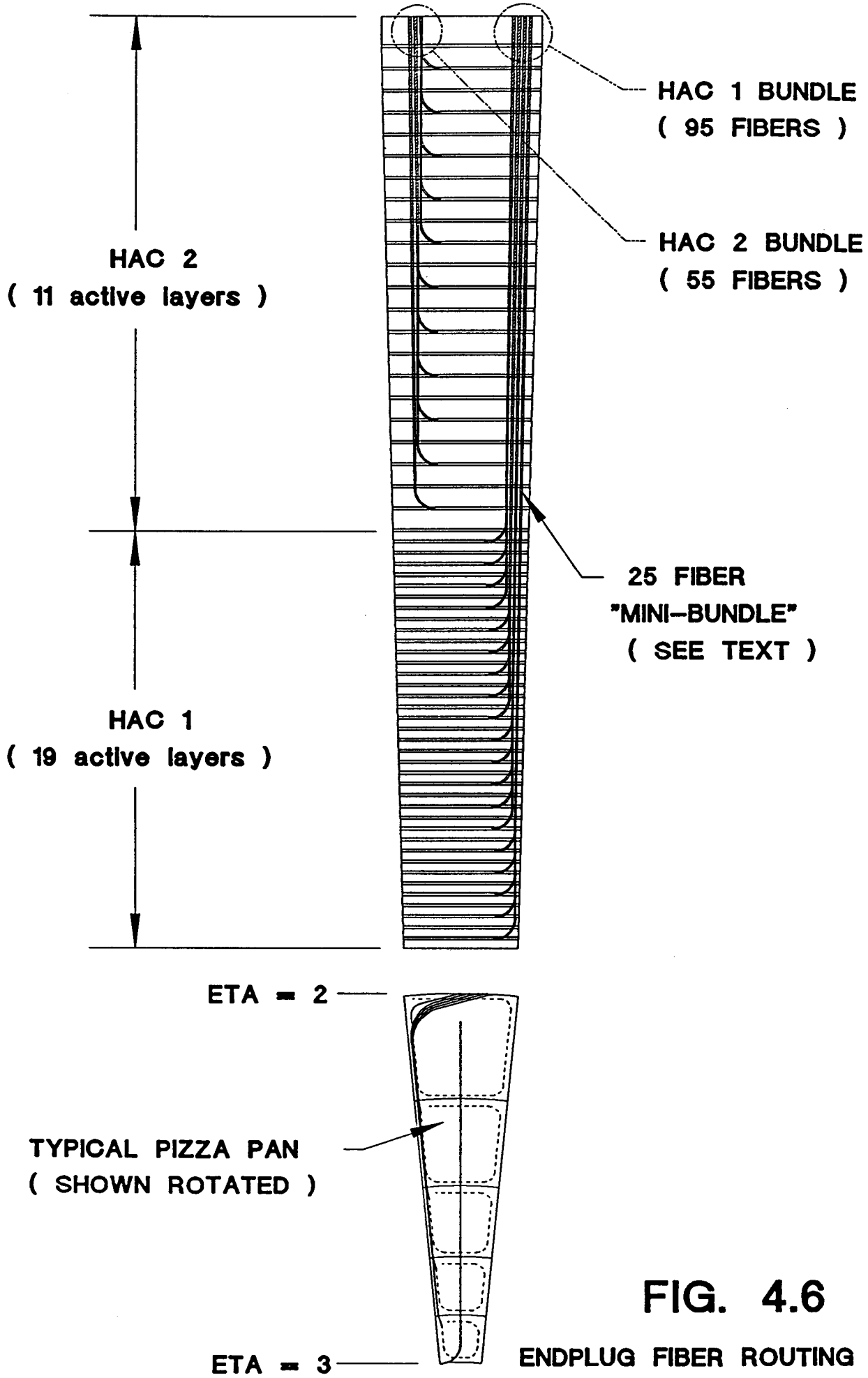

FIG. 4.6

ENDPLUG FIBER ROUTING DETAILS

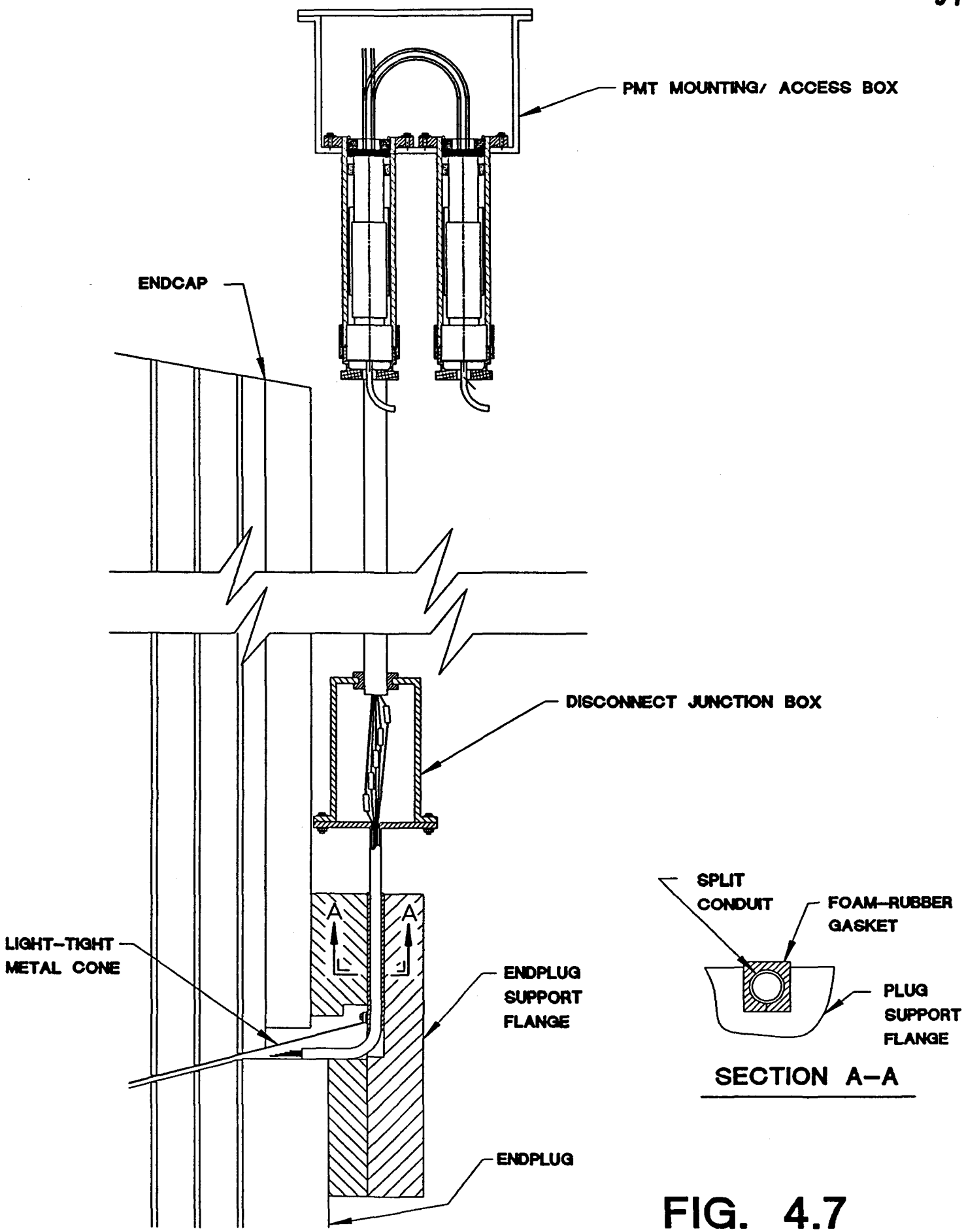

FIG. 4.7

TYPICAL RADIAL CROSS-SECTION THROUGH THE ENDPLUG SUPPORT FLANGE

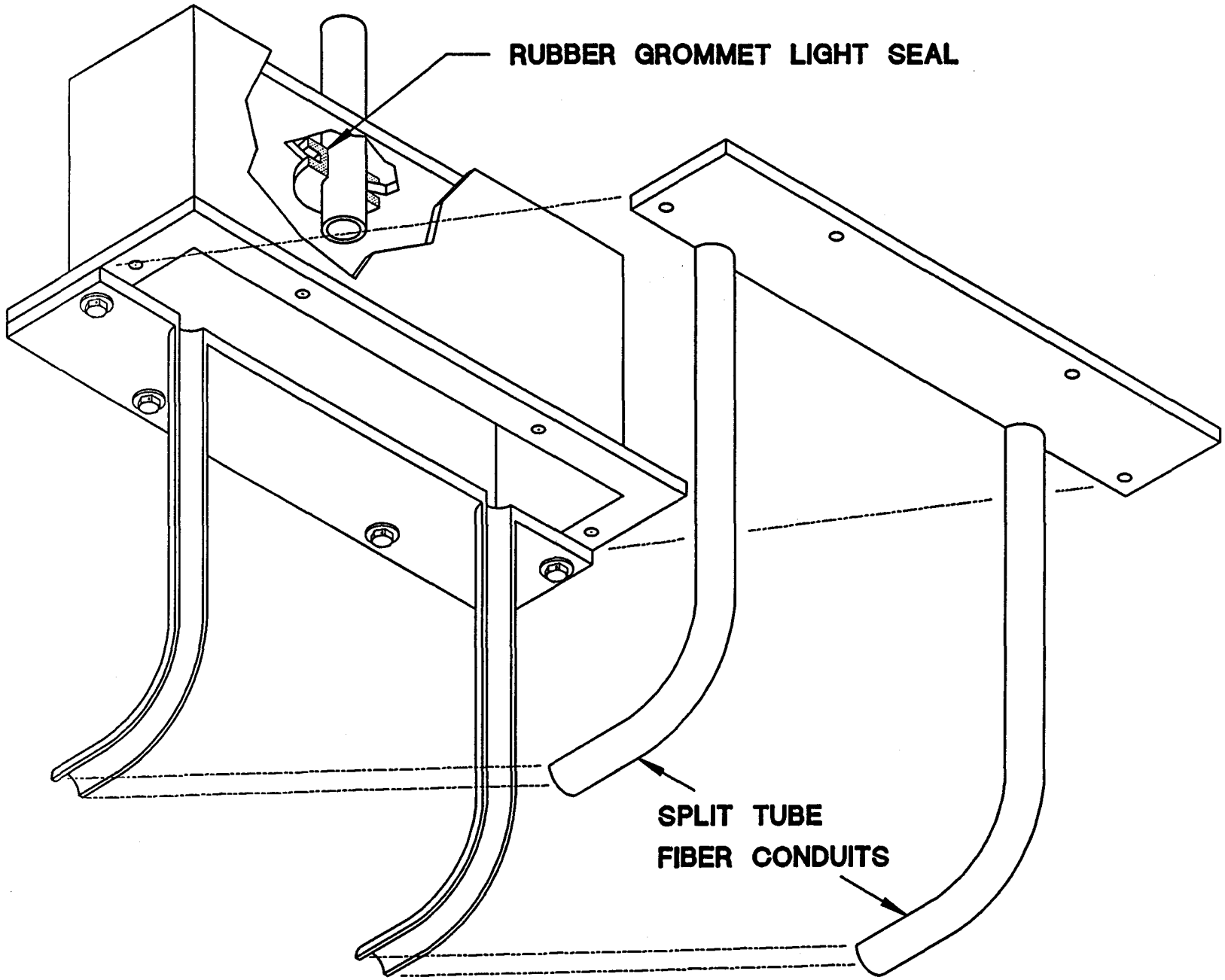

FIG. 4.8 FIBER-DISCONNECT JUNCTION BOX

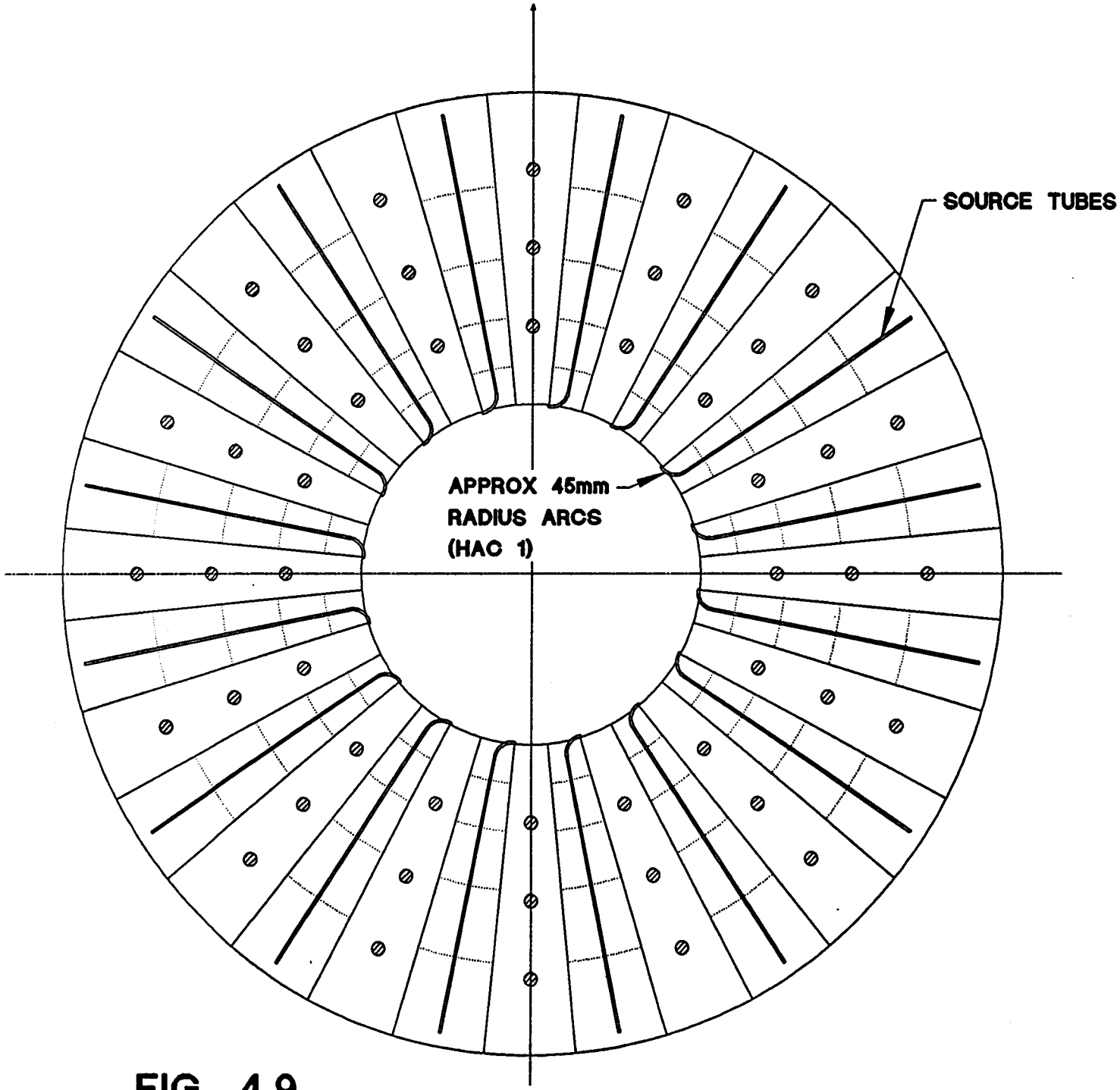

FIG. 4.9

TYPICAL ROUTING OF SOURCE TUE 'N ENDPLUG ABSORBER LAYERS

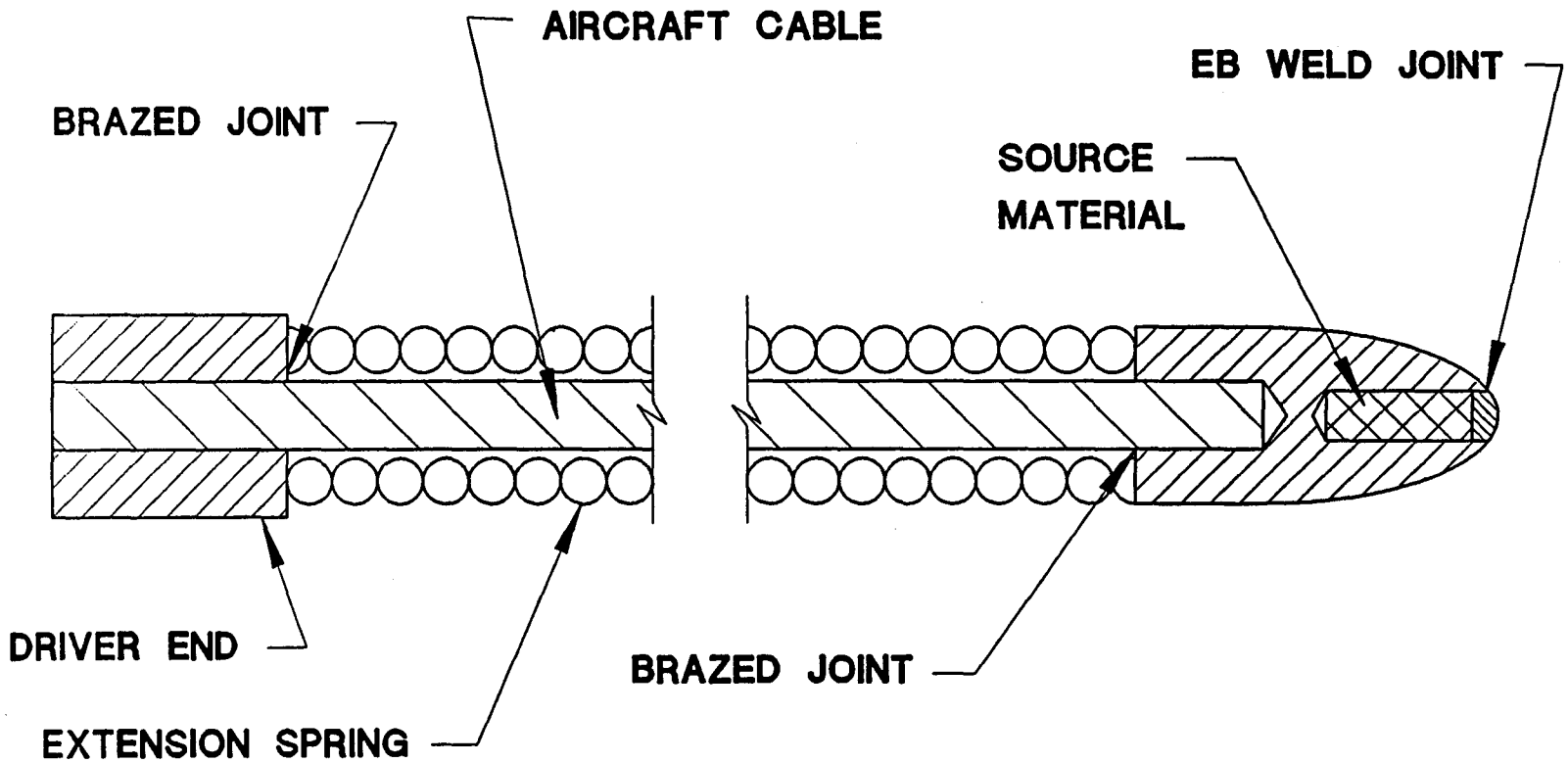

FIG. 4.10

COMPOSITE SOURCE WIRE

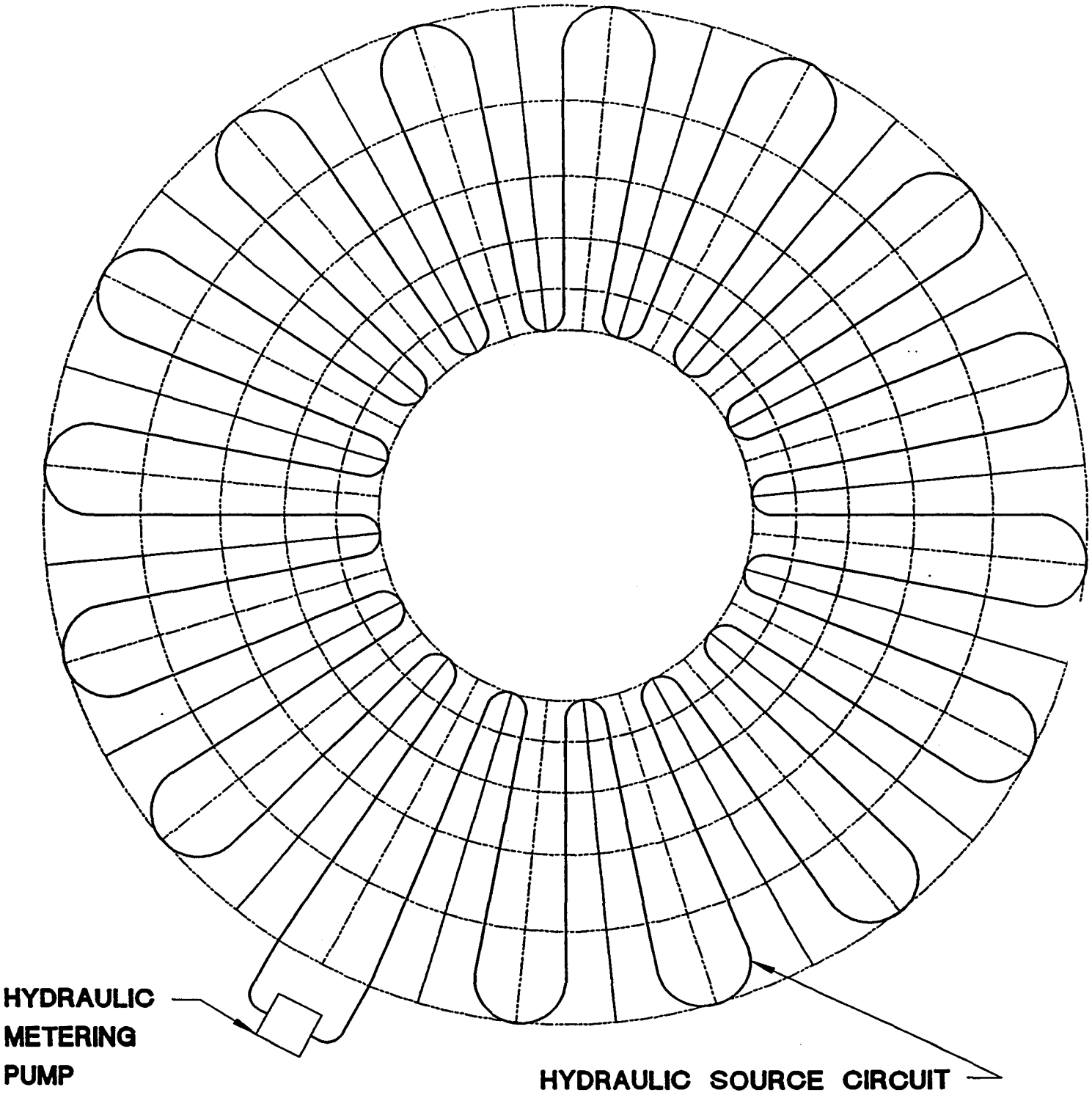

FIG. 4.11

CONCEPTUAL HYDRAULIC SOURCE CIRCUIT PATH

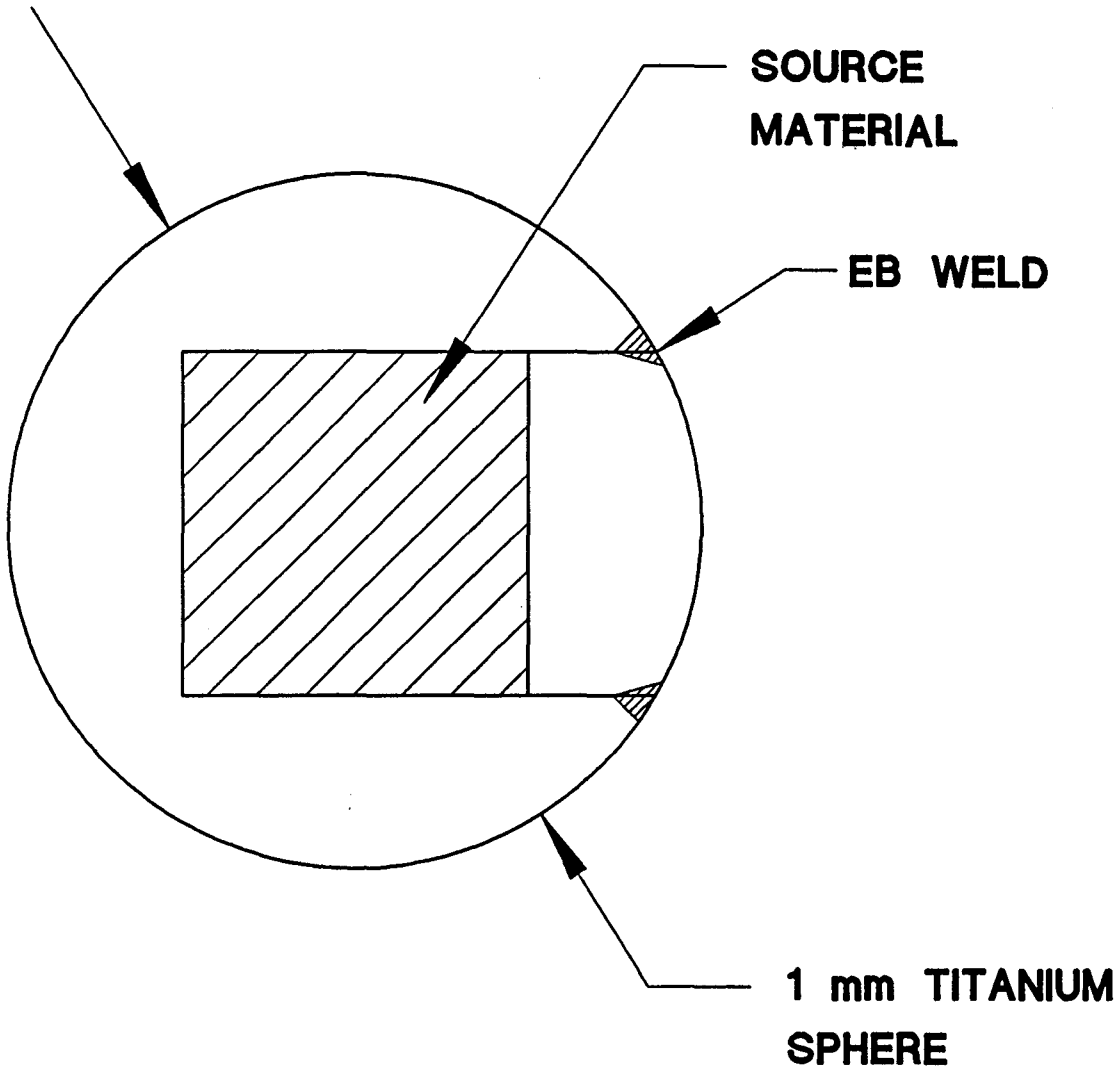

FIG. 4.12

SOURCE SPHERE FOR THE HYDRAULIC
SOURCE POSITIONING OPTION

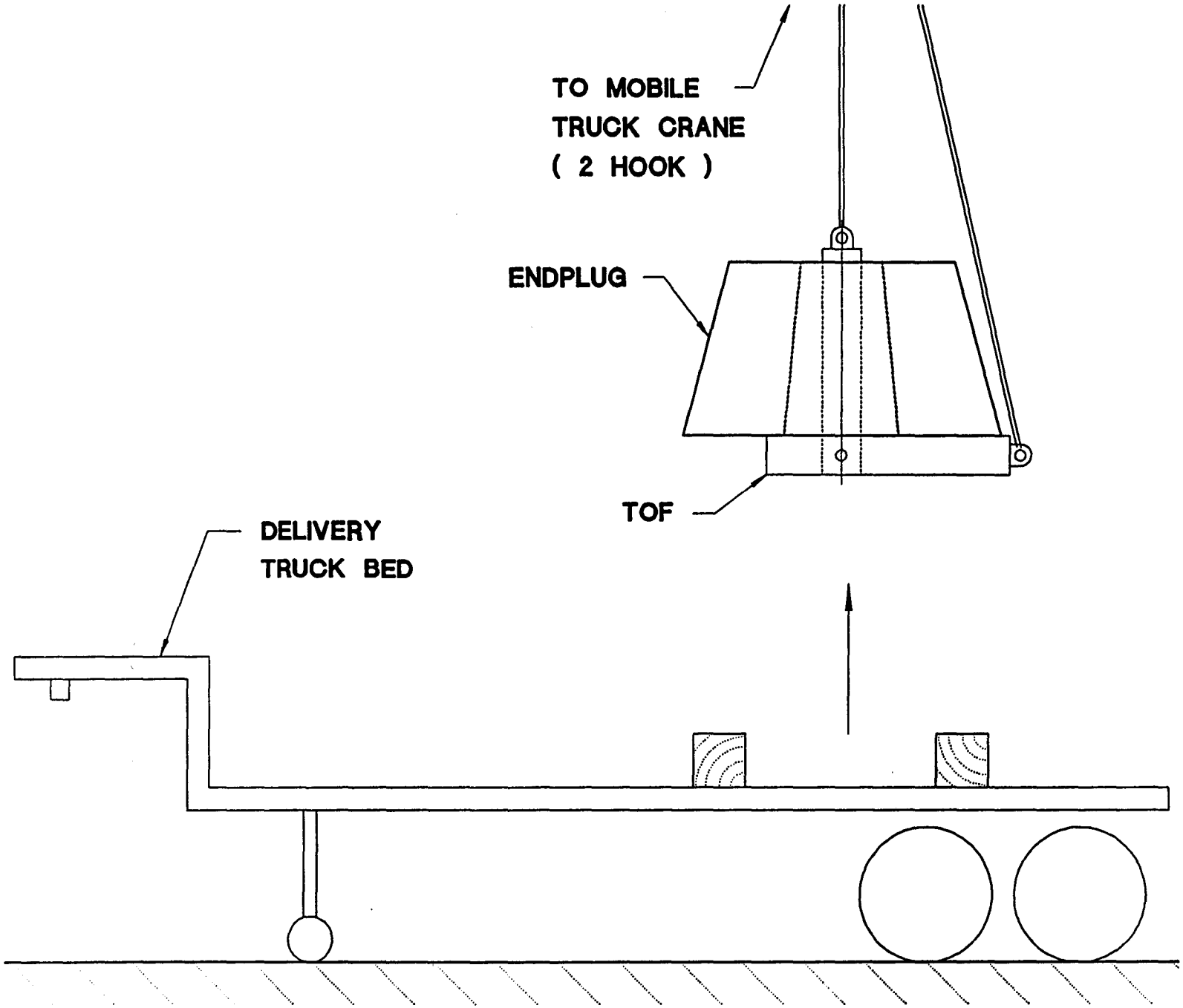

FIG 5.1
ENDPLUG FF LOADING

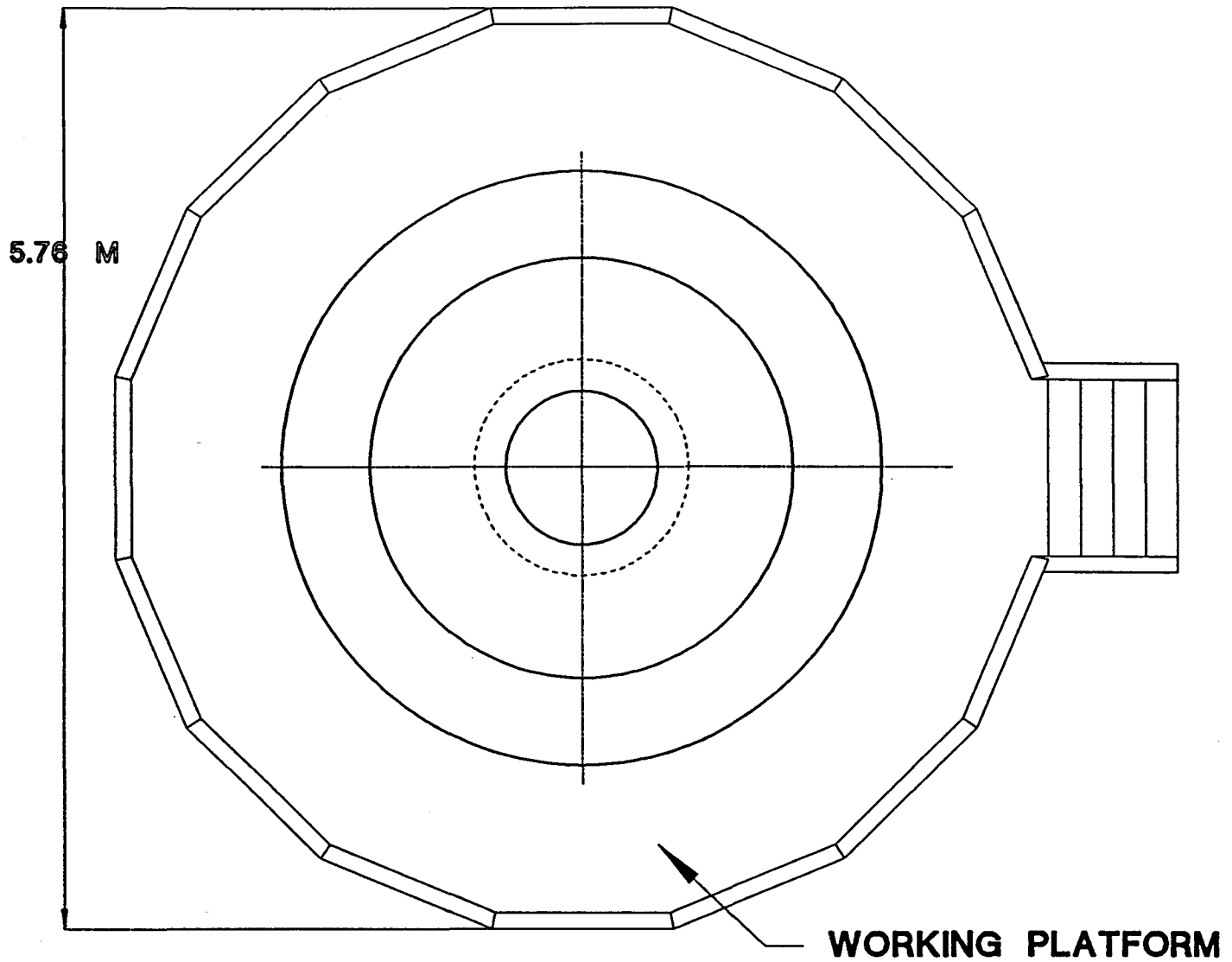

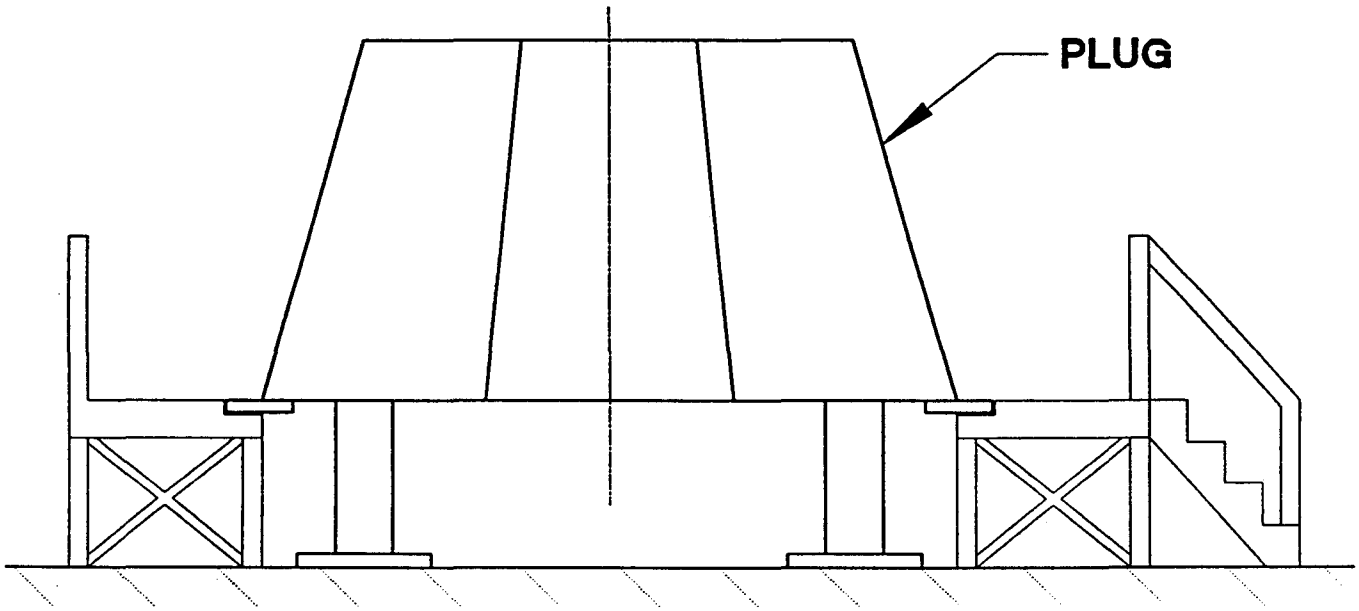

FIG. 5.2

ENDPLUG ASSEMBLY WORK STATION AT LBL

REQ	ITEM	PART NUMBER	DESCRIPTION
			PLATE, MILD STEEL, SAE 1020

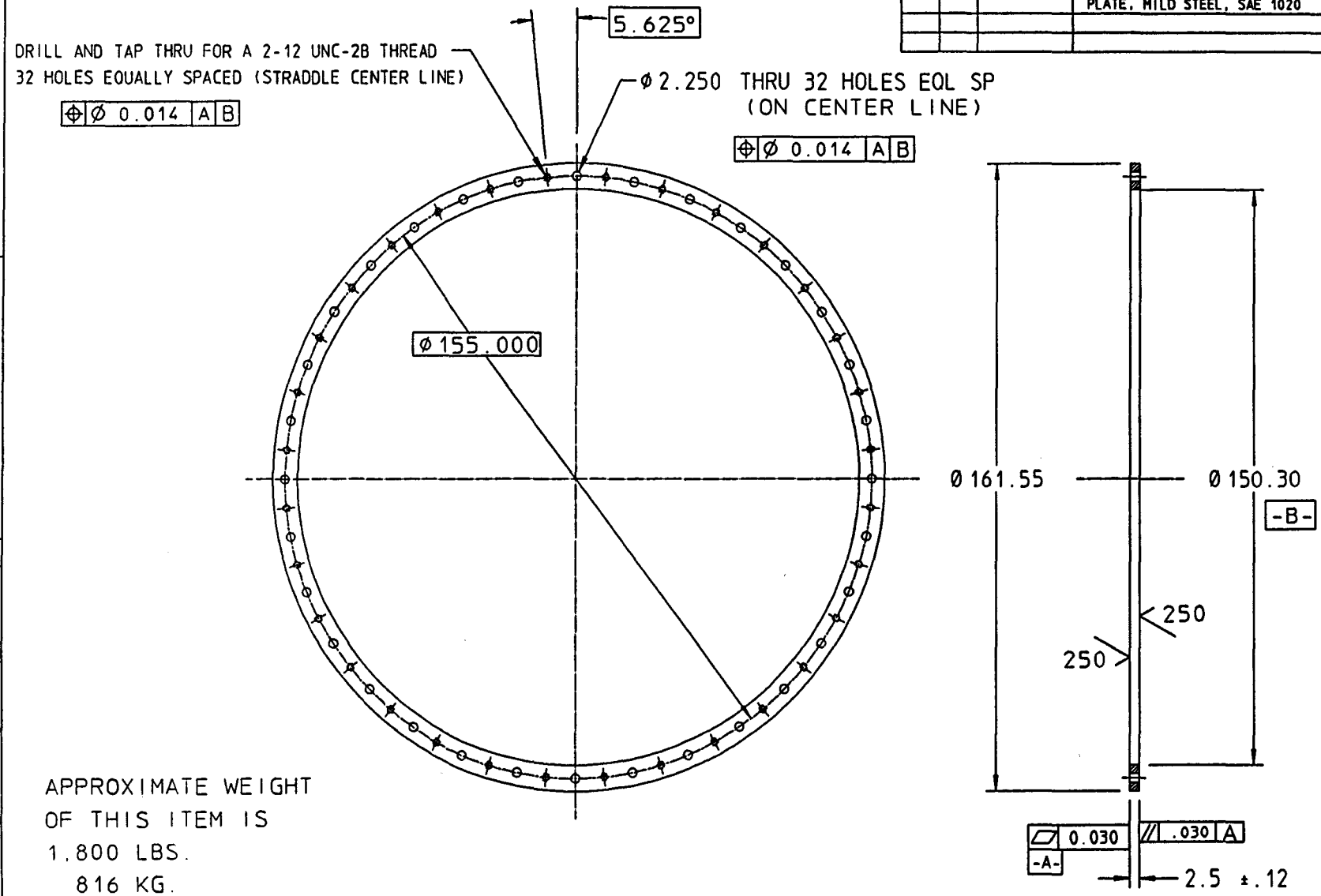

APPROXIMATE WEIGHT
OF THIS ITEM IS
1,800 LBS.
816 KG.

20M6173

REV	DWG	CHK	ZONE	DATE	CHANGES

UNLESS OTHERWISE SPECIFIED

TOLERANCES		
	.X ±	FRAC. ±
	.XX ± .03	ANGLES ±
	.XXX ± .015	FINISH 250

THREADS ARE CLASS 2
CHAMFER ENDS OF ALL SCREW THREADS 30°.
CUT 1.5 PITCH RAD RELIEF WITH ROUND NOSE TOOL ON MACHINE CUT THREADS.
BREAK EDGES .016 MAX. ON MACHINED WORK
REMOVE [illegible] SPLATTER & LOOSE SCALE
REFE[illegible] ASI Y14.5 & B46 1.

SHOP ORDERS

ACCT. NO.		SERIAL NO.	
DATE ISSD	DATE REQD.	NO. REQD.	
DELIVER TO			
SURFACE TREATMENT	DEGREASE		
IDENT. METH.	TAG		
DWG BY	MATT HOFF	DATE	9-21-92
CHK. BY		DATE	

LAWRENCE BERKELEY LABORATORY
UNIVERSITY OF CALIFORNIA-BERKELEY

SSC
2.0 SDC PLUG
ENDCAP ADAPTER RING

PATENT CLEAR	DWG. TYPE	SHOWN ON	SCALE	DO NOT SCALE PRINTS
	DETAIL		N.T.S.	
MICROFILMED	DESIGN ACCT. NO.	CATEGORY CODE	DWG. NO.	SIZE / REV.
	4213-01	2.02.10	20[illegible]173	

REQ	ITEM	PART NUMBER	DESCRIPTION
			PLATE, MILD STEEL, SAE 1020

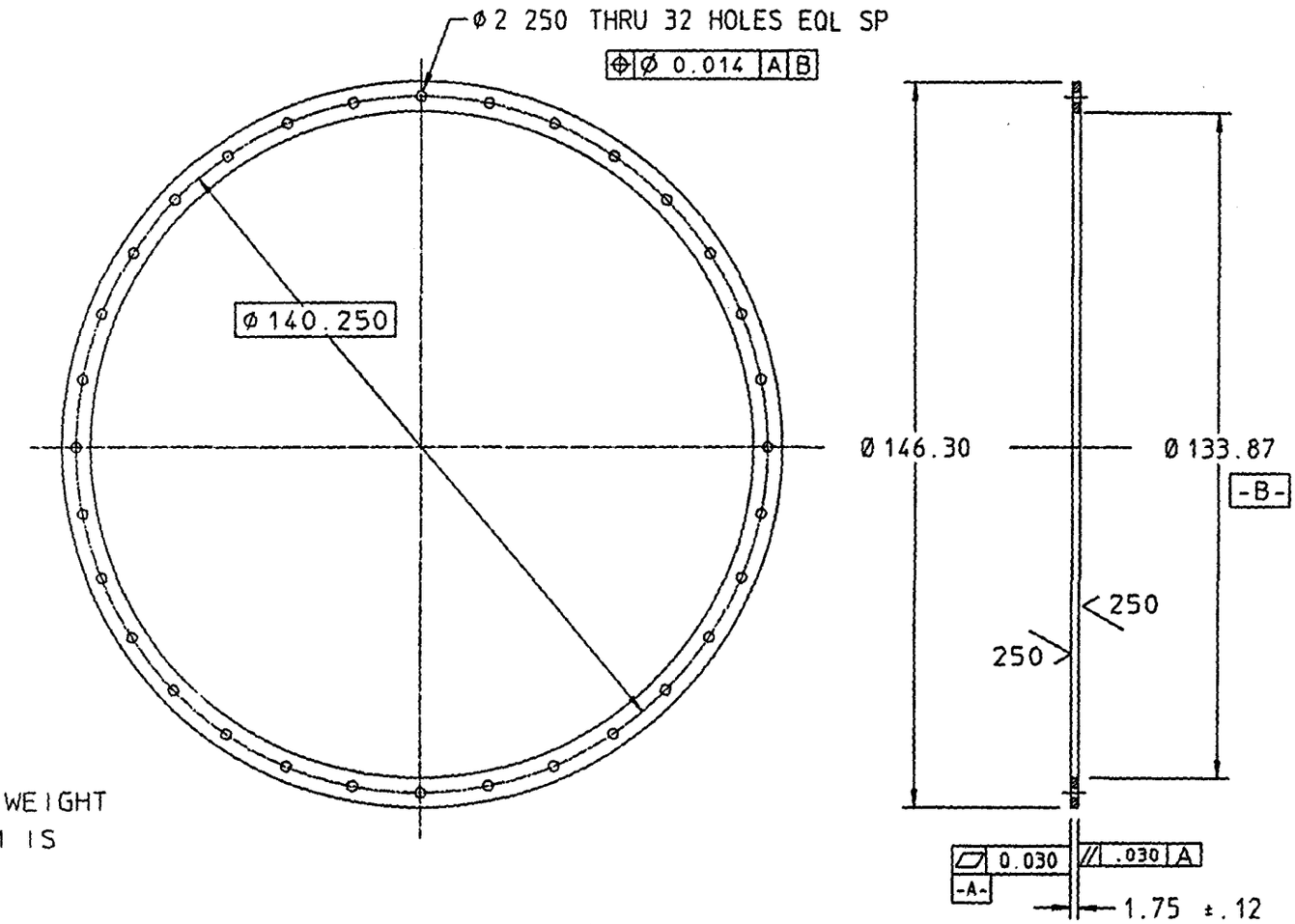

20M6133B

APPROXIMATE WEIGHT
OF THIS ITEM IS
1,300 LBS.
590 KG.

REV	DWG	CHK	ZONE	DATE	CHANGES
B	MDH			9-21-92	REDESIGNED
A	MDH			8/27/92	Ø155.000 WAS Ø154.500

UNLESS OTHERWISE SPECIFIED
TOLERANCES: .X ± FRAC. ± ; .XX ± .03 ANGLES ± ; .XXX ± .015 FINISH 250
THREADS ARE CLASS 2
CHAMFER ENDS OF ALL SCREW THREADS 30°.
CUT 1.5 PITCH THRD RELIEF WITH ROUND NOSE TOOL ON MACHINE CUT THREADS.
BREAK EDGES .016 MAX. ON MACHINED WORK
REMOVE BURRS WELD SPLATTER & LOOSE SCALE
REFERENCES: ANSI Y14.5 & B46.1.

SHOP ORDERS
ACCT. NO. | SERIAL NO.
DATE ISSD | DATE REQD | NO. REQD
DELIVER TO
SURFACE TREATMENT: DEGREASE
IDENT METH.: TAG
DWG. BY: MINAMIHARA | DATE: 5-26-92
CHK. BY | DATE

LAWRENCE BERKELEY LABORATORY
UNIVERSITY OF CALIFORNIA-BERKELEY
SSC
2.0 SDC PLUG
ENDPLUG ADAPTER RING

PATENT CLEAR | DWG. TYPE: DETAIL | SHOWN ON | SCALE: N.T.S. | DO NOT SCALE PRINTS
MICROFILMED | DESIGN ACCT. NO.: 4213-01 | CATEGORY CODE: 2.02.10 | DWG. NO.: 20M6133 | SIZE | REV.: B

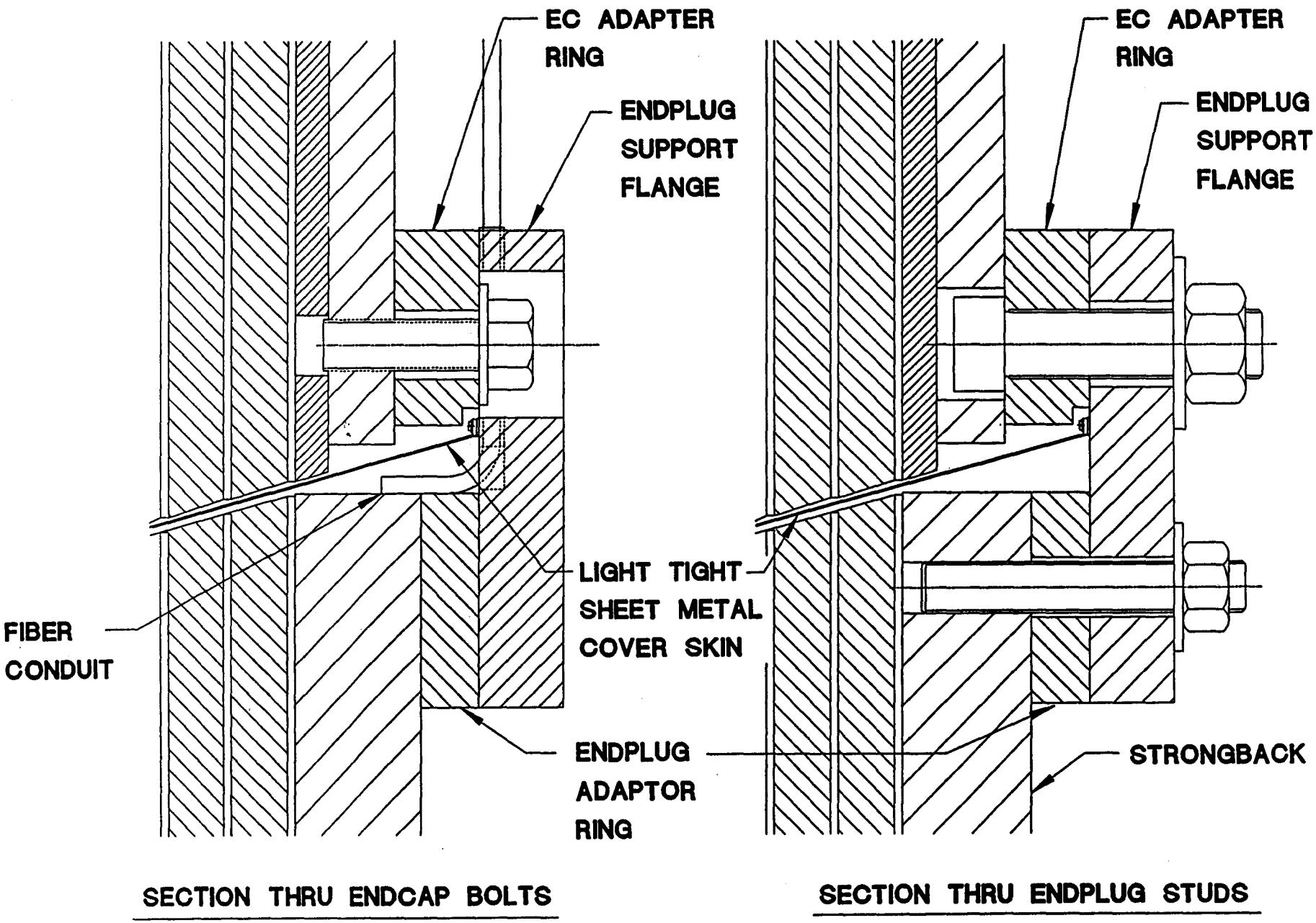

FIG. 6.1
ENDPL SUPPORT

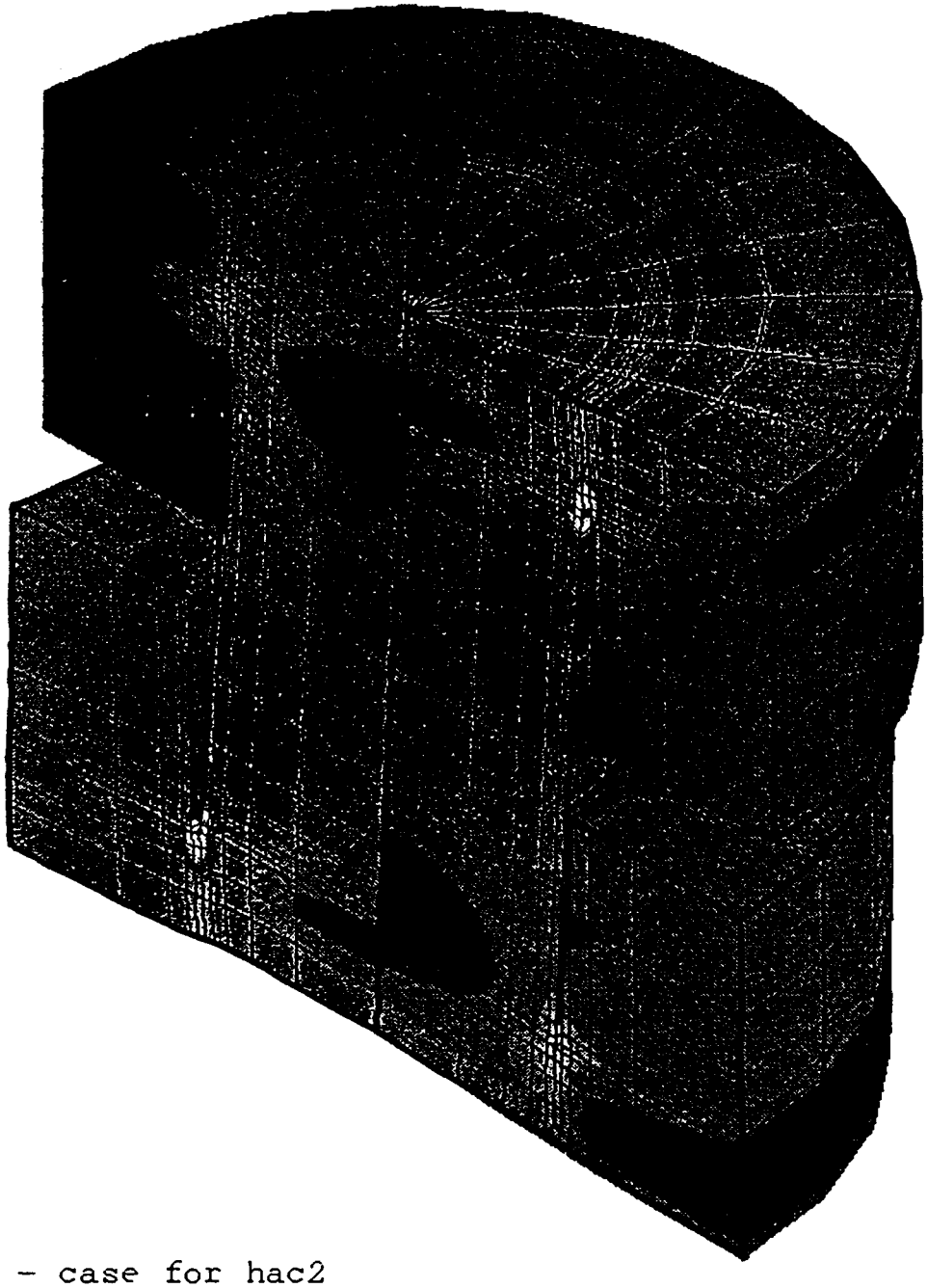

tr3dpl - case for hac2

Fig. 7.1 ANSYS generated plot of the tie rod/plate junction's stress and deflection (exaggerated, illustrating the stress concentration at the weld bottom. Plastic analyses techniques prove this to be a non-problem.

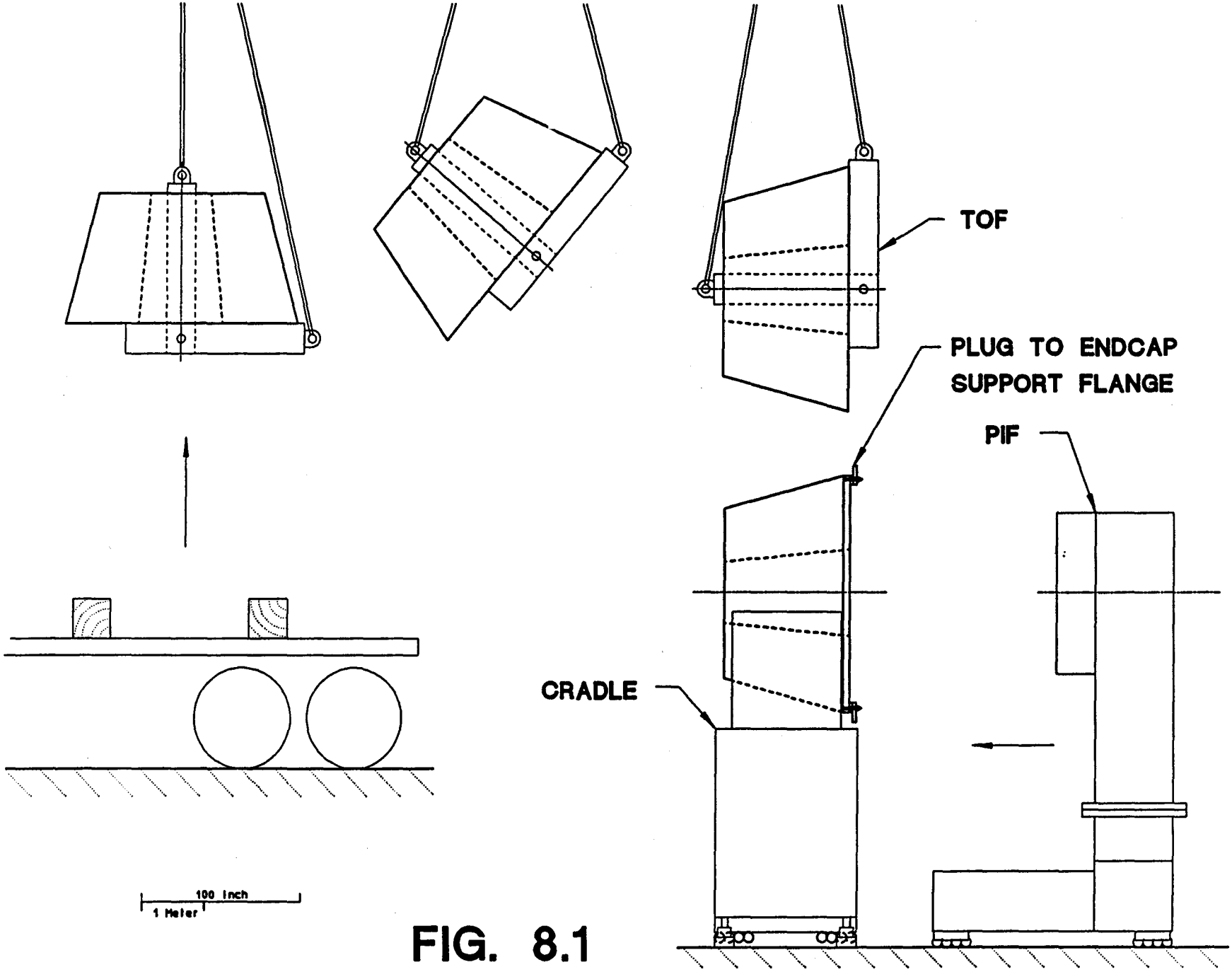

FIG. 8.1

SSC SITE ENDPLUG TRANSFER STEPS

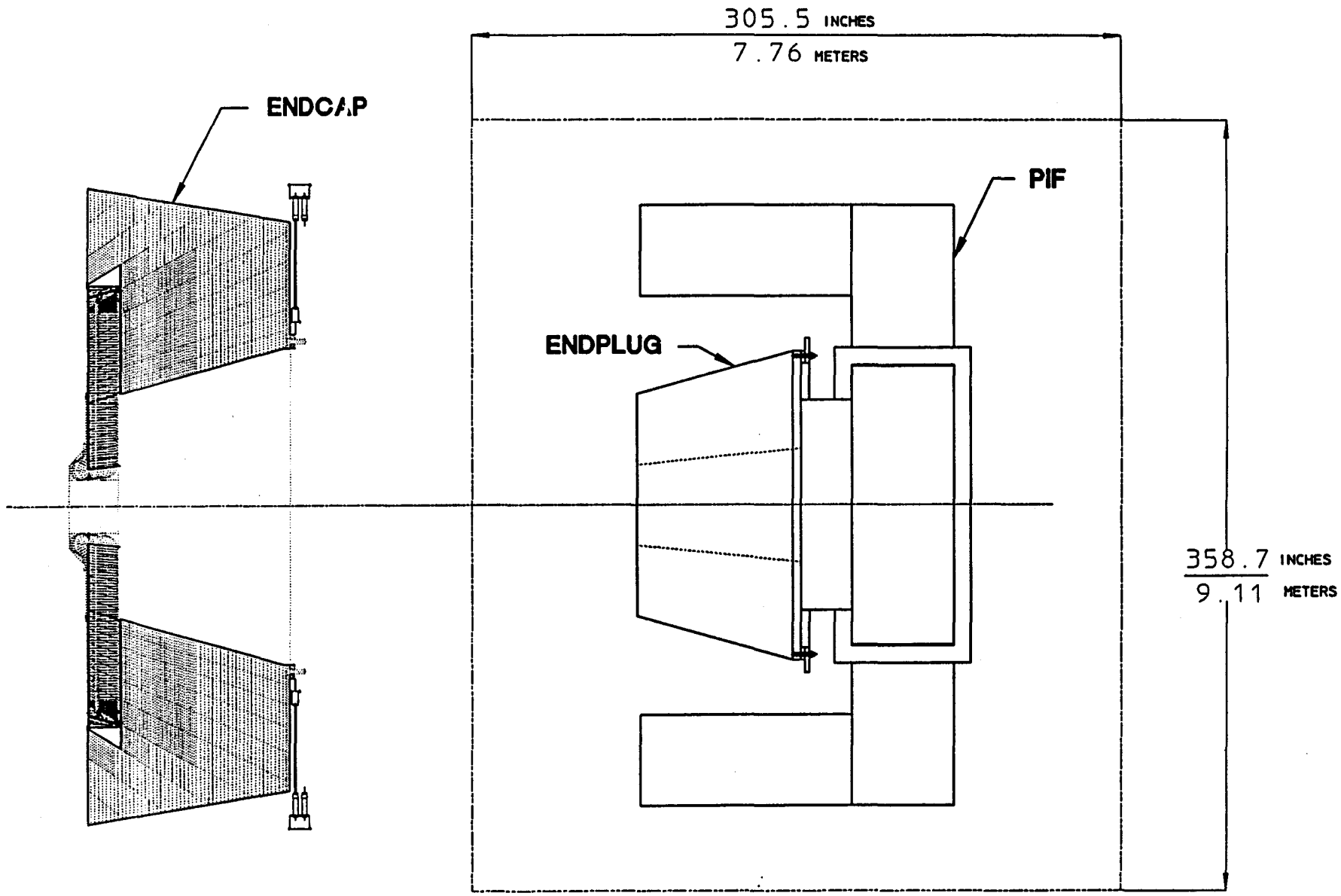

FIG. 8.2 PLAN VIEW OF WORKING SPACE FOR PLUG ASSEMBLY AND INSTALLATION

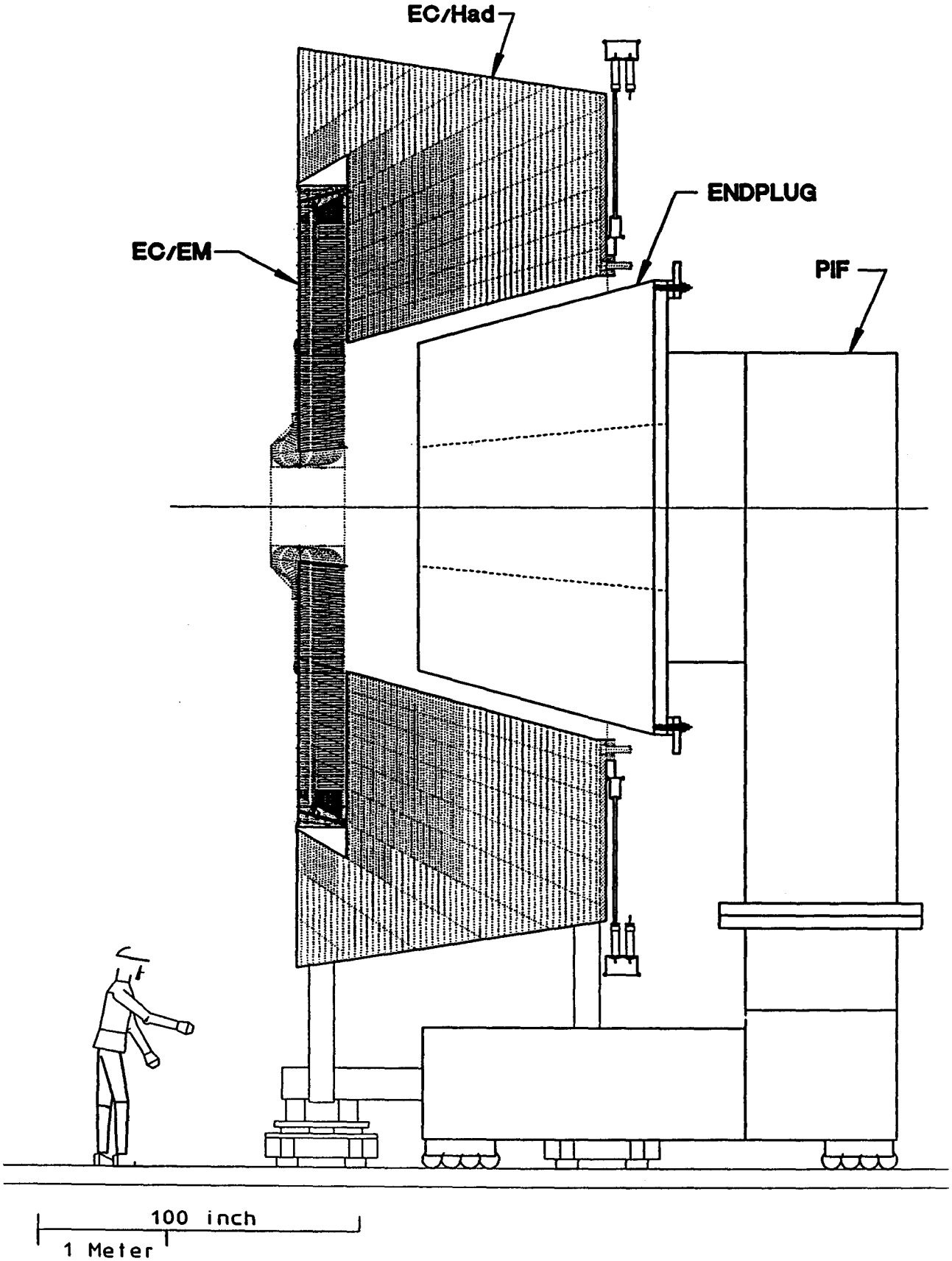

FIG. 8.3 INSTALLATION OF THE ENDPLUG INTO THE ENDCAP IN THE SURFACE ASSEMBLY BUILDING.

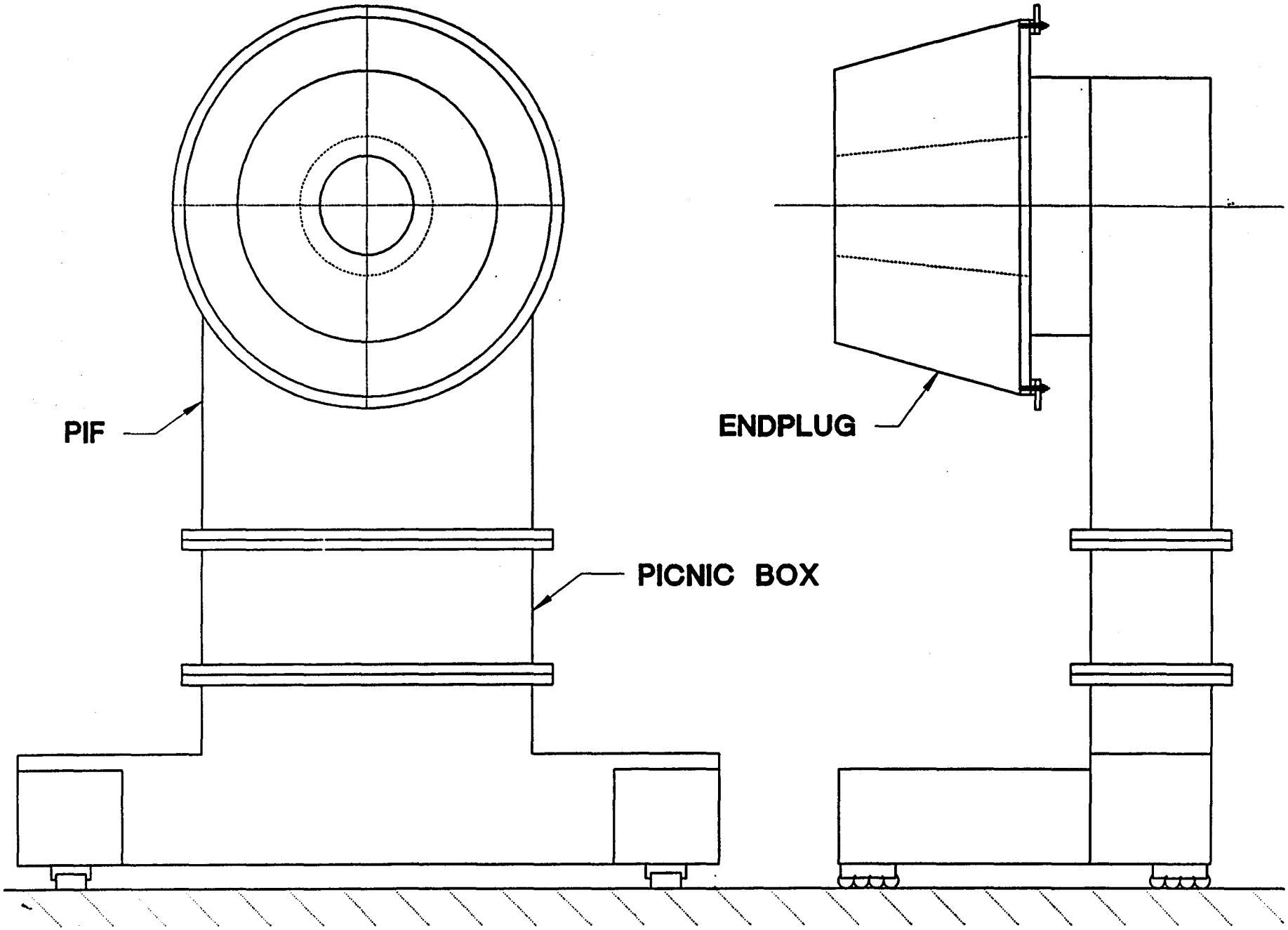

FIG. 8.4 MODIFICATION OF THE ENDPLUG INSTALLATION FIXTURE (PIF) FOR HALL OPERATIONS.

OPEN PLAN

Project: CALORIM
Report: SOCBARIC
Status as of: 01OCT92
Current Date: 23OCT92
Page: 1

LEVEL III SUMMARY BASELINE SCHEDULE

2.2 End Cap Calorimeter

SOLENOIDAL DETECTOR COLLABORATION

Summary Description	Baseline Start/Finish	Projected Start/Finish	%Comp
MILESTONES			
START MODULE DESIGN		30SEP92 30SEP92	
POR-ENDCAP MODULE STRUCTURE		18JUN93 18JUN93	
COMPLETE PROTOTYPE BEAM TEST		05MAY94 05MAY94	
FOR-ENDCAP MODULE STRUCTURE		31AUG94 31AUG94	
FOR-ENDCAP SUPPORT STRUCTURE		28SEP94 28SEP94	
FOR-ENDCAP SCINT & MISC		05MAY95 05MAY95	
COMPLETE 1ST HAD WEDGE (64)		20JUN95 20JUN95	
COMP.1ST-EM LEAD CASTING (ENDCAP)		09JAN96 09JAN96	
START-ASSY OF END PLUGS		02FEB96 02FEB96	
ASSEMBLY START (OFF-SITE)-ENDCAP		03MAY96 03MAY96	
ASSEMBLY START (SSCL)-ENDCAP		05NOV96 05NOV96	
ABOVE GROUND FACILITY REQUIRED-ENDCAP		05NOV96 05NOV96	
SHIPPING TO SSCL BEGINS-ENDCAP		17JAN97 17JAN97	
COMP.SHIPMENT OF ENDPLUGS		24JUN97 24JUN97	
START ENDPLUG SURFACE ASSY		25JUN97 25JUN97	
COMP.ENDCAP S.ASSY-READY T.O.H.		10NOV97 10NOV97	
INITIAL TOP OF HOLE CAPABILITY-ENDCAP		11NOV97 11NOV97	
INSTALLATION IN HALL BEGINS-ENDCAP		11NOV97 11NOV97	

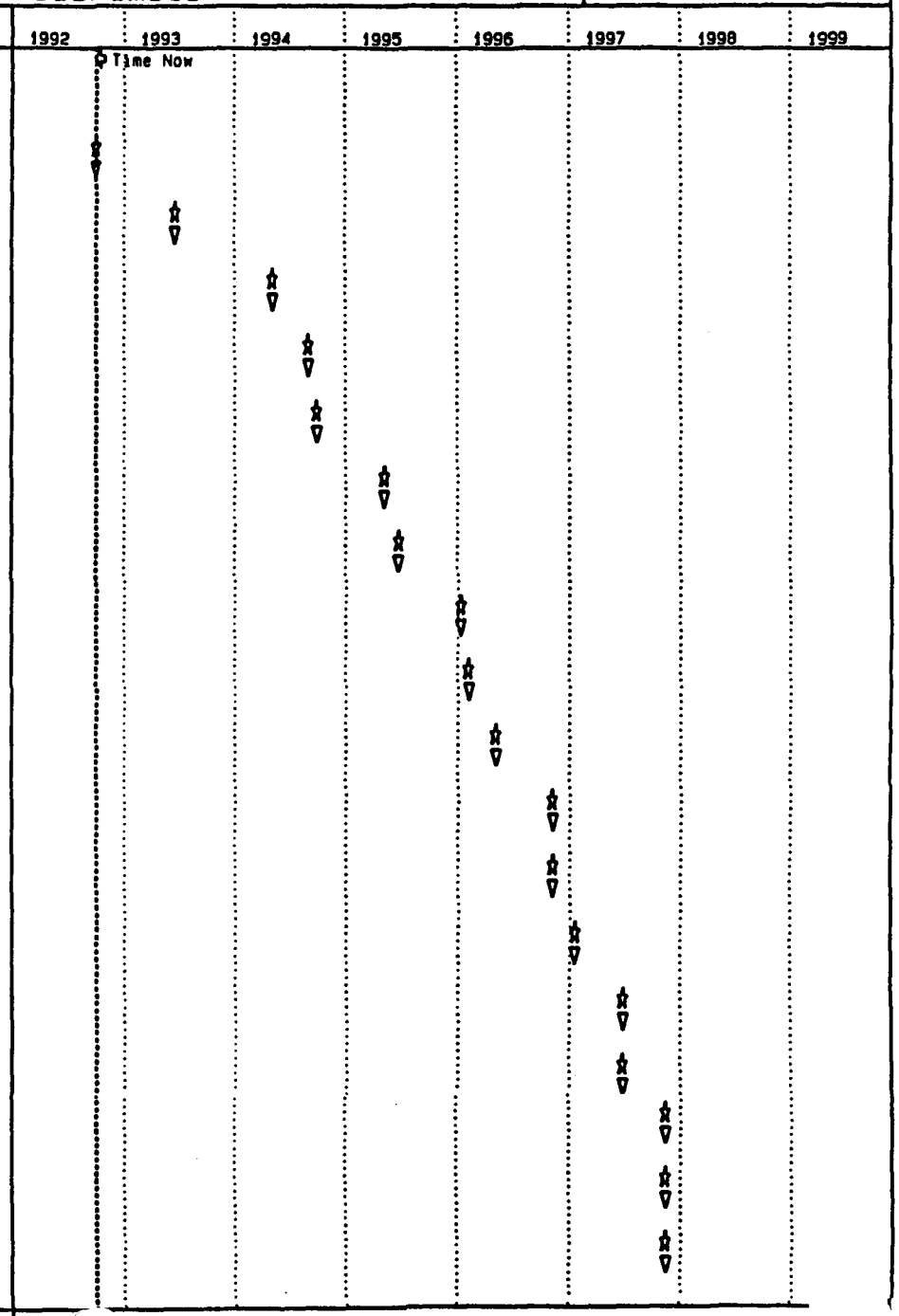

Legend
Br[illegible]
% [illegible]te of Total
% [illegible]f Planned to date
Projected/Actual Start
Projected/Actual Finish
Float

Fig 9.1